MYELOID CELL FUNCTION AND KINETICS IN ARTERIAL DISEASE

INVESTIGATING THE IMPACT OF CIGARETTE SMOKE ON MYELOID CELL FUNCTION AND KINETICS DURING THE PATHOGENESIS OF ATHEROSCLEROSIS AND AORTIC ANEURYSM

By DHARNEYA (DANYA) THAYAPARAN, B.Sc.

A Thesis

Submitted to the School of Graduate Studies

in Partial Fulfillment of the Requirements

for the Degree

Doctor of Philosophy

DOCTOR OF PHILOSOPHY (2021)

Faculty of Health Sciences, Medical Sciences Graduate Program

McMaster University, Hamilton, Ontario, Canada

TITLE: Investigating the impact of cigarette smoke on myeloid cell function and kinetics during the pathogenesis of atherosclerosis and aortic aneurysm

AUTHOR: Dharneya (Danya) Thayaparan, B.Sc. (McMaster University)

SUPERVISOR: Martin R Stämpfli, PhD

NUMBER OF PAGES: xxii, 175

LAY ABSTRACT

Diseases that affect the heart and major blood vessels are one of the leading causes of illness and death worldwide. Atherosclerosis is one such disease caused by the buildup of fatty deposits in the walls of major blood vessels called arteries. This buildup can eventually block the artery and lead to a heart attack or stroke. Abdominal aortic aneurysms are another type of disease that affects arteries. In this case, the walls of the artery grow weak and begin to balloon out until the artery eventually breaks causing severe internal bleeding and death. One of the most important cells involved in the development of atherosclerosis and aneurysms is the macrophage, a type of white blood cell that is an important part of the immune system and found in diseased arteries. Although we know that cigarette smoking is one of the most significant risk factors for developing atherosclerosis and abdominal aneurysms, we do not fully understand why. Therefore, the goal of this thesis project was to investigate how cigarette smoke affects the development of arterial disease with a focus on understanding how it impacts the movement and function of macrophages. Using a mouse model, we found that the development of atherosclerosis and aneurysm are likely related, and also identified ways that exposure to cigarette smoke increases the numbers of macrophages in arteries. This work advances our understanding of how arterial diseases may be related and provides insight into how smoking can increase the risk of developing arterial disease.

ABSTRACT

Rationale. Cigarette smoking is a well-known risk factor for cardiovascular disease, including arterial diseases such as atherosclerosis and abdominal aortic aneurysm. However, our understanding of how exposure to cigarette smoke impacts arterial disease pathogenesis is not well known. Consequently, this doctoral thesis focuses on understanding the development of atherosclerosis and aortic aneurysm in the context of exposure to cigarette smoke. In particular, since monocytes and macrophage are key immune cells implicated in arterial pathology, this work concentrates on understanding the impact of cigarette smoke exposure on the function and kinetics of monocytes and arterial macrophages.

Main Findings. Using a mouse model that combines two clinically relevant risk factors, hyperlipidemia and cigarette smoke, we showed that smoke exposure increases atherosclerosis and induces the spontaneous formation, progression, and rupture of abdominal aneurysms. We also provide experimental evidence that atherosclerosis strongly associates with regions of elastin damage and arterial dilation, suggesting atherogenesis may directly contribute to abdominal aneurysm formation.

Given the importance of macrophages in arterial disease, we investigated arterial macrophage heterogeneity and function following exposure to cigarette smoke. We report that cigarette smoke exposure increased the abundance of arterial monocytes and macrophages, whereas heterogeneity was primarily driven by hypercholesterolemia in aneurysmal tissue. Specifically, hypercholesterolemia is

associated with an increase in macrophage populations with putative functions in inflammation and tissue remodelling including Trem2 foamy macrophages, inflammatory macrophages, and interferon-inducible macrophages. Moreover, we demonstrated that arterial macrophages play a critical role in elastin fragmentation within the arterial wall of smoke exposed mice.

Finally, we investigated the impact of cigarette smoke on kinetic factors that can contribute to arterial macrophage accumulation. We found that, despite increased development of arterial disease, exposure to cigarette smoke is associated with an overall suppression of circulating monocytes and pro-inflammatory cytokines. Using a parabiosis model, we show monocyte recruitment is significantly increased and is likely a key factor contributing to accumulation of arterial macrophages following exposure to cigarette smoke. We also present evidence suggesting that endothelial dysfunction, related to a loss of endothelial nitric oxide synthase, contributes to increased arterial monocyte recruitment following exposure to cigarette smoke.

Conclusions and Significance. Overall, we provide evidence that atherosclerosis likely contributes to abdominal aneurysm pathology in a model of cigarette smoke-induced aneurysm formation. We further provide insight into how tobacco smoke promotes arterial disease development through increased local accumulation of arterial macrophages despite suppressed monopoiesis and systemic inflammation. We identify monocyte recruitment and endothelial dysfunction as key factors contributing to the increased accumulation of arterial macrophages, with no overall

differences in macrophage heterogeneity, following smoke exposure. In addition to providing insight into the increased risk of arterial disease following exposure to cigarette smoke, this study also provides experimental evidence that atherogenesis can contribute to abdominal aneurysm pathology. Overall, this thesis furthers our understanding of arterial disease pathogenesis and can provide a foundation for further mechanistic or therapeutic focused research aimed at reducing the burden of cardiovascular disease.

ACKNOWLEDGEMENTS

Pursuing doctoral research is no easy task and the completion of this thesis would not have been possible without the support of many, many people who I will do my best to acknowledge here. Apologies in advance for anyone I may have missed, the omission is not intentional, and you have my gratitude, nonetheless.

To begin, I was extremely fortunate in the guidance of Dr. Martin Stämpfli whose mentorship has shaped both my personal and professional development over the last eight years. Martin's pragmatism, humor, expertise, and arsenal of anecdotes created the perfect combination of advice and support for any situation and was critical in helping me to navigate the rocky roads of research.

An equal share of my mentorship is owed to Dr. Clint Robbins who didn't simply offer a passive collaboration but, instead, welcomed me as a member of his own lab. This thesis project would not exist without Clint's whole-hearted collaboration and guidance. Research is often filled with unexpected obstacles, and the number of times I hit a roadblock with this project, only to have a ten-minute conversation with Clint and walk away bursting with new ideas and renewed excitement is countless. Clint's passion for science, agile-thinking, and tenacity challenged my own approach to scientific research and helped me see that with enough grit and adaptability, even the loftiest of goals are achievable.

I must admit, I was spoiled for good mentorship in graduate school and am incredibly grateful for the advice and expertise of both Dr. Manel Jordana and Dr.

Dino Trigatti. Their scientific excellence and thoughtful questions never failed to create productive discourse during my committee meetings and significantly helped to shape my own critical thinking skills, as well as the research presented in this thesis.

I am incredibly grateful to the members of the Robbins lab who adopted me into the lab and spent hours training me in difficult and highly technical lab skills, in addition to contributing to this project themselves. Dr. Takuo Emoto, a co-first author on the manuscript based on this work, displayed an incredible work ethic and was absolutely instrumental in advancing this project. He pioneered several techniques that significantly improved our efficiency and enabled incredibly productive experiments. Dr. Ricky Besla and Dr. Angela Li were among the first members of the Robbins lab involved in this collaboration and shared in all the challenges of establishing a multi-center collaboration. Although not a member the Robbins lab, Marwan Althagafi (Cybulsky lab) provided his time, expertise, and training which allowed us to generate the beautiful *en face* immunofluorescence images presented in this thesis. Finally, for performing experiments, co-ordinating logistics, and providing scientific expertise, I must also thank Dr. Tara Sivasubramaniyam, Aniqa Khan, Amina Abow, Dr. Antigona Ulndreaj, Stephanie Schroer-McFarland, Shaun Pacheco, Emily Chen, Felix Chiu, and Elvira Paneda.

The amount of thanks I owe to members of the Stämpfli lab, both past and present, is difficult to articulate. Many individuals have contributed to this project

and/or my development as a scientist including Dr. Mathieu Morissette, Dr. Pam Shen, Dr. Jake Nikota, Ashley Beaulieu, Joanna Kasinska, Rachel Heo, Bruce Ly, Bomi Park, Peipei Wang, and Matthew Fantauzzi, to name a few. I owe an especial debt of gratitude to Josh McGrath and Steven Cass who have spent endless hours editing documents, listening to presentations, and performing incredibly demanding amounts of lab work with me while somehow making it all fun. Grad school was certainly challenging but it helped knowing that there was always someone ready with an ear or a beer to discuss science, life, the universe, and everything, oftentimes within the same conversation. I hope you all know that you have set the bar impossibly high for future coworkers and friends.

I do not have enough space to thank all the other members at MIRC or UHN (PMCRT) who have worked with me over the years in the lab, as a teaching assistant, in graduate courses, or on volunteer committees, although everyone's help and support are very much appreciated. However, I would be remiss if I did not thank the excellent technical staff at both animal research centres as well as members of the Cybulsky, Epelman, Jordana, Kaushic, and Xing labs including Dr. Shabana Vohra, Dr. Sara Nejat, Dr. Corey Scipione, Tina Walker, Talveer Mandur, Josh Koenig, Dr. Puja Bagri, Dr. Alison Felker, Dr. Sam Afkami, Dr. Rocky Lai, Mike D'Agostino, and Dr. Joni Hammill for all of the help they've provided for me and for the work presented in this thesis.

Last, but certainly not least, I would like to thank my family for endless amounts of unconditional love and support even as you all gradually realized how long doctoral studies actually take. For my Appappa, Appamma, Ammamma and Thatha, who were among my earliest teachers and showed me the doors that are opened by education. For my Appa who is an unapologetic nerd and taught me learning is not limited to a classroom. For my Amma who instilled the importance of street smarts in addition to academic pursuits, and for the endless cups of tea. For my cousins who kept me on my toes by racing me to the end of their own milestone accomplishments. For my aunts and extended family who always checked in on me and did their best to remember mice are different from rats. And, of course, for my Acca and brother-in-law who spent my entire graduate career kindly reminding me that an education alone does not pay the bills. This achievement was only possible because of you all, and I can not thank you guys enough!

TABLE OF CONTENTS

LIST OF FIGURES AND TABLES

CHAPTER 3.1: Aortic aneurysm formation strongly associates with atherosclerosis in smoke exposed mice

CHAPTER 3.2: Hypercholesterolemia induced macrophages are increased by smoke exposure and mediate arterial elastin damage

LIST OF ABBREVIATIONS AND SYMBOLS

7AAD – 7-Aminoactinomycin D

AAV – Adeno-associated viral vector

ABC – ATP-binding cassette

ACTA2 – Actin

Adgre1 – Adhesion G protein-coupled receptor E1

AIM – Apoptosis inhibitor expressed by macrophages (aka Spα or Api6)

AMP – Adenosine monophosphate

ANOVA – Analysis of Variance

APOB – Apolipoprotein B

APOE – Apolipoprotein E

Arg1 – Arginase 1

ATP – Adenosine triphosphate

AU – Arbitrary units

Bax – Bcl-2 associated X protein

Bcl-2 – B cell lymphoma 2

BrdU – Bromodeoxyuridine

BSA – Bovine serum albumin

$CaCl_2$ – Calcium chloride

CCL – C-C motif ligand

CCR – C-C motif receptor

CD – Cluster of Differentiation

CD209a (aka DC-SIGN) – Dendritic cell-specific intercellular adhesion molecule-3-grabbing non-integrin

CD3d – T-cell surface glycoprotein CD3 delta chain

CD79a – B cell antigen receptor complex associated protein alpha chain

cDC – Conventional dendritic cells

Cebpb – CCAAT enhancer binding protein beta

c-Myb – proto-oncogene, transcription factor

COX-2 – inducible cyclo-oxygenase

Cre – Cre recombinase (targets Lox sequences)

CRP – C reactive protein

CSF1 – colony stimulating factor 1

Cts – Cathepsin

CX_3CR1 – C-X3-C motif chemokine receptor (aka fractalkine receptor or G-protein coupled receptor 13)

CXCL – CXC chemokine ligand

CXCR – CXC chemokine receptor

CyTOF – mass cytometry by tome of flight

DAPI – 4′,6-diamidino-2-phenylindole

DNA – Deoxyribonucleic acid

EDTA – Ethylenediaminetetraacetic acid

eNOS – Endothelial nitric oxide synthase

EVG – Elastin van Gieson

EYFP – enhanced yellow fluorescent protein

FACS – fluorescence activated cell sorting

FDR – False discovery rate

FITC – Fluorescein

Flt3 (CD135) – fms like tyrosine kinase 3 or fetal liver kinase 2

FSC – Forward scatter

Fscn1 – Fascin actin bundling protein 1

G1 – Gap/growth phase 1 (RNA and protein synthesis prior to replication)

G2 – Gap/growth phase 2 (DNA replication complete)

Gata 3 – trans-acting T cell specific transcription factor GATA-3 (aka GATA-binding factor 3)

G-CSF – Granulocyte colony stimulating factor

GO – Gene ontology

Gzmk – granzyme K

H&E – Hematoxylin and eosin

H2O2 – Hydrogen peroxide

HCD – High cholesterol diet

HCL – Hydrochloric acid

HDL – High density lipoprotein

HMG-CoA – 3-hydroxy-3-methylglutaryl-coenzyme A

ICAM-1 – Intercellular adhesion molecule 1

IFN – Interferon

IFNIC – Interferon inducible macrophages

Ig – Immunoglobulin

IL - Interleukin

ILC2 – Innate lymphoid cell 2

Irf – Interferon response factor

Isg – Interferon stimulated gene

Itgam – Integrin subunit alpha M (subunit of CD11b)

KEGG – Kyoto Encyclopedia of Genes and Genomes

Ki67 – Antigen Ki-67

Klra9 – Killer cell lectin-like receptor subfamily A membrane 9

LDL – Low density lipoprotein

LDLR – Low density lipoprotein receptor

LFA-1 – Lymphocyte function-associated antigen 1 (CD11a/CD18)

Lgals3 – Galectin-3

Lin – Lineage

L-NAME – Nω-Nitro-L-arginine methyl ester hydrochloride

LoxP – short specific DNA sequences (targeted by Cre)

Ly6c2 – lymphocyte antigen 6C2

Lys - Lysine

Lyve1 – Lymphatic vessel endothelial hyaluronan receptor 1

M – Mitosis (cell division)

Mac^{AIR} – Aortic intimal resident macrophages

MARCO – macrophage receptor with collagenous structure

MCP-1 – Monocyte chemoattractant protein 1 (aka CCL2)

MIBI - multiplexed ion beam imaging

MIP – Macrophage inflammatory protein

MMP – Matrix metalloproteinase

Mrc1 – Mannose receptor C-type 1

mRNA – Messenger RNA

MSR-1 – Macrophage scavenger receptor 1 (aka CD204)

MYH11 – myosin heavy chain

NK – Natural Killer

NLRP3 – NOD-, LRR- and pyrin-domain containing protein 3

NO – Nitric oxide

NOS – Nitric oxide synthase

Nr4a1 – Nuclear receptor subfamily 4 group A member 1

Ntn – netrin-1

OPN – Osteopontin

ORO – Oil red O

p/s/cm2/s – photons per second per cm squared per steradian

PBS – phosphate buffered saline

PCA – Principal component analysis

PCSK9 – Proprotein convertase subtilisin/kexin type 9

Pct.1 – percent of cells in a cluster expressing a gene in sample population 1

pDC – Plasmacytoid dendritic cell

Pecam1 – Platelet endothelial cell adhesion molecule

Pf4 – Platelet factor 4 (CXCL4)

PFA – Paraformaldehyde

qPCR – Quantitative polymerase chain reaction

RBC – Red blood cell

RNA – Ribonucleic acid

Rorc – Nuclear receptor ROR-gamma

S – Cell cycle phase between G1 and G2 when DNA is replicated

S100a9 – S100 calcium binding protein A9 (aka calgranulin B or migration inhibitory factor-related protein 14 (MRP14))

Sca1 – Stem cell antigen-1

scRNA-seq – single cell RNA sequencing

SEM – Standard error of the mean

SMC – Smooth muscle cell

SOD – Superoxide dismutase

Spp1 – Secreted phosphoprotein 1 (aka osteopontin)

SSC – Side scatter

TimD4 – T cell immunoglobulin and mucin domain containing protein 4

TLR – Toll-like receptor

TNFα – Tumor necrosis factor alpha

Trem2 – Triggering receptor expressed on myeloid cells 2

UMAP – Uniform manifold approximation and projection

UMI – Unique molecular identifiers

UNC5b – Unc-5 netrin receptor B

VCAM-1 – Vascular cell adhesion molecule 1

VLA-4 – Very late antigen 4 (aka integrin α4β1 or CD49d/CD29)

Xcr1 – X-C motif chemokine receptor 1

α – Alpha

β – Beta

γ – Gamma

μ – Micro

DECLARATION OF ACADEMIC ACHIEVEMENT

A manuscript based on the research presented in this thesis is currently under peer-review at *Nature* (May 2021) with myself listed as first author and shared with Dr. Takuo Emoto and Dr. Rickvinder Besla. I significantly contributed to all aspects of this work including project conceptualization, experimental design and execution, and data analysis and presentation while under the supervision of Dr. Martin Stämpfli and Dr. Clint Robbins. This work would not have been possible without the technical assistance of Joshua J. C. McGrath, Steven P. Cass, Marwan Althagafi, Aniqa Khan, Amina Abow, Angela Li, Shaun Pacheco, Rachel Heo, Matthew Fantauzzi, Stephanie Schroer-McFarland, Dr. Tharani Sivasubramaniyam, Dr, Antigona Ulndreaj, Emily Chen, Felix Chiu, and Joanna Kasinska who assisted with complex animal work, sample processing for flow cytometry and/or histology, confocal microscopy, and logistical support. Bioinformatic analysis of the single cell RNA sequencing data presented in chapter 3.2 was performed by Dr. Shabana Vohra, Dr. Sara Nejat, and Edouard Al-Chami. Dr. Shabana Vohra also kindly provided the methodology for single cell RNA sequencing-related work described in chapter 2.5. Finally, Drs. Myron I. Cybulsky, Slava Epelman, Mansoor Husain, Barry B. Rubin, and Peter Libby kindly provided reagents and key expertise to facilitate completion of the work presented in this thesis.

CHAPTER 1: INTRODUCTION

1.1 BURDEN OF CARDIOVASCULAR DISEASE

Cardiovascular disease is a broad term that encompasses several conditions primarily affecting the heart and vasculature and includes coronary artery disease, peripheral arterial disease, cerebrovascular disease, and aortic aneurysms, among others. It is the number one cause of mortality in the world and is increasing globally.[1] In fact, cardiovascular disease accounts for 20-24% of the overall global burden of disease.[2] Notably, half of this burden is due to ischemic arterial diseases, which is characterized by the development of atherosclerosis.[2] Atherosclerosis is an occlusive arterial disease and can lead to acute events such as myocardial infarction and stroke, which contribute to the majority of cardiovascular related deaths.[3] Another significant contributor to cardiovascular mortality is aortic aneurysms. Although the prevalence of aneurysm is much lower, the insidious nature of the disease coupled with sudden rupture leads to death in over 50-80% of cases even with emergency surgical intervention.[2,4] Thus, despite current therapeutic strategies, cardiovascular diseases such as atherosclerosis and aortic aneurysm remain a pressing global health issue.

1.2 ATHEROSCLEROSIS

1.2.1 CLINICAL OVERVIEW

Atherosclerosis is a chronic and progressive arterial disease characterized by the gradual accumulation of lipids and immune cells at focal sites forming a plaque in

the arterial wall.[5] These plaques grow over time and can become fibrous and calcified leading to stenosis which is the gradual hardening and narrowing of the arteries. As the plaque grows into the lumen of the artery, it can become occlusive and lead to restricted blood flow to key organs including the heart or brain. Eventually, plaque rupture and the subsequent formation of blood clots (thrombosis) can completely block the blood vessel and result in severe acute events such as myocardial infarction or stroke. Importantly, atherosclerosis should not be thought of as the passive build up of lipids and cells or static occlusions of the aorta, but rather dynamic sites of activity and inflammation.[6–8] Current clinical guidelines on the treatment of atherosclerosis focus on identification and management of key risk factors.[9] In particular, hyperlipidemia has been confirmed as a critical causative factor in the development of atherosclerosis.[9,10] Additional considerations of note include physiological risk factors such as hypertension and hyperglycemia, as well as behavioural risk factors including tobacco use, cholesterol-rich diet, and low physical activity. Management of these risk factors is approached through a combination of lifestyle changes and pharmacological interventions.[9]

1.2.2 RISK FACTORS AND TREATMENT

1.2.2.1 Hypercholesterolemia

Cholesterol

One of the major risk factors for the development of atherosclerosis is hyperlipidemia, an excess of circulating lipids, which can be caused by a high cholesterol diet or a deficiency in effective lipid processing.[10–14] Normally,

cholesterol and other lipids synthesized in the liver or obtained through the diet are transported to and from various tissues in the body by lipoproteins. There are different types of lipoproteins primarily characterized by their density as well as their lipid and protein components. In general, low density lipoproteins (LDL) are high in lipid content (cholesterol, triglycerides, and phospholipids) and are involved in delivering lipids to tissues, whereas high density lipoproteins (HDL) are involved in removing lipids from cells through cellular efflux. Following efflux these lipids are then transported by HDL to the liver for recycling or excretion in a process termed reverse cholesterol transport.[13]

Apolipoproteins are the protein component of lipoproteins which facilitate the transport of non-polar, or amphipathic, lipids though the circulation, in addition to acting as ligands for lipid uptake and transfer receptors. For example, apolipoprotein A-I in HDL interacts with ATP-binding cassette protein A1 (ABCA1) on cells to facilitate lipid efflux from the cell to HDL. Similarly, apolipoprotein B (apoB) in LDL interacts with LDL receptors (LDLR) to enable receptor-mediated endocytosis of LDL allowing for delivery of lipids into the cells of various tissues. Apolipoprotein E is also a notable component of lipoproteins and interacts with LDLR to facilitate lipid transport as well as the clearance of lipoprotein remnants by liver cells. However, when an excess of lipids are consumed or produced, or a defect in lipid clearance occurs, this homeostatic balance is disrupted and results in the accumulation of circulating lipids.[10–14] Specifically, an increase in circulating LDL has been causally linked to

atherosclerosis and is the major therapeutic target of most currently available pharmacologic treatments.[10,15]

Lipid-lowering Therapies

It is important to note that cholesterol is an essential lipid that forms an integral component of cell membranes and also serves as a precursor for many hormones and, as such, is produced by most mammalian cells. Cholesterol biosynthesis involves many steps with 3-hydroxy-3-methylglutaryl-coenzyme A (HMG-CoA) acting as a key intermediate for cholesterol synthesis, and HMG-CoA reductase being a rate-limiting enzyme for this process.[14,16] In 1976, an HMG-CoA reductase inhibitor (compactin) was isolated from penicillium mold and observed to have cholesterol lowering effects.[17] This led to a new class of drugs called statins which were soon shown to have clinical efficacy in lowering LDL cholesterol in patients with diet-induced hypercholesterolemia and familial hypercholesterolemia caused by heterozygous loss of LDL receptors.[18,19] Interestingly, statins do not appear to have the same efficacy in patients with homozygous loss of LDL receptors, suggesting a mechanism dependent on functional LDL receptors.[20] Since statins are HMG-CoA reductase inhibitors they block endogenous cholesterol synthesis which leads to activation of transcription factors that increase expression of LDL receptors in addition to genes involved in cholesterol synthesis. However, since statins functionally inhibit cholesterol synthesis, this process leads to a positive feedback loop of increased LDL receptor expression, which leads to reduced circulating LDL

cholesterol by increasing cellular uptake and clearance.[14] Thus statins can effectively lower cholesterol in the context of functional LDL receptor expression.

Given the significant role elevated LDL has on the development of atherosclerosis, it is unsurprising that lipid-lowering therapies like statins are the first line pharmacotherapy recommended for individuals at risk.[9] The safety and efficacy profile of statins are will established with an approximately 22% reduction in risk of major adverse cardiovascular events for every mmol/L reduction in LDL cholesterol.[15] Recently, additional cholesterol lowering therapies have also shown clinical success including ezetimibe which reduces dietary cholesterol absorption in the intestine. The IMPROVE-IT trial demonstrated further LDL cholesterol lowering and improved cardiovascular outcomes when ezetimibe was added to statins compared to statin alone.[21] Another therapy that has shown recent clinical success are monoclonal antibodies that inhibit proprotein convertase subtilisin/kexin type 9 (PCSK9). PCSK9 binds to hepatic LDL and promotes its degradation leading to lower LDL receptor expression on liver cells. It was observed, clinically, that loss-of-function mutations in PCSK9 lead to lower circulating LDL levels and gain-of-function mutations resulted in hypercholesterolemia.[22,23] Thus, anti-PCSK9 monoclonal antibodies such as alirocumab and evolocumab were developed into pharmacotherapies that have shown success in reducing LDL cholesterol in statin-treated patients, with a concomitant decrease in adverse events.[24–26] Therefore, although statins have shown impressive efficacy in the treatment of atherosclerosis and reduction of

major cardiovascular events, additional therapies can help further improve patient outcomes.

Residual Inflammatory Risk

Patients with well controlled cholesterol levels still exhibit residual risk since cholesterol-lowering therapies do not halt disease progression or completely mitigate risk of adverse events.[27–30] Recent evidence suggests that inflammation may be an important contributor to this residual risk. For example, there is evidence that elevated circulating C-reactive protein (CRP) is associated with increased risk of adverse cardiovascular events independent of LDL levels. The JUPITER trial demonstrated that statin treatment of patients with below-threshold LDL but high CRP, benefited from statin treatment. Specifically, it was observed that high baseline CRP was associated with higher risk, and that increased CRP reduction was associated with higher risk reduction.[31,32]

Furthermore, CANTOS, a recent clinical trial, demonstrated a modest decrease in risk of acute cardiac events as a result of an anti-IL-1β therapy without affecting LDL levels.[27–29,33] CANTOS specifically recruited patients with a previous myocardial infarction and elevated CRP. Similar to JUPITER, the investigators also observed the most benefit in patients with the largest CRP reduction.[34] Moreover, a similar pattern of benefit was observed with reductions in IL-6, highlighting a role for inflammation in residual risk.[35] However, this benefit in reduced cardiovascular risk was offset by a significant increase in fatal

infections, demonstrating a pressing need to better understand the nuances of residual inflammatory risk in order to refine therapeutic strategies.[30,33,36]

1.2.2.2 Cigarette Smoke

Tobacco smoking is a well established risk factor for atherosclerosis and is associated with an increase in acute coronary events, stroke and all-cause mortality in cardiovascular disease patients.[37] In fact, smoking is associated with earlier cardiovascular mortality with an advance of more than 5 years.[37] Smoking, which emerged as a risk factor of interest in the 1950s, has been a recognized risk factor associated with a 2-3 fold increased risk of cardiovascular disease since the 1970s.[38–40] Interestingly, despite significant advances in hyperlipidemia and hypertension treatments since the 1970s, the risk attributed to smoking has remained consistent, highlighting smoking as an important independent risk factor for cardiovascular disease.[40] Thus, current clinical guidelines recommend smoking cessation as early as possible given that the benefit of smoking cessation is dose-dependent and increases with time.[37] However, former smokers remain at increased risk of cardiovascular disease and adverse events compared to individuals who have never smoked, indicating a potential gap in treatment and a need to further understand smoking related disease pathogenesis.[9,37]

1.2.3 PATHOGENESIS

1.2.3.1 Arterial Anatomy

Atherosclerotic plaques form in the arteries, which are the major blood vessels responsible for carrying oxygenated blood from the heart to the rest of the body. The aorta is an elastic blood vessel composed of 3 major layers: the intima, media, and adventitia, each of which has a distinct composition.[41] The intima (innermost layer) primarily consists of a single endothelial cell layer while the adventitia (outermost layer) principally consists of fibroblasts and collagen fibers. The media (middle layer) is predominantly composed of vascular smooth muscle cells and the extracellular matrix, which includes structural proteins such as elastin and collagen. Together, the vascular smooth muscle cells and extracellular matrix form the elastic lamina, the fundamental fibromuscular unit of the media, responsible for evenly distributing stress and providing elasticity to accommodate dynamic blood flow.[41] More recent evidence has also identified the presence of myeloid cells both within the intima and the adventitia of aortic tissues during homeostasis.[42,43] Atherosclerotic plaques mainly form in the intima, with advanced plaques involving migration of the smooth muscle cells from the media and plaque growth into the luminal space.[5,6,44]

1.2.3.2 Mouse Models

Much of our knowledge regarding the pathogenesis of atherosclerosis has been gained through the use of preclinical animal models. The two primary mouse

models used to investigate atherosclerosis are the apolipoprotein E-deficient (*Apoe-/-*) mouse and the low-density lipoprotein receptor-deficient (*Ldlr-/-*) mouse, both of which were generated on a C57BL/6 background.[45,46] In both models, loss of efficient lipid processing capabilities leads to significant increases in hypercholesterolemia. Notably, atherosclerosis development in the *Ldlr-/-* mouse is dependent on atherogenic diets which are high in fat and/or cholesterol diet such as the "Western"-type diet (0.2% cholesterol, 21% fat). The *Apoe-/-* mouse, however, can develop atherosclerosis on a normal diet and is hypercholesterolemic at baseline, with atherogenic diets accelerating this process.[46–48] The transgenic and experimental manipulations of both these models have allowed for significant mechanistic insights into the *in vivo* development of atherosclerosis.

1.2.3.3 Initiation of Atherogenesis

The exact sequence of the earliest events in atherogenesis is difficult to decipher but is generally agreed to be consistent of subendothelial lipid accumulation and compromised endothelial function. The concept of lipid accumulation initiating atherosclerosis was proposed as the 'response to retention' model 25 years ago, and has been well supported with LDL cholesterol identified as a causative risk factor of atherosclerosis.[10,49,50] The 'response to injury' model was initially proposed 45 years ago and suggested that atherosclerosis was initiated by loss of endothelial cells in athero-susceptible regions.[51,52] However, subsequent observations including the presence of intact endothelium overlying developing atheroma in

clinical samples led to the evolution of this theory over time.[53,54] Now, it is generally proposed that endothelial dysfunction plays an important role in early atherogenesis, particularly in regards to inflammation and immune cell infiltration.[55]

Subendothelial Lipid Accumulation

Hypercholesterolemia is a well established risk factor for atherosclerosis with strong clinical evidence to support a causal role for elevated LDL cholesterol.[10] Circulating LDL are able to bind proteoglycans, often exposed in athero-susceptible arterial branch points, allowing for LDL infiltration and retention in the aortic wall.[56] This retention is typically mediated by an ionic interaction between basic amino acids in apoB and the negatively charged sulphate groups on proteoglycans.[50,57] Notably, although endothelial permeability may contribute to increased lipid accumulation, it is not a necessary factor.[50] Early work in rabbits with labelled LDL showed hypercholesterolemia did not affect endothelial permeability and that increased lipid accumulation at atheroprone sites was likely due to reduced LDL degradation and increased retention.[58] More recent evidence has shown that early lipid accumulation also involves intimal myeloid cells that are capable of internalizing lipids prior to the onset of immune cell infiltration.[42,59,60] Together, clinical evidence of atherosclerosis risk factors and mechanistic studies regarding subendothelial lipid accumulation have led to strong support for the 'response to retention' model of atherogenesis.[49,50]

It should also be noted that modifications of circulating and retained LDL are also thought to contribute to the development of atherosclerosis by generating immunogenic neoepitopes. For example, endogenous reactive oxygen species and immune cell associated enzymes, such as myeloperoxidase, can mediate oxidative damage of LDL.[7,61] Oxidized LDL contain neoepitopes that share molecular mimicry with conserved pathogen associated molecular patterns and are recognized by a number of innate immune receptors.[62] Therefore, recognition of oxidized LDL by innate immune receptors can lead to endothelial activation, pro-inflammatory responses (TLR4), or receptor-mediated phagocytosis (CD36, MSR-1), and foam cell formation which can all contribute to atherogenesis.[61]

Endothelial Dysfunction

Initially, the 'response to injury' model proposed by Ross and colleagues postulated that extensive damage and loss of the endothelium was the major initiating event in atherosclerosis.[51,52] However, clinical histology samples were observed to show intact endothelium overlaying plaques which contradicted this model and led to a gradual shift in focus to endothelial function and dysfunction.[53–55] In particular, it was observed that atheroprone regions are often in areas of disturbed blood flow or low shear stress which prompted investigation into the impact of fluid dynamics on endothelial activation and dysfunction. Several *in vitro* studies have used models that can mimic blood flow patterns over cultured cells and have shown that laminar, turbulent, and pulsatile flow can lead to differential morphological and functional

changes in cultured endothelial cells which mimic *in vivo* phenotypes. In particular, atheroprone regions with turbulent flow or low shear stress are observed to have increased expression of pro-inflammatory cytokines including MCP-1, IL-1, IFNγ, and TNFα, as well as increased expression of adhesion receptors such as VCAM-1 and ICAM-1 compared to regions with high shear stress and laminar flow.[63,64] Furthermore, laminar flow was associated with expression of athero-protective genes including endothelial nitric oxide synthase (eNOS), superoxide dismutase (SOD) and inducible cyclo-oxygenase (COX-2) which exert anti-oxidative, anti-inflammatory, and anti-adhesion effects on endothelial cells.[55,64] Interestingly, exposure to other risk factors associated with atherosclerosis including LDL and cigarette smoke are observed to induce similar effects on endothelial cell activation and dysfunction.[65–69] Therefore, initiating events in atherogenesis likely also include endothelial cell activation and dysfunction characterized by increased expression of adhesion receptors and inflammatory cytokines, and decreased expression of antioxidative enzymes in atheroprone regions of the aorta.[55]

1.2.3.4 Early Atherogenesis

Intimal lipid accumulation

The formation of early atherosclerotic lesions is characterized by the accumulation of lipid-laden foam cells within the intima of the aorta in atherosclerosis-prone regions. Initially it was thought that these foam cells were exclusively derived from infiltrating monocytes; however, recent work suggests the involvement of resident

myeloid cells. Specifically, myeloid cells already present within the intima of the aorta are capable of recognizing and internalizing lipids, leading to the early accumulation of lipid-laden foam cells prior to monocyte recruitment.[42,59,60] In one study, $CD11c^{+}$ intimal cells were shown to internalize lipids prior to monocyte recruitment, and depletion of these cells using a transgenic inducible knockout model lead to significantly reduced intimal lipid accumulation.[59] A more recent study using sophisticated fate-mapping techniques demonstrated that these intimal myeloid cells are likely macrophages and named them aortic intimal resident macrophages (Mac^{AIR}). The authors show that Mac^{AIR} cells are present in healthy aortas and begin accumulating lipids under hyperlipidemic conditions prior to monocyte recruitment, in accordance with data from earlier studies.[42] This initially accumulation of lipids within intimal myeloid cells then leads to foam cell formation, inflammation, and monocyte recruitment.

Foam cell formation

Macrophages are one of the main immune cells involved in the response to excess lipids and are fundamental to the development of atherosclerosis.[60,70–72] In addition to intrinsic phagocytic ability, macrophages have several pattern recognition receptors capable of recognizing and mediating the uptake of oxidized lipids including MSR1, MARCO, and CD36, resulting in efficient uptake of excess cholesterol and damaged lipids. Normally, in response to lipid uptake, macrophages can activate pathways involved in lipid efflux including increasing the expression

of ATP-binding cassette transporters such as ABCA1 and ABCG1. Processed lipids can then undergo efflux from within the macrophage through ABCA1 or ABCG1 to extracellular apolipoprotein AI-containing HDL.[73,74] HDL can then transport these lipids to the liver to be recycled or secreted in the bile. However, in the context of hyperlipidemia, this homeostatic process is overwhelmed, and cholesterol intake exceeds efflux capacity. This leads to intracellular free cholesterol getting converted to cholesteryl ester which forms the cytosolic lipid droplets that characterize foam cell morphology.[72] Moreover, ineffective efflux of lipids or their intracellular crystallization can trigger production of inflammatory cytokines, such as IL-1β, via NLRP3 activation.[75–78] Thus hyperlipidemia and dysregulated lipid processing contribute to formation of lipid-laden foam cells which accumulate in the artery over time and form a major component of atherosclerotic plaques.[70]

Monocytosis and Recruitment

Early atherosclerosis development relies on the recruitment of Ly6C^{hi} monocytes from the circulation into athero-susceptible regions of the aorta.[8,79] Hyperlipidemia can induce monocytosis and is particularly associated with increased circulating levels of classical Ly6C^{hi} monocytes which correlate with disease severity.[80,81] The process of monocyte recruitment involves many receptor ligand interactions and is not fully dependent on a single interaction. Leukocyte adherence at atheroprone sites is primarily mediated by VCAM-1, as well as selectins and ICAM-1, which are expressed on activated endothelium and capable of binding VLA-4 and LFA-1

on monocytes.[82–85] After adherence, monocytes are able to undergo extravasation into the aortic tissue and enter the intimal space. Monocytes also express CCR2, CCR5, and CX_3CR1, allowing them to migrate along the chemotactic trails of their cognate ligands including CCL2 (MCP-1), CCL3 (MIP1α), CCL4 (MIP1β), and CX_3CL1 which are increased in atherosclerosis.[61,82,84,86] It should be noted that CCR2 appears to predominantly affect monocyte mobilization from the bone marrow whereas CCR5 and CX_3CR1 are directly involved in recruiting monocytes to atherosclerotic plaques.[87,88] Recruited immune cells and the activated endothelium produce many additional inflammatory mediators including IL-1α, IL-1β, IL-6, and TNFα, leading to continued leukocyte recruitment, endothelial cell activation, and chronic low-grade inflammation.[70,80,89] Once in the tissue, recruited $Ly6C^{hi}$ monocytes can differentiate into macrophages and contribute to foam cell formation and early plaque growth.[90]

1.2.3.5 Advanced Atherogenesis

Over time, atherosclerotic plaques can grow in size and complexity. Although early plaque growth is dependent on continual monocyte infiltration, macrophage burden in established plaques is predominantly maintained through local macrophage proliferation.[79,88] Other immune cells are also recruited to the atherosclerotic lesion including neutrophils, T cells, and B cells.[6] However, accumulated cells are ineffectively cleared from the atherosclerotic plaque, which contributes to

accumulation of dead cells and the formation of a necrotic core in advanced lesions.[91]

Vascular smooth muscle cells of the media also begin to migrate into the atherosclerotic plaque where they mediate a number of different functions. Initially, it was thought that smooth muscles cells were primarily athero-protective as they contribute to formation of a fibrous cap and production of extracellular matrix proteins which help stabilize the plaque, separate it from the lumen, and prevent rupture.[44,46,92] However, more recent work utilizing *in vivo* lineage tracing of smooth muscle cells has shown that these cells are more versatile than initially thought. In particular, it appears that smooth muscle cells can undergo 'phenotypic switching' characterized by decreased expression of smooth muscle associated markers such as myosin heavy chain (MYH11) and actin (ACTA2) and upregulation of macrophage associated markers including F4/80, CD68, and CD11b.[93,94] This suggests that vascular smooth muscle cells may be partly contributing to features of atherosclerosis previously attributed to macrophages alone such as foam cell formation and calcification.[44,93–96] Vascular calcification involves mineral deposition reminiscent of bone and cartilage formation and is sometimes referred to as osteogenesis or ossification of arterial tissue.[97] This process contributes to the hardening of aortic tissue characteristic of advanced atherosclerosis.[98,99] Initially, calcification was attributed to macrophages, but more recently has been attributed to osteoclast-like and chondrocyte-like cells that appear to be derived from vascular smooth muscle cells.[44,94–96] Thus, vascular smooth

muscle cells are implicated in both athero-protective and pathogenic functions in advanced lesions.

Overall, atherosclerotic plaques grow in size and complexity over time with advanced plaques containing increased immune cells, vascular smooth muscle cells, fibrous caps, necrotic cores, and/or calcification.

1.2.3.6 Rupture and Thrombosis

Some atherosclerotic plaques can proceed to rupture and thrombosis which is often the underlying cause of acute cardiovascular events such as myocardial infarction and stroke.[46,60,100,101] Some features that are associated with a non-stable or vulnerable plaque include a thin or damaged fibrous cap, a large necrotic core, and/or increased accumulation of macrophages, particularly in close proximity to the fibrous cap or shoulder region.[101] Thinning of the fibrous cap is thought to be mediated by increased expression of proteases by plaque macrophages and other immune cells, as well as decreased matrix production by smooth muscle cells.[46,94,100,102] Eventually, this progressive damage to the fibrous cap can lead to plaque rupture and the release of plaque contents, including thrombogenic factors, which cause the formation of blood clots.[101] Finally, it is the occlusion of arteries by blood clots that often leads to acute cardiac events such as myocardial infarction or strokes which are frequently associated with morbidity and mortality.

1.2.4 MACROPHAGE POPULATIONS AND FUNCTION

Macrophages are highly versatile cells found in most major organs with widely varied functions in both homeostasis and disease. To better understand these complex cells, several studies have been dedicated to uncovering factors that influence macrophage heterogeneity and function and have identified key factors including ontogeny and tissue microenvironment.[103–105] With the complexity of atherosclerosis and dynamic plaque environment, characterizing macrophage subtypes and functions has proven challenging. However, recent advances in single cell technologies and *in vivo* lineage tracing capabilities have contributed to an increased understanding of the diversity of these versatile cells and provides insight into potential functions.

1.2.4.1 Traditional and Novel Approaches to Macrophage Classification

Historically, macrophages were broadly categorized as classically activated pro-inflammatory "M1" or alternately activated pro-resolving or reparative "M2" macrophages based on *in vitro* phenotypes. M1 macrophages were characterized by increased expression of inflammatory cytokines including IL-1β, IL-6, and TNFα whereas M2 macrophages were characterized by increased expression of IL-4 and IL-10, in addition to differential expression of cell surface receptors and transcription factors. In atherosclerosis M1 macrophages were described to co-localize with the rupture-prone shoulder region of plaques compared to M2 macrophages which were localized to the adventitia and areas of

neovascularization.[106] However, this same study also identified the presence of ambiguous macrophage populations, including macrophage foam cells that expressed both M1 and M2 markers.[106] It became clear that not all macrophages fit into this dichotomous model and additional subsets were proposed including macrophages with a redox-regulatory gene expression profile (Mox) that form in response to oxidized lipids.[107] However, the reliance on predefined markers, often with overlapping expression, resulted in difficulty identifying distinct macrophage subsets *in vivo* in a useful or meaningful way.[72,108]

More recently, it has been proposed that classifying macrophages based on functional phenotypes may provide a better foundation to build further investigation and understanding of these heterogenous cells.[108] Recent advances in single cell RNA sequencing (scRNA-seq) has allowed for the unbiased assessment of whole transcriptome expression at an individual cell level, facilitating identification of cell clusters with similar expression profiles. This approach allows for identification of populations of cells that likely share similar functions without relying on a narrow set of predefined genes or markers. Similarly, protein expression-based techniques like mass cytometry by time of flight (CyTOF) has allowed for expanded panels of cell identifying markers compared to traditional flow cytometry leading to increased resolution of complex populations like macrophages. The combination of scRNA-seq and CyTOF data has provided enhanced resolution resulting in the identification of discrete macrophage subsets with potentially distinct functional roles in atherosclerosis. A recent meta-analysis of nine scRNA-seq datasets and two

mass cytometry datasets in both *Apoe*$^{-/-}$ and *Ldlr*$^{-/-}$ mouse models has identified five macrophage subtypes present in atherosclerotic aortas.[109] These populations include resident macrophages, inflammatory macrophages, interferon (IFN)-inducible macrophages, Trem2 (triggering receptor expressed on myeloid cells-2) foamy macrophages, and cavity macrophages. This meta-analysis also confirmed that leukocyte diversity increases in the context of hyperlipidemia and decreases with plaque regression or reversal of hyperlipidemia.[110,111]

1.2.4.2 Resident Macrophages

Resident macrophages are the predominant macrophage population residing in healthy aortas, but can also be found at decreased levels in atherosclerotic aortas.[109,112] These macrophages have low pro-inflammatory gene expression and express markers such as *Lyve1* and *Mrc1* which are associated with yolk-sac and embryonic precursor-derived tissue resident macrophages.[112] Within resident like macrophages are a subset of CCR2^{hi} LYVE1^{lo} cells, which may be monocyte-derived macrophages that adopt a resident cell like phenotype.[112,113] Resident arterial macrophages typically populate the adventitia and, although resident macrophages are detected in atherosclerotic tissue, it is difficult to determine whether these cells are within the atherosclerotic plaques or in the adventitial tissue.[43,112] In general, tissue resident macrophages are thought to play a role in maintaining homeostasis and are decreased or dysregulated in the context of injury or disease.

1.2.4.3 Trem2 Foamy Macrophages

Although foam cells are not exclusive to atherosclerosis or macrophages, lipid-laden macrophage foam cells are well-known as the characteristic immune cell in atherosclerotic plaques. These cells are not typically observed in healthy aortic tissue but are quickly detected in early atherogenesis and were initially thought to significantly contribute to local inflammation in addition to lipid uptake.[75,77,112] Insight into potential functions of foamy macrophages has been provided by scRNA-seq analyses which identify high expression levels of Trem2 and CD11c (*Itgax*) in addition to genes associated with lipid uptake, processing, and transport including *Abca1, Cd36, Msr1,* and *Lipa* in these cells.[112,114] Furthermore, an elegant experimental approach by Kim *et al*., used a lipid-specific fluorescent dye to sort macrophage foam cells from non-foamy cells and allowed for generation of differential gene expression profiles in each population. This allowed the authors to specifically compare transcriptomic profiles of lipid positive versus negative macrophages isolated from atherosclerotic aortas and provided insight into the potential functions of each population. Notably, this study demonstrated that macrophage foam cells express high levels of protease genes including *Mmp12, Mmp14, Ctsd,* and *Ctsl,* but have low expression of proinflammatory mediators including *Il1b* and *Cxcl2*. This surprising observation was confirmed in a separate scRNA-seq study and in a meta-analysis of all currently available atherosclerosis scRNA-seq and CyTOF datasets.[109,112,114] Previously, macrophage foam cells were thought to contribute to arterial plaque inflammation, but these recent findings

suggest that foam cells are predominantly involved in processing lipids with a separate population of macrophages involved in driving inflammation.

1.2.4.4 Inflammatory Macrophages

Inflammatory macrophages,also called chemokine^{high} macrophages, are not found in healthy aortic tissue. As the name suggests, these macrophages are characterized by increased expression of pro-inflammatory cytokines and chemokines including IL-1β, IL-6, and TNFα, and exhibit upregulation of pathways associated with chemokine signalling and response. This population also expresses CCR2 suggesting that they may be monocyte-derived. Of particular interest is that these inflammatory cytokines have been distinctly identified as non-foamy macrophages.[110,112,114] These findings challenge previous pathogenesis models that propose foamy macrophages as key sources of inflammatory cytokines and suggest a smaller, non-foamy macrophage population may be driving inflammatory processes in atherosclerotic plaques.

1.2.4.5 Interferon (IFN)-inducible Macrophages

IFN-inducible macrophages express high levels of IFN-inducible genes such as *Irf7* and *Isg15*, and exhibit upregulated pathways associated with anti-viral defense responses. The detection of this smaller population is variable between studies but is normally observed in studies with a larger amount of cells and in higher powered meta-analyses.[109,110,114] Interestingly, these cells are detected in both steady state and after ischemic injury, so it is still unclear whether they play a homeostatic or

disease-driving role. However, the general increase in pro-inflammatory-associated genes suggests potential contribution to disease progression in atherosclerosis.[109,113]

1.2.4.6 Cavity Macrophages

Cavity macrophages make up the smallest cluster of macrophages identified in atherosclerotic aortas. In fact, this cluster is so small it was only revealed through meta-analysis of pooled scRNA-seq data of atherosclerotic aortas, including data from *Apoe*$^{-/-}$, *Ldlr*$^{-/-}$, and PCSK9-augmented models. This macrophage subpopulation exhibits a gene expression profile similar to macrophages found in peritoneal and pleural cavities; however, their function and origin in aortic tissue is unclear.[109]

1.2.4.7 Protein-based Evidence of Macrophage Heterogeneity

Although scRNA-seq is a powerful tool allowing for a broad and unbiased approach to identifying cell populations, it should also be acknowledged that gene expression does not always translate to differential protein expression or function. Thus, experimental approaches based on differential protein expression or *in vivo* cell tracking are important complementary analyses to identify distinct macrophage populations and their potential impact on disease progression. CyTOF analysis is a particularly strong technique for resolving heterogenous cell populations given its ability to generate higher dimensional protein expression data at the single cell level compared to traditional fluorescence-based flow cytometry. CyTOF datasets generated to date typically show a different number of immune cell clusters

compared to scRNA-seq analysis.[109,111,115] This may be due to a number of factors including the fact that some cell cluster formations in scRNA-seq datasets can be driven by upregulated genes that have insufficient or poorly detected protein expression. Alternatively, scRNA-seq analysis may not be able to separate cell populations that have overlapping functions and are primarily distinguished by a few differentially expressed key proteins.[109,111] However, data comparisons between the different techniques have provided stronger evidence for the presence of specific macrophage subsets in atherosclerotic aortas.

Currently, there are no set panels that can be used to definitively differentiate scRNA-seq-based macrophage populations by CyTOF. This is not surprising given the high dimensionality of transcriptomic data compared to protein-based technologies. Nonetheless, two studies using CyTOF to assess myeloid cells in atherosclerotic aortas were able to identify 3-4 macrophage clusters using panels of 33-35 protein targets.[111,115] An additional study using transgenic fluorescent reporter genes to differentially label CX_3CR1^+ cells and $CD11c^+$ cells in *Apoe*$^{-/-}$ mice also identified 4 macrophage populations *in vivo* with unique transcriptomic profiles.[116] When these datasets were compared to each other and to scRNA-seq datasets, it became apparent that three of these macrophage populations likely correspond to resident macrophages, Trem2 foamy macrophages, and inflammatory macrophages.[109] Resident macrophages were observed to express CX_3CR1, CD206, CD169, Lyve1, and TimD4 in addition to the commonly used macrophage markers CD64 and CD11b. Trem2 foamy macrophages, on the other

hand, exhibited high expression of CD11c with low expression of resident cell markers CD206 and CD169. Inflammatory macrophages mapped less clearly to CyTOF- or reporter gene-defined populations but the putative cluster expresses high levels of CCR2, which may indicate a monocyte-derived population.[109,111,115,116]

1.2.4.8 Summary

Overall, CyTOF and scRNA-seq data provide novel tools to address the ever-evolving question of macrophage heterogeneity and function in atherogenesis, with a focus on identifying distinct populations. To date, these two approaches have confirmed previous observations of increased myeloid cells in the context of hyperlipidemia, and further reveal an increase in overall myeloid cell heterogeneity.[81,109] Key macrophage populations currently identified include resident macrophages, which are decreased in atherosclerosis, and Trem2 foamy macrophages and inflammatory macrophages, which are increased and likely involved with disease progression.

1.2.5 MACROPHAGE ONTOGENY AND KINETICS

1.2.5.1 Arterial Macrophage Ontogeny

In vivo Fate-mapping

With increased appreciation for macrophage heterogeneity, the interest in the influence of both tissue environment and ontogeny on macrophage function and survival during homeostasis and in response to stress has also increased. Impressive

advances in genetic engineering technologies have led to the development of transgenic mice with inducible reporter genes under the control of specific promoters allowing for *in vivo* labelling of target cells and their progeny at defined points in development. For example, embryonic macrophages express the fractalkine receptor CX_3CR1, so a tamoxifen-inducible Cre-Lox system under the control of the *Cx3cr1* promoter can be used to fate-map these cells *in vivo*. Briefly, mice engineered to express tamoxifen-inducible Cre-recombinase under the control of the *Cx3cr1* promoter are crossed with mice containing the constitutively and ubiquitously expressed ROSA26 locus with an inserted stop codon flanked by *loxP* sequences upstream of a gene encoding the Enhanced Yellow Fluorescent Protein (EYFP) reporter gene. When these mice receive tamoxifen-containing diet, expression of the Cre recombinase protein is activated in cells expressing *Cx3cr1* and allows for excision of the *loxP*-flanked stop codon in the ROSA26 locus resulting in permanent EYFP expression in all CX_3CR1^+ cells and their progeny.[104] By inducing reporter gene expression at specific developmental periods and tracking labelled cells *in vivo*, this approach has allowed for fate-mapping of embryonically-derived macrophages in various tissues.

Tissue Macrophage Ontogeny

In general, it has been observed in mouse models that macrophage colonization of tissues typically occurs in three waves over the course of development.[105] The first wave consists of yolk sac derived macrophages and occurs around day 8.5 of

embryogenesis.[117,118] The second wave consists of fetal liver monocytes between embryonic days 10.5 – 16.5.[118] Although fetal liver monocytes are initially derived from yolk sac progenitor cells, unlike yolk sac derived macrophages, fetal liver derived monocytes express c-Myb which is critical for hematopoiesis in the fetal liver.[119,120] This second wave of macrophages replaces most yolk sac derived macrophages in tissues, with the brain being a notable exception.[119] The third wave occurs postnatally when hematopoiesis shifts to the bone marrow as observed in mature mice. However, the contribution of this wave of bone marrow derived macrophages differs between tissue compartments. Some tissues, like the brain, remain mostly independent of monocyte-derived macrophages, whereas tissues like the intestines require frequent monocyte input to maintain macrophage populations throughout adult life.[105,118,121]

Arterial Macrophage Ontogeny

To determine the origins of aortic macrophages during homeostasis and in response to acute inflammation and resolution, Ensan *et al.*, used multiple fate-mapping and *in vivo* cell tracking techniques.[43] The results of this study demonstrated that aortic macrophages can arise from yolk sac derived erythroid-myeloid progenitor cells during embryogenesis (both yolk sac derived and fetal liver derived) followed by a brief period of monocyte recruitment postnatally. Therefore, adult aortas contain both embryonic and bone marrow-derived macrophages. Arterial macrophages in healthy tissues predominantly reside in the adventitia and express Lyve-1,

consistent with other resident macrophage populations. Notably, macrophage turnover in aortic tissue is dynamic and, under homeostatic conditions, is maintained primarily through self-renewal via proliferation.[43] Overall, aortic macrophages in healthy tissue arise from embryonic and postnatal precursors, and are largely maintained independently of blood monocytes under homeostatic conditions.

1.2.5.2 Monocyte Recruitment

Early atherosclerosis is characterized by the accumulation of lipids and leukocytes in the arterial wall. As such, the trafficking of key immune cells into the tissue plays a crucial role in disease progression. Hypercholesterolemia is a causative risk factor for atherosclerosis and is associated with monocytosis. Specifically, an increase in classical Ly6C^{hi} monocytes which is the combined result of increased survival, proliferation, and reduced conversion to Ly6C^{lo} monocytes in the context of hyperlipidemia.[90] Circulating Ly6C^{hi} monocytes are recruited to athero-susceptible regions by adherence to activated endothelial cells and extravasation into the subendothelial space along chemotactic trails. This process of monocyte recruitment is critical for early plaque growth and can occur through multiple receptor ligand interactions including VCAM-1 and VLA-4 as well as ICAM-1 and LFA-1 for adhesion and CCR2 (CCL2/MCP-1), CCR5 (MIP-1α and β), and CX_3CR1 (CX_3CL1) for chemotactic migration.[81–86] VCAM-1 in particular has been shown to be a major contributor to monocyte recruitment in the context of

atherosclerosis compared to other endothelial adhesion receptors.[85] Notably, VCAM-1 expression on endothelial cells is also upregulated following exposure to multiple atherosclerosis risk factors including turbulent flow, modified LDL, and cigarette smoke.[63,66–69] Overall, monocytes are increased in the context of hyperlipidemia and their recruitment to atheroprone regions of the aorta is critical for early plaque development and involves multiple receptor-ligand interactions.

1.2.5.3 Proliferation

The role of self-renewal or local proliferation in maintaining tissue macrophage populations in the aorta during homeostasis and aortic disease has been increasingly highlighted in recent years. One study by Williams *et al*., found that intimal myeloid cells, which have been implicated in early atherogenesis, are likely specialized macrophages which the authors termed aortic intimal resident macrophages (Mac^{AIR}).[42,59,60] This study showed that Mac^{AIR} cells begin to take up lipids prior to monocyte recruitment, which is in accordance with earlier observations of intimal myeloid cells. This study also paired lineage-tracing with parabiosis models and found Mac^{AIR} cells are self-renewed through proliferation under homeostasis, but are replaced by monocyte-derived macrophages that adopt gene expression profiles similar to Mac^{AIR} cells in the context of atherosclerosis.[42] This is similar to observations by Ensan *et al.*, who report self-renewal of aortic macrophages under homeostasis but monocyte infiltration during polymicrobial-induced acute inflammation.[43] In the context of atherosclerosis development, earlier work by

Robbins *et al.*, showed that, although monocyte recruitment is critical for early plaque formation, macrophage burden in established plaques is predominantly maintained through local proliferation. This was shown through an elegant set of experiments including tracing *in vivo* bromodeoxyuridine (BrdU) incorporation into newly proliferated cells and signal decay over several weeks within aortic macrophages, as well as parabiotic models.[79] Thus proliferation is a key kinetic parameter that contributes to macrophage maintenance and dynamic responses during homeostasis and disease.

1.2.5.4 Survival

Cell survival is another important factor that affects the accumulation or depletion of macrophages within the tissue. In the case of aortic macrophages, CX_3CR1 plays an important role in cell survival. Arterial macrophages mostly retain CX_3CR1 expression, unlike many other tissue resident macrophage populations and interference with the CX_3CR1-CX_3CL1 axis results in significant depletion of arterial macrophages.[43,104] Specifically, CX_3CR1 inhibition and knock-out didn't affect proliferation, but did increase positive TUNEL staining in macrophages populating the arterial adventitia. This data suggests the reduction in macrophages following CX_3CR1 interference was due to increased cell death rather than decreased proliferative capacity.[43] Notably, although survival of tissue-resident arterial macrophages occurs in a CX_3CR1-dependent manner, the residual presence

of a small population of macrophages in *cx3cr1*$^{-/-}$ mice suggests other pathways are also involved in arterial macrophage survival.[43]

1.2.5.5 Death

Another major factor affecting the accumulation of macrophages in aortic tissue is cell death. In early atherogenesis, macrophage apoptosis can help limit plaque development and multiple studies have shown that inhibiting apoptosis can increase atherosclerotic lesions.[122] For example, transplantation of bone marrow derived cells deficient in the proapoptotic Bcl-2 associated X protein (Bax) into *Ldlr*$^{-/-}$ mice resulted in increased atherosclerosis.[123] This provides evidence that that apoptosis in hematopoietic cells contributes to limiting plaque size in the context of atherosclerosis. Similarly, promoting atherosclerosis by knocking out the apoptosis inhibitor expressed by macrophages protein (AIM, alternatively Spα or Api6) in *Ldlr*$^{-/-}$ mice resulted in reduced atherosclerotic lesions.[124] Since AIM is involved in promoting macrophage survival by inhibiting apoptosis, the loss of this protein increases apoptosis and subsequently leads to reduced plaque formation. Boesten *et al*., used a Cre-loxP system to knock out the proapoptotic p53 gene (tumor suppressor p53) in macrophages in early and established atherosclerosis. As expected, this resulted in reduced apoptosis and increased macrophage content in early and advanced lesions. Interestingly, p53 loss in established atherosclerosis also lead to larger necrotic cores suggesting that apoptosis normally contributes to reducing necrotic core formation.[125] This is understandable given that controlled

cell death via apoptosis can facilitate formation of membrane-bound apoptotic blebs that can be cleared by phagocytic cells, and protect against necrotic cell death. Thus, controlled cell death in macrophages is an important factor that impacts the dynamic accumulation of cells in early and late atherosclerosis.

1.2.5.6 Egress

Egress or migration of cells out of atherosclerotic plaques can also impact macrophage accumulation; however, it should be noted that macrophage egress is not readily observed in most mouse models of atherosclerosis. One model where egress is observed used aortic tissue transplantation wherein segments of atherosclerotic aortas are transplanted into either hypercholesterolemic mice, like *Apoe*$^{-/-}$, or normocholesterolemic mice, like C57BL/6. Transplantation into hypercholesterolemic mice is used as a model of plaque progression whereas transplantation into normocholesterolemic mice is used as a model of plaque regression.[126] To assess macrophage egress, transplantation was performed in a model where donor and recipient mice were congenic and expressed either CD45.1 or CD45.2 which allowed cells from transplanted tissues to be tracked *in vivo*.[127] In the regression model where hypercholesteremia is rapidly and significantly lowered, macrophage egress can be observed. This egress seems to at least partly involve the CCR7 ligands CCL19 and CCL21, as inhibition of these ligands prevents plaque regression in the transplant model.[128]

One notable study that did not use the transplant model, identified factors involved in macrophage retention that normally inhibits egress. The authors showed that a secreted protein, netrin-1 and the netrin receptor, UNC5b, are increased under hypercholesterolemic conditions *in vivo*. Interestingly, bone marrow derived cells deficient in netrin-1 transplanted into *Ldlr*$^{-/-}$ mice result in significantly less atherosclerosis. By using *in vivo* tracking of bead-labelled cells, van Gils *et al*., were able to show this reduction in atherosclerosis was through an increase in macrophage egress, indicating that netrin-1 promotes macrophage retention in atherosclerotic plaques.[129] Together, these studies provide strong evidence that macrophage egress, or lack thereof, impacts the accumulation of macrophages in aortic tissue during atherogenesis.

1.2.5.7 Significance of Macrophage Ontogeny and Kinetics

Understanding macrophage origin and dynamics can facilitate a deeper understanding of how different populations of macrophages behave under homeostatic and disease conditions. Importantly, this may help better delineate protective versus pathogenic functions in macrophages and their differential contributions over the course of disease development. To date, several lines of evidence suggest that tissue resident macrophages are depleted under acute stress and replaced by monocyte-derived macrophages which exhibit increased pro-inflammatory responses. Following resolution of inflammation, the kinetics of how resident macrophage populations recover can vary based on tissue and injury.

Importantly, the origin of the cells that repopulate the tissue macrophage pool may impact subsequent functional capabilities and secondary responses to stress.

Cardiac Macrophages in Ischemic Injury

The impact of ontogeny on function is clearer in some instances such as in models of cardiac injury. In this case, embryonic-derived resident cells are observed to promote tissue repair through cardiomyocyte proliferation and angiogenesis, whereas monocyte-derived macrophages are observed to infiltrate the tissue following injury and drive proinflammatory responses.[130] Interestingly, using sophisticated fate-mapping and single-cell technologies, Dick *et al.*, demonstrated that following ischemic injury recruited monocytes differentiate into multiple distinct macrophage subsets. One of these subsets appears to adopt nearly identical transcriptional and surface marker profiles as self-renewing resident cardiac macrophages. However, functionally, these cells were not as effective at cardioprotective functions as authentic resident macrophages resulting in impaired cardiac function and increased adverse remodelling following injury. This provides compelling evidence that ontogeny can impact macrophage function during challenge regardless of phenotypic presentation under homeostatic tissue environment.[113]

Arterial Macrophages in Sepsis

Alternatively ontogeny may have minimal impact on function, but may significantly impact another factor, such as survival, thus influencing key

population kinetics both during inflammation and following resolution.[105] For example, arterial macrophages are maintained locally through proliferation during homeostasis and, although their homeostatic function is not well described, are thought to involve phagocytosis and maintenance of tissue integrity.[43,105] However, during sepsis they are transiently depleted with a concomitant increase in recruited monocytes and monocyte-derived macrophages. Interestingly, recruited monocyte-derived macrophages appear to display greater *in vivo* phagocytosis of bacteria compared to resident macrophages suggesting these cells may respond more effectively during microbial exposure.[43] Following resolution of inflammation, resident macrophages were restored through proliferation, rather than replacement by monocyte-derived macrophages. This restored population of arterial macrophages displayed comparable self-renewal, phagocytic capacity, and transcriptomic profiles, suggesting a return to normal functional homeostasis after challenge.[43] Interestingly, similar kinetics are also observed with lung macrophages, with restoration of depleted resident macrophages mediated through self-proliferation independent of circulating monocytes.[131] Thus it appears in the context of acute microbial challenge, monocyte-derived macrophages respond rapidly and play a critical role in host defense with recovery of the resident macrophage population mediated by self-renewal following resolution.

Summary

Both cardiac and arterial resident macrophage populations are depleted and replaced by monocyte-derived macrophages in the context of acute injury and inflammation. Interestingly, monocyte-derived macrophages appear to partially replace embryonically derived resident cardiac macrophages following resolution of ischemic injury, but exhibit reduced protective functionality. Conversely, arterial resident macrophages exhibit intact self-renewal capacity following transient depletion during sepsis and are able to repopulate the tissue without continued monocyte influx. In both scenarios, macrophage ontogeny impacted population function and kinetics and have facilitated a more nuanced understanding of tissue responses to injury and recovery.

1.3 AORTIC ANEURYSM

1.3.1 CLINICAL OVERVIEW

Abdominal aortic aneurysms are characterized by the progressive weakening or bulging of the aorta in the abdominal region that becomes prone to rupture when unable to withstand the pressure of blood flow.[132] This increase in diameter can either be a fusiform aneurysm, which involves the entire circumference of the aorta, or a saccular aneurysm, which only involves enlargement on one side of the aorta. Clinically, abdominal aortic aneurysms are defined as a ≥50% increase in diameter (or >3cm), with larger diameters associated with increased risk of rupture. Since size is a predictor of rupture, abdominal aortic aneurysms are often classified based

on the size of aortic dilation where aneurysms <5cm are considered benign but requiring monitoring, and those ≥5cm in women and ≥5.5cm in men as requiring surgical intervention when possible.[132] Given their insidious, asymptomatic nature, aneurysms often go undetected until rupture. Unfortunately, rupture results in severe internal hemorrhaging which is fatal if untreated and has a mortality rate of 50-80% even with emergency surgical intervention.[133–135] Currently, there are no pharmacological therapies for aortic aneurysms so treatment options are limited to screening at-risk populations and surgical repair.[136–139] Part of the difficulty in identifying potential therapeutics is an incomplete understanding of the pathogenesis of abdominal aortic aneurysms which represents a clinically-relevant gap in knowledge.

1.3.2 RISK FACTORS AND TREATMENT

1.3.2.1 Genetic

Abdominal aortic aneurysms have a complex etiology including significant genetic contribution to risk. Male sex is one of the well established genetic risk factors with abdominal aortic aneurysm prevalence in patients over 65 years old being 4-8% in men compared to 1-2% in women.[140,141] Abdominal aneurysms are also more prevalent in individuals with rare genetic disorders, including Marfan syndrome and Ehlers-Danlos syndrome; however, this comprises a small portion of the overall population with aneurysms.[142] More commonly, abdominal aortic aneurysm is associated with a positive family history with complex inheritance patterns

indicating multifactorial etiology.[143–145] Moreover, large scale studies with twins estimate that 70-80% of susceptibility to aneurysm is due to genetic contributions.[146,147] The remaining risk is largely attributed to environmental risk factors and comorbid conditions.

1.3.2.2 Cigarette Smoke

The most significant, non-genetic risk factor for abdominal aortic aneurysm by far is tobacco smoking.[142,148,149] In fact, current smokers are 7-13 times more likely to develop aneurysm compared to non-smokers.[149–151] Current smoking is also associated with faster growth rate as well as increased rupture risk and mortality.[152–155] Although smoking cessation can reduce this risk, former smokers are still 3 times more likely to develop AAA compared to non-smokers.[151] Despite the strong clinical association with smoking, the mechanisms underlying this increased risk remain poorly understood.

1.3.2.3 Atherosclerosis

Although atherosclerosis and AAA are often observed to occur in the same patient, no shared mechanistic relationship has been unambiguously defined for both diseases.[142,156–158] One theory is that atherosclerosis and AAA are independent pathologies that occur concurrently as a result of shared risk factors.[158,159] Although it should be noted that the contribution of some of these shared risk factors may differ between both diseases, as well as the existence of opposing risk factors. For example, male sex and smoking are much more dominant risk factors for abdominal

aortic aneurysms than for atherosclerosis, whereas hyperlipidemia is a critical risk factor for atherosclerosis but weakly associated with AAA.[148,155,160] One of the most frequently cited examples of divergent mechanisms of pathology for atherosclerosis and abdominal aortic aneurysms is the contrasting association with diabetes mellitus. Whereas diabetes is associated with a significantly increased risk of atherosclerosis, aneurysm incidence amongst diabetic patients is lower than the general population.[155,161] This clinical evidence, in addition to the fact that atherosclerosis is not observed in all aneurysm patients, provides compelling evidence that these are two distinct aortic diseases that are not causally linked.[142,157]

The second theory is that inflammatory processes within atherosclerotic plaques may promote aneurysm formation at the abdominal aorta, or vice versa.[162] This is plausible given that both diseases are associated with leukocyte infiltration and inflammation of arterial tissue. However, the localization of this inflammation is slightly different with atherosclerosis primarily involving the intimal layer and aneurysms predominantly involving the medial and adventitial layers.[71,142,163–165] Although it has been proposed that atherosclerosis may promote aneurysm formation, this paradigm has not been adequately addressed experimentally to the best of our knowledge.

Since there is evidence to support and refute both theories, this question remains controversial and represents a significant gap in knowledge. Part of the difficulty in investigating the potential interplay of atherosclerosis and abdominal

aortic aneurysm is the lack of a suitable animal model that engages clinically relevant risk factors that recapitulate key disease pathologies.

1.3.3 PATHOGENESIS

1.3.3.1 Arterial Anatomy

The abdominal aorta is the region of aorta below the diaphragm and is responsible for supplying oxygenated blood to tissues of the abdomen. The formation of abdominal aortic aneurysms involves dilation of all layers of the vascular wall which differentiates it from pseudoaneurysms or aortic dissections. Aortic dissection normally involves intimal tearing and blood accumulation in the vessel wall resulting in secondary dilatation of the external layer of the aorta, rather than the medial thinning and degeneration underlying true aneurysm formation.[142] The major features of abdominal aneurysm, typically observed using histological analysis, include medial degeneration characterized by extracellular matrix degradation and vascular smooth muscle cell apoptosis, in addition to increased oxidative stress and inflammation.[4,156,166–169] Notably, the abdominal aorta contains less elastic lamellar units compared to other regions of the aorta and shows increased susceptibility to other arterial diseases, which may partially account for the susceptibility of this region to aneurysm formation.[4,170,171]

1.3.3.2 Mouse Models

The three main murine models of abdominal aortic aneurysm currently used require the delivery of elastase, calcium chloride ($CaCl_2$) or phosphate ($Ca_3(PO_4)_2$), or

angiotensin II, in order to induce aneurysm formation. Both elastase and $CaCl_2$/ $Ca_3(PO_4)_2$ delivery models require direct access to the aorta, necessitating invasive surgery that may elicit potentially confounding factors. Although these models recapitulate features of tissue pathology observed clinically, neither elastase nor $CaCl_2$/$Ca_3(PO_4)_2$ represent clinically relevant risk factors for the development of aneurysm. Additionally, the nature of these models involves acute tissue injury followed by a resolution phase which limits the ability to observe extended disease progression. Therefore, both these models may engage mechanisms that poorly model clinical disease and would not provide interventional targets if explored.[172–174] Angiotensin II is also capable of inducing aneurysms when delivered subcutaneously to mice.[175,176] This model uses more clinically relevant stimuli given that it induces hypertension and is primarily used in hypercholesterolemic mice. However, the aneurysms induced in this model differ from clinically observed pathology, including less elastin degradation, aneurysm formation throughout the aorta, and intima tearing preceding aneurysm formation leading to frequent aortic dissection.[142,174,177] Lastly, the formation of aneurysms in all these models is rapid and occurs within hours to days which is in sharp contrast to the gradual progression and late-onset of disease in humans.[142,174] Therefore, the fundamental design of current models of abdominal aortic aneurysm may be contributing to the difficulty in successfully identifying key mechanisms which can be therapeutically targeted.

1.3.3.3 Inflammation and Tissue Damage

Our current understanding of the pathogenesis of AAA is incomplete and primarily relies on histological and molecular assessment of diseased tissue. This approach has established that AAA is characterized by media degeneration, including elastin fragmentation and loss of vascular smooth muscle cells, as well as increased oxidative stress and inflammation. Unfortunately, since clinical samples often represent end-stage disease only, and murine models differ in major features of AAA, the roles and necessity of specific immune cell populations in the pathogenesis of AAA has not yet been unambiguously determined.[4,142,156,174,178]

The predominant immune cells observed within human AAA are macrophages and lymphocytes (mainly $CD4^+$ T cells), followed by neutrophils within medial and adventitial layers of the aorta.[4,178–181] This is similar to observations in angiotensin-II induced aneurysm models which feature monocyte and macrophage recruitment to the adventitia where these cells are implicated in tissue remodelling and inflammation.[163–165] In general, leukocyte infiltration is thought to contribute to aneurysm pathology through the production of pro-inflammatory cytokines (MCP-1, IL-6) and reactive oxygen species. This leads to continual immune cell recruitment, as well as damage to structural proteins and cell membranes, resulting in increased apoptosis of vascular smooth muscle cells and subsequent weakening of the aortic wall.[4,156]

Furthermore, proteolytic activity is increased in abdominal aortic aneurysm and includes matrix metalloproteinases (MMPs-2, 8, 9, and 12) as well as collagenases (cathepsin K, L, and S) produced by macrophages, neutrophils, and vascular smooth muscle cells,.[168,181–183] Increased proteolytic activity in abdominal aneurysms contributes to elastin damage and rapid turnover of the extracellular matrix. This increased turnover is associated with decreased quality of deposited structural proteins which may also contribute to the progressive weakening of the aortic wall.[41,184] Notably, smokers have been shown to have decreased collagen content in the aorta compared to non-smokers which may contribute to the increased susceptibility of smokers to abdominal aortic aneurysms.[185]

Therefore, although the pathology of abdominal aortic aneurysms is complex and incompletely understood, it is currently thought to consist of a local inflammatory response with concurrent proteolytic activity in the media and adventitia, which ultimately results in progressive damage and weakening of the aortic wall and aneurysm formation.[4,156]

1.4 SMOKING AND ARTERIAL DISEASE

1.4.1 CLINICAL EVIDENCE

Despite the significant progress achieved by decades of anti-smoking campaigns and legislation, cigarette smoking remains a significant global issue. In fact, since 1980, the number of global smokers has increased by 250 million people, which is associated with 1 trillion more cigarettes sold per year.[186] Furthermore, in North

America the decline in smoking prevalence has plateaued with approximately 15-30% of the population continuing to smoke.[186,187] Unsurprisingly, cigarette smoking has a significant impact on the health of the consumer and those exposed to second hand smoke, including increased risk of cardiovascular diseases such as atherosclerosis and abdominal aortic aneurysms.[188] In fact, one-third of deaths attributed to cigarette smoking are associated with cardiovascular disease.[188,189] Although the strong link between smoking and increased risk of developing cardiovascular disease is well established, our understanding of the mechanisms underlying this process remains incomplete.

1.4.2 PRE-CLINICAL EVIDENCE

1.4.2.1 *In vitro* Models

Several studies have aimed to understand how cigarette smoke exposure promotes the development of cardiovascular diseases such as atherosclerosis and aneurysm using *in vitro* models of cell culture. These models primarily investigated the impact of smoke-conditioned media on endothelial cell function and leukocyte adhesion to interrogate mechanisms related to leukocyte infiltration and inflammation observed in aortic disease. Cigarette smoke has been shown to increase leukocyte adhesion receptor expression on endothelial cells *in vitro*, including ICAM-1 and VCAM-1.[68,69,190] Smoke exposure *in vitro* has also been shown to promote leukocyte migration and adhesion to endothelial cells in a dose-dependent manner.[67] Of note, a critical mediator of endothelial cell homeostasis is

nitric oxide (NO) which is produced by endothelial nitric oxide synthase (eNOS). NO is a vasoactive mediator that helps maintain arterial tone and can limit inflammation by reducing adhesion receptor expression and inflammatory cytokine production by endothelial cells.[191,192] Cigarette smoke has been shown to contribute to endothelial cell dysfunction by reducing NO bioavailability through eNOS uncoupling, which is a potential mechanism that could contribute to smoking-associated inflammation *in vivo*.[193–195] Overall, *in vitro* data provides evidence that smoking increases endothelial dysfunction and leukocyte adhesion, potentially through disrupting NO mediated pathways, which could contribute to arterial disease development *in vivo*.

1.4.2.2 *In vivo* Models

Few studies have investigated the impact of cigarette smoke on the development of atherosclerosis or aneurysm using *in vivo* mouse models. However, the studies that have been done to date demonstrate that exposure to cigarette smoke or nicotine usually increases atherosclerosis and/or aneurysm *in vivo*, which is consistent with clinical observations. Smoke exposure of elastase models resulted in increased aneurysm size but did not impact overall incidence.[196,197] Two studies showed increased atherosclerosis in smoke exposed *Apoe*$^{-/-}$ mice, but focused on the impact of smoke exposure on tissue lipid profiles.[198,199] Smoke exposure of angiotensin II-treated *Apoe*$^{-/-}$ mice resulted in a non-significant increase in aneurysm formation and increased protease expression.[200] Similarly, another study demonstrated

nicotine infusion induced aneurysm formation in *Apoe*$^{-/-}$ mice and identified mechanisms related to smooth muscle cell-mediated protease activity.[183] However, to the best of our knowledge, no studies to date have investigated the impact of cigarette smoke on monocyte and macrophage function or kinetics *in vivo* in the context of arterial disease pathogenesis. Given the critical role of myeloid cells in atherosclerosis and abdominal aneurysms, in addition to the fact that smoking is an established risk factor for both diseases, this represents an important area of investigation.

1.5 CENTRAL PARADIGM

Cigarette smoking is a well-known risk factor for cardiovascular disease, including arterial pathologies such as atherosclerosis and abdominal aortic aneurysm.[40,188,189] Yet, how exposure to cigarette smoke impacts disease pathogenesis is not well understood. Given that cigarette smoke has been shown to mediate significant and complex effects on immune cell function, and the known critical role of myeloid cells in atherosclerosis and aneurysm, this represents a significant gap in knowledge. Consequently, this thesis focuses on understanding the development of atherosclerosis and aortic aneurysms in a mouse model of cigarette smoke exposure and hypercholesterolemia. Since monocytes and macrophages are key immune cells for both arterial pathologies, this project specifically focuses on understanding the function and kinetics of these cells during arterial disease progression over the course of cigarette smoke exposure.

1.5.1 RESEARCH OBJECTIVES

Research Focus

In this study, we aim to use a mouse model that engages the clinically relevant risk factors of cigarette smoke and hyperlipidemia to investigate the development of arterial pathologies with a focus on understanding monocyte and macrophage function and kinetics.

Central Hypothesis

We hypothesize that cigarette smoke exposure will lead to increased development of atherosclerosis and aortic aneurysm characterized by greater accumulation of inflammatory and proteolytic arterial macrophage subsets through increased local macrophage proliferation and monocyte recruitment.

Specific Objectives

Using a mouse model of hypercholesterolemia and cigarette smoke exposure, we aim to:

1) Characterize the development of atherosclerosis and abdominal aortic aneurysm
2) Examine macrophage heterogeneity and function in arterial disease
3) Investigate monocyte and macrophage kinetics underlying arterial disease development

1.6 STUDY SUMMARIES

1.6.1 CHAPTER 3.1

By engaging the clinically relevant risk factors of hypercholesterolemia and cigarette smoke, we aim to improve our ability to model the pathogenesis and potential interaction of concurrent arterial disease development. Data presented in chapter 3.1 demonstrate that exposure to cigarette smoke increases atherosclerosis and induces aneurysm formation in hyperlipidemic mice. Furthermore, we show that our model recapitulates clinical observations regarding the impact of smoking cessation on aneurysm incidence. Lastly, our data provide experimental evidence that atherosclerosis is strongly and specifically associated with regions of elastin damage and arterial dilation, suggesting a potential role in abdominal aortic aneurysm formation.

1.6.2 CHAPTER 3.2

Given the importance of macrophages in arterial disease, we next investigated arterial macrophages in our model including their abundance, heterogeneity, and overall functional contribution to tissue pathology. The data presented in chapter 3.2 provide novel insight into the diversity and function of macrophages in smoking induced aneurysmal disease. Here we show that cigarette smoke exposure increases the abundance of arterial monocytes and macrophages, whereas hypercholesterolemia drives arterial macrophage heterogeneity. Specifically, hypercholesterolemia is associated with an increase in macrophage populations

with putative functions in inflammation and tissue remodelling including Trem2 foamy macrophages, inflammatory macrophages, and IFN-inducible macrophages. Notably, we provide evidence that recruited monocytes can differentiate into Trem2 foamy macrophages in aneurysmal tissue, and that Trem2 macrophages have increased expression of proteolytic enzymes implicated in extracellular matrix degradation. Lastly, we demonstrate that macrophages play a critical role in elastin fragmentation within the arterial wall of smoke exposed mice. Together these data highlight the capacity of atherosclerosis-associated macrophages to damage the arterial wall and directly contribute to aneurysm associated pathology. Importantly, this study addresses a contentious question in the field and provides experimental evidence that atherogenesis can contribute to abdominal aneurysm pathology.

1.6.3 CHAPTER 3.3

Finally, we investigated the impact of cigarette smoke on kinetic factors that can contribute to arterial macrophage accumulation including monopoiesis, local proliferation, and monocyte recruitment. The data presented in chapter 3.3 demonstrate that cigarette smoke significantly impacts hematopoiesis and is associated with an overall suppression of circulating monocytes and pro-inflammatory cytokines, despite increased development of arterial disease. We also report an increase in the total number of proliferating macrophages in arterial lesions although this increase is not proportional to overall lesion size. Furthermore, using a parabiosis model, we show monocyte recruitment is significantly increased

and is likely a key kinetic factor underlying the increased accumulation of arterial macrophages following exposure to cigarette smoke. Lastly, we propose that endothelial dysfunction contributes to increased monocyte recruitment and provide evidence that smoke exposure results in reduced eNOS expression in arterial tissue. As a proof-of-concept, we demonstrate NOS inhibition significantly worsens arterial pathology including increased arterial macrophage accumulation and aneurysm formation and rupture. Taken together these data suggest that increased monocyte recruitment and endothelial dysfunction are key factors contributing to the increased risk of arterial disease development following exposure to cigarette smoke.

CHAPTER 2: MATERIALS AND METHODS

2.1 ANIMALS

C57BL/6J, apolipoprotein E–deficient (*Apoe*$^{-/-}$) mice (B6.129P2-Apoe^{tm1Unc}), and low-density lipoprotein receptor-deficient (*Ldlr*$^{-/-}$) mice (B6.129S7-Ldlr^{tm1Her}/J) were purchased from The Jackson Laboratory. *Ldlr-/-* purchased from The Jackson Laboratory express CD45.2 on immune cells. Congenic *Ldlr*$^{-/-}$ mice expressing CD45.1 were bred in the Animal Resources Centre at the University Health Network (Toronto, ON) by backcrossing *Ldlr-/-* mice with CD45.1 mice (B6.SJL-Ptprc^{a}Pepc^{b}/BoyJ) purchased from The Jackson Laboratory. At 8-10 weeks old, *Apoe*$^{-/-}$ mice were placed on a Western diet (HCD, 21.2% fat/weight; 0.2% cholesterol) (Harlan Teklad, Madison, WI) and *Ldlr*$^{-/-}$ mice were placed on a high cholesterol diet (20% fat/weight, 1.25% cholesterol) (Research Diets Inc., New Brunswick, NJ). Mice were housed under specific pathogen free conditions with 12h light-dark cycle and access to food and water *ad libitum*. All animal work was conducted according to guidelines set by the Canadian Council on Animal Care and all procedures were approved by the Animal Research Ethics Board at McMaster University and the University Health Network Animal Care Committee in Toronto.

2.2 *in vivo* MODELS AND INTERVENTIONS

2.2.1 Cigarette smoke exposure: At 8-10 weeks old, mice were exposed to room air or cigarette smoke for 4, 8, 12, or 16 weeks. Mice were exposed to the mainstream cigarette smoke of 12 cigarettes over a 50min period, twice a day, five

times per week using a whole-body exposure system (SIU48, Promech Inc., Sweden). Details of the experimental protocol have been reported previously.[201]

2.2.2 Hypercholesterolemia: Hypercholesterolemia in our mouse model was assessed using The Center for Phenogenomics (Toronto, ON), a dedicated core facility providing pathology services including clinical chemistry analysis of mouse samples. Plasma samples were analyzed for total cholesterol, high density lipoprotein cholesterol, low density lipoprotein cholesterol, and triglycerides using a Beckman AU480 Biochemistry Analyzer (Beckman Coulter).

2.2.3 Parabiosis: The surgical procedure of joining mice in parabiosis was conducted as previously described.[202] Briefly, after shaving the corresponding lateral aspects of each mouse, matching skin incisions were made from behind the ear to the tail of each mouse, and the subcutaneous fascia was bluntly dissected to create about 1⁄2 cm of free skin. The scapulas were sutured using a mono-nylon 5.0 (Ethicon, Albuquerque, NM), and the dorsal and ventral skins were approximated by continuous suture. Mice were joined for intervals of 9 to 10 weeks. Percent chimerism in the blood and aortic tissue was defined for either gated monocytes or macrophages as %CD45.1 / (%CD45.1 + %CD45.2) in CD45.2 mice, and as %CD45.2 / (%CD45.2 + %CD45.1) in CD45.1 mice.

2.2.4 CSF1 Blockade: A blocking antibody against macrophage colony stimulating factor (anti-CSF1, 1mg/ml, BE0204, BioXCell) or an isotype control antibody (anti-trinitrophenol RatIgG2a, 1mg/ml, BE0089, BioXCell) were delivered using

subcutaneously implanted mini osmotic pumps (Alzet, model 2004) at a dose of 0.25µl/hour for 3 weeks.

2.2.5 BrdU Incorporation: Contribution of newly proliferated cells to different cell populations was determined by *in* vivo labeling with bromodeoxyuridine (BrdU, BD Biosciences), a thymidine analog that is incorporated into the DNA of dividing cells. BrdU was administered by injecting mice intraperitoneally with 100µg of BrdU 3h, 12h, or 24h before sacrifice.

2.2.6 L-NAME: Nitric oxide synthase activity was inhibited by administering L-NAME (Nω-Nitro-L-arginine methyl ester hydrochloride, 0.5g/L, Sigma) in the drinking water of mice. Control mice received normal sterile water.

2.2.7 Prosense680 Imaging: To quantitatively and spatiotemporally assess inflammatory leukocytes in lesions, we used dual channel imaging to report cathepsin activity based on lys-lys cleavage of Prosense-680. Prosense-680 is a protease-activatable fluorescence sensor based on a polymeric scaffold that allows imaging of Cathepsin B activity (and to a lesser extent cathepsins K, L, and S). Macrophages and neutrophils ingest and activate Prosense-680, indicating intracellular cysteine protease activity. Prosense680 was delivered intravenously 24h before sacrifice. Whole aortas were collected and imaged using Xenogen IVIS spectrum.

2.3 HISTOLOGY

2.3.1 Sample Collecting and Embedding: Whole aortas from the aortic root to the iliac bifurcation were collected from mice after whole-body perfusion using 20-30ml of PBS. Aortas were then sectioned and either immediately embedded in O.C.T. compound (Sakura, Finetek) and flash-frozen in isopentane and dry ice or placed in a fixative solution (10% formalin or 4% PFA) for a minimum of 1h, and up to 24h, prior to embedding.

2.3.2 Sectioning: Serial cross sections (10 μm) were cut using a cryostat and air dried onto microscope slides (Fisher Scientific, Pittsburgh, PA). The aortic root, suprarenal aorta (region below the diaphragm and above the renal arteries), and ascending aorta (region between the aortic root and the brachiocephalic artery) were sectioned into 10μm slices, generating approximately 60-180 consecutive sections that spanned the entirety of the region of interest.

2.3.3 Staining: Hematoxylin and eosin (H&E) (Sigma), Elastin van Gieson (EVG) (Sigma), and Oil Red O (Sigma) staining were performed by to visualize overall tissue morphology, elastin, or lipid content. Elastin content was also visualized using Russell Movat Pentachrome (American MasterTech Scientific) staining or autofluorescence (FITC channel). Images were captured using an Aperio Scanscope AT2 (Leica Biosystems).

2.3.4 Immunofluorescence staining. Aortic tissue cross-sections were permeabilized with 0.1% tritonX-100 and blocked with 10% goat serum in PBS.

Slides were then incubated with primary antibodies at 4°C overnight, following by incubation with secondary antibodies at room temperature for 1h, and Hoechst staining for 30min at room temperature. Slides were washed three times with PBS between each step. For detection of BrdU or Ki67, BD antigen retrieval A solution (BD550524) was used prior to blocking according to manufacturer's instructions. Slides were mounted with DAKO Fluorescence Mouting Medium (DAKO) and images were acquired using the Axio Imager.A2 microscope (Zeiss).

2.3.5 *En face* immunofluorescent staining: Aortic arch and suprarenal tissue sections were isolated and fixed in 4% PFA for 60min on ice, and permeabilized in 0.5% tritonX-100 with 1mM glycine in PBS for 15min at room temperature. Tissues were then quenched in 3% H2O2 for 20min and antigen retrieval was performed using 1N HCL at 37°C for 30min. Tissues were washed and then stained overnight with the primary antibodies. Antibodies used were either directly conjugated to a fluorophore or biotin and can be found in **Supplementary Table 1**. Tissues were washed and then incubated with streptavidin conjugated to horseradish peroxidase (1:200) for 30min. Tissues were washed and stained with Hoechst (1:400, Invitrogen 33342) for 30min. Tissue sections were then carefully flattened and mounted on slides for imaging. Images were captured using a Nikon A1R confocal microscope (Nikon, USA).

2.3.6 Quantification: Morphology and positive staining were quantified using the open-source software, Image J (National Institute of Health). To assess aneurysms

maximal diameter in the suprarenal region was measured and compared to adjacent non-aneurysmal thoracic aorta. Aortic dilations that had a diameter ≥50% larger than non-affected arterial tissue were considered aneurysms. For comparison of lesion size, elastin damage, and luminal diameter between the groups, 6 consecutive sections with 100μm intervals were used. Elastin scores were determined as followed; 1 (no damage), 2 (single strand break within the elastic lamina), 3 (multiple strand breaks within the elastic lamina), 4 (disruption of all layers of the elastic lamina). The highest level of elastin degradation observed in the 6 consecutive sections was reported for each sample. Total numbers of regions with severe damage was defined as number of regions with 4 or more elastin breaks in all 6 consecutive cross-sections. Luminal diameter was estimated by measuring the luminal circumference and then using the equation diameter = circumference/pi. Antibodies used for immunohistochemical staining and isotype controls can be found in **Supplementary Table 1**.

2.4 FLOW CYTOMETRY

2.4.1 Sample collection and processing: Peripheral blood for flow cytometric analysis was collected by cardiac puncture using a 50 mM EDTA solution as anticoagulant. Erythrocytes were lysed using RBC Lysis Buffer (BioLegend). The total white blood cell count was determined by preparing a 1:20 dilution of (undiluted) peripheral blood obtained from the orbital sinus using heparin- coated capillary tubes in RBC Lysis Buffer (BioLegend). After organ harvest, single-cell

suspensions were obtained as follows: for bone marrow, the femur of one leg was crushed with mortar and pestle and homogenized through a 40-µm-nylon mesh. For aortic tissue, the aorta was perfused with 10 ml PBS before digestion. The entire aorta (from the aortic sinus to the iliac bifurcation) was cut in small pieces and subjected to enzymatic digestion with 450 U ml^{-1} collagenase I, 125 U ml^{-1} collagenase XI, 60 U ml^{-1} DNase I and 60 U ml^{-1} hyaluronidase (Sigma-Aldrich) for 10–40 min (depending on age) at 37 °C while shaking. Single-cell suspensions of digested tissues were obtained by homogenizing digested tissue though 40-µm-nylon mesh.

2.4.2 Staining and analysis: Antibodies used for flow cytometric analyses are provided in **Supplementary Table 2**. Data was acquired on an LSRII flow cytometer (BD Biosciences) and analyzed with FlowJo v8.8.6 (Tree Star, Inc.). Digested aortic cells were treated with FcBlock (BD Biosciences) for 15 min before incubation with antibody cocktail for an additional 30 min. Samples were fixed before flow analysis (BD Cytofix). BrdU+ cell were assessed with the FITC BrdU+ Flow Kit (BD Biosciences).

2.4.3 Cell markers: Immune cell populations were identified as follows: neutrophils ($CD45^+CD11b^+Ly6G^+$), monocytes ($CD45^+Ly6G^-CD11b^+CD115^+Ly6C^{lo-hi}$), B cells ($CD45^+B220^+$), $CD4^+$ T cells ($CD45^+CD3^+CD4^+$), $CD8^+$ T cells ($CD45^+CD3^+CD8^+$). Aortic monocytes/macrophages were identified as ($CD45^+Ly6G^-CD11b^+F480^+$). Bone

marrow hematopoietic stem and progenitor cells were identified as follows: Lineage (CD3, CD127, CD11b, CD11c, NK1.1, TER119, B220), MPP ($Lin^-Ckit^+Sca1^+CD48^-CD150^-$), HPC-1 ($Lin^-Ckit^+Sca1^+CD48^+CD150^-$), HPC-2 ($Lin^-Ckit^+Sca1^+CD48^+CD150^+$), HSC ($Lin^-Ckit^+Sca1^+CD48^-CD150^+$), CMP and GMP ($Lin^-Ckit^+Sca1^-CD16/32^+CD34^+$), and MEP ($Lin^-Ckit^+Sca1^-CD16/32^-CD34^-$). Myeloid restricted progenitors were identified as follows: Lineage (CD3, Ly6G, B220, NK1.1, CD90.2), MDP ($Lin^-CD45^+CD115^+CD135^+CD117^+CD11b^-Ly6C^-$), cMOP ($Lin^-cKit^+CD115^+CD135^-CD11b^-Ly6C^+$) and transitional $CxCR4^{hi}$ pre-monocytes ($Lin^-cKit^-CD115^+CD135^-CD11b^+Ly6C^+CxCR4^{hi}$), as well as mature monocytes ($Lin^-cKit^-CD115^+CD135^-CD11b^+Ly6C^+CxCR4^{lo}$).[43,203,204]

2.5 SINGLE CELL RNA SEQUENCING AND ANALYSIS

2.5.1 Sample collection and processing: Four experimental groups were included in the single cell RNA sequencing analysis: C57BL/6 mice (n=5, Naïve), *Apoe*$^{-/-}$ mice exposed room air (n=5, Room Air), *Apoe-/-* exposed to cigarette smoke without aneurysm (n=2, Smoke), and *Apoe-/-* mice exposed to cigarette smoke with aneurysm (n=4, Aneurysm). *Apoe*$^{-/-}$ mice were on a high fat diet and exposed for 16 weeks. Suprarenal aortas were isolated and pooled for each group and total $CD45^+CD31^-$ and $CD45^-CD31^+$ cells were FACS sorted using the MoFlo Astrios BRVY.

2.5.2 Single cell sequencing library preparation: Generation of single cell sequencing libraries were prepared as outlined in the 10x Genomics Single Cell 3′

v2 Reagent Kit user guide. Briefly, the samples were washed twice in PBS (Life Technologies) + 0.04% BSA (Sigma) and re-suspended in PBS + 0.04% BSA. Cell viability was determined using Trypan Blue (Thermo Fisher) and counting on a haemocytometer (Thermo Fisher). A total of 6059 cells from four different experimental groups (Naïve:782, Room Air:1851, Smoke:584, and Aneurysm:2842) were analyzed. Viability for the samples were as follows: Naïve (73%), RA (91%), Aneurysm (94%), Smoke (90%). Following counting, the appropriate volume for each sample was calculated for a target capture 2000-4000 cells. Samples below the required cell concentration as defined by the user guide (i.e., <400 cells/µl) were pelleted and re-suspended in a reduced volume and counted again using a haemocytometer prior to loading onto the 10x Genomics single-cell-A chip. Droplet emulsions containing single cells were transferred to a pre-chilled 96-well plate (Eppendorf). The plates were heat-sealed using a Bio-Rad heat sealer and transferred to a Veriti 96-well thermal cycler (Thermo Fisher) for reverse transcription. After the reverse transcription, cDNA was recovered using Recovery Agent provided by 10x followed by a Silane DynaBead clean-up (Thermo Fisher) as outlined in the user guide. Purified cDNA was amplified for 13 cycles before being cleaned using SPRIselect beads (Beckman). Samples were diluted 4:1 (elution buffer (Qiagen):cDNA) and run on a Bioanalyzer (Agilent Technologies) to determine cDNA concentration. cDNA libraries were prepared as outlined by the Single Cell 3′ Reagent Kits v2 user guide with appropriate

modifications to the PCR cycles based on the calculated cDNA concentration (as recommended by 10X Genomics).

2.5.3 Sequencing: The concentration of each library was calculated based on library size as measured using a bioanalyzer (Agilent Technologies) and qPCR amplification data (Kappa/Roche). Samples were pooled and normalized to 10 nM, and then diluted to 2 nM using elution buffer (Qiagen) with 0.1% Tween20 (Sigma). Each 2 nM pool was denatured using 0.1 N NaOH at equal volumes for 5 min at room temperature. Library pools were further diluted to 20 pM using HT-1 (Illumina) before being diluted to a final loading concentration of 14 pM. 150 µl from the 14 pM pool was loaded into each well of an 8-well strip tube and loaded onto a cBot (Illumina) for cluster generation. Samples were sequenced on a HiSeq 2500 with the following run parameters: Read 1—26 cycles, read 2—98 cycles, index 1—8 cycles. Samples were sequenced to a read depth of ~60,000 reads/cell and run through the 10X Genomics cell ranger platform.

2.5.4 Single cell RNA-seq analysis: The sequenced data was processed into expression matrices with the Cell Ranger software (version 2.2.0) from 10X Genomics (http://10xgenomics.com/). Raw base call files from HiSeq2500 sequencer were demultiplexed into library specific FASTQ files. Sequencing reads were aligned to the mouse transcriptome using STAR aligner. Subsequently, cell barcodes and Unique Molecular Identifiers (UMIs) underwent filtering and

correction. Reads associated with the retained barcodes were quantified and used to build a transcript count table.

2.5.5 Pre-processing and normalization: The standard procedures of filtering, normalization, dimensionality reduction and clustering were performed using an R package Seurat (v.3.2).[205,206] Genes not detected in at least three cells and low-quality cells expressing less than 200 genes were removed. Potential doublets or multiplets, and dead or lysed cells were excluded by removing cells with a high number of genes and high percentage of transcripts mapping to mitochondrial genes After quality control, 14731 genes across 5159 cells in three datasets were retained for downstream analysis. The data was normalized using the log normalization method and highly variable genes were selected using the mean-variance method (FindVariableFeatures).

2.5.6 Dimensionality Reduction and Clustering: Principal component analysis (PCA)was used for linear dimensionality reduction and the number of significant principal component for subsequent analysis was determined based on the elbow point showing the standard deviations of each principal component. Clusters were identified by a graph-based clustering approach implemented by the FindClusters function in Seurat. Cells were embedded in a k-nearest neighbors graph based on the Euclidean distance matrix constructed on the significant PCs. The Louvian modularity optimization algorithm was applied to iteratively group cells together

into clusters. Non-linear dimensionality reduction and visualization was performed using UMAP (Uniform Manifold Approximation and Projection).

Differential gene expression analysis was performed using the Wilcoxon rank sum test with the FindAllMarkers function to identify genes uniquely expressed in each cluster relative to all other clusters.[207] Lastly, biological pathway analysis was performed using gProfiler (https://biit.cs.ut.ee/gprofiler/gost) to identify enriched pathways based on the differentially expressed genes in each cluster.[208]

2.5.7 Statistical analysis of cell type composition: To test the association of cluster composition between the Room Air and Aneurysm samples, we performed a chi-square test. In quantifying the fraction of cells corresponding to each cluster, two assumptions were made. The first is that 10X captures and sequences cells in an unbiased manner, and the other is that the frequencies of cells are representative of their frequencies in the aorta. The fraction of cells corresponding to each cluster was obtained by counting the number of cells assigned to each cluster in room air and aneurysm sample and dividing over the total number of cells. Empirical P values were obtained by permuting genotype 20,000 times and obtaining the fraction of cells corresponding to each cluster for each permutation. These fractions were sorted, and the P value was obtained by counting the number of times a fraction was more extreme or equal to the observed fraction in the non-permuted data divided by 20,000 and multiplied by 2 for a two-tailed test. P values were

adjusted for multiple comparison testing using the Benjamini-Hochberg FDR procedure.

2.5.8 Trajectory Analysis: We used Monocle3 to investigate inferred developmental trajectories between macrophage and monocyte clusters.[209–211] Monocle uses the Reverse Graph Embedding to learn the sequence of gene expression changes that each cell undergoes within the dynamic biological sample provided. It then places each cell at an appropriate position along this trajectory of gene expression changes. The data previously analysed with Seurat was imported into monocle. Dimensionality reduction was done using principal component analysis with highly variable genes from Seurat. Non-linear dimensionality reduction was performed using UMAP followed by clustering with Leiden community detection.[212] In addition to grouping cells into clusters, this method divides cells into large well-defined groups called partitions. These partitions will subsequently represent separate or disjoint trajectories. Finally, the trajectory was built within each partition from the reduced dimension space using reversed graph embedding. Data was visualized with UMAP embeddings and trajectories derived from Monocle and overlaid with clusters annotated from the Seurat analysis.

RNA velocity analysis was performed using the python package Velocyto.[213] Briefly, Velocyto uses raw data to count the spliced (mRNA) and unspliced (Introns) reads for each gene to generate RNA velocity maps that were projected onto the UMAP plot.

2.6 STATISTICS

Data are expressed as mean ± SEM. Statistical tests include unpaired Student's t test using Welch's correction for unequal variances, 1-way ANOVA followed by Tukey's or Bonferroni's post-hoc correction for multiple comparisons, Fisher's exact test or chi-squared analysis followed by a post-hoc pairwise comparison. Adjusted P values of 0.05 or less were considered to denote significance.

CHAPTER 3: RESULTS

3.1: AORTIC ANEURYSM FORMATION STRONGLY ASSOCIATES WITH ATHEROSCLEROSIS IN SMOKE EXPOSED MICE

The data presented in this chapter characterize the development of arterial pathology in cigarette smoke exposed hypercholesterolemic mice. To our knowledge, this is the first murine model that demonstrates spontaneous aneurysm formation using only the clinically relevant risk factors of hypercholesterolemia and cigarette smoke exposure. Here we show smoke exposure increases the size of atherosclerotic lesions and that atherosclerosis localizes with regions of elastin damage and aortic dilation. These data suggest atherosclerosis may be mechanistically linked to aneurysm formation, addressing a longstanding controversial question in the field.

3.1.1. Cigarette smoke exposure increases atherosclerosis in *Apoe*$^{-/-}$ mice.

To assess the impact of cigarette smoke exposure on the development of atherosclerosis, we used *en face* oil red O staining of neutral lipids in the lesser curvature of the aortic arch and the abdominal aorta, as well as staining serial cross-sections of the aortic root. Our data show that cigarette smoke exposure results in larger atherosclerotic lesions in the aortic arch and abdominal aorta of male *Apoe*$^{-/-}$ mice fed a Western-type high cholesterol diet (HCD) compared to room air controls at 12 weeks of exposure **(Figure 1 A-D)**. Increased atherosclerosis within the lesser curvature of the aortic arch was also observed within 4 weeks of exposure and became more pronounced at 12 weeks **(Figure 1 A-B)**. Although there was a trend

towards increase, no significant difference was observed in oil red O positive area in the aortic root **(Figure 1E-G)**. Overall, these data demonstrate increased atherosclerosis following exposure to cigarette smoke in *Apoe*$^{-/-}$ mice.

3.1.2. Cigarette smoke exposure induces aortic aneurysm formation and rupture in *Apoe*$^{-/-}$ mice.

Next, we assessed the development of abdominal aortic aneurysms, which are another smoking-associated arterial pathology. We observed exposure to cigarette smoke induces spontaneous aortic aneurysm formation in the supra-renal region of the aorta in a dose-dependent manner, with no gross abnormalities observed in other regions of the aorta **(Figure 2A-C)**. Aneurysms were characterized by an increase in both gross and luminal aortic diameter **(Figure 2C-D)**. In approximately 10% of smoke-exposed mice, aortic aneurysms proceeded to spontaneous rupture resulting in sudden death **(Figure 3A-B)**.

3.1.3. Female sex and smoking cessation are associated with reduced incidence of aortic aneurysms in *Apoe*$^{-/-}$ mice.

To assess whether aneurysm formation was dependent on sex in our model, we also assessed aneurysm formation in female mice. We observed that 18% of female *Apoe*$^{-/-}$ mice on a HCD developed aneurysm following 12 weeks of exposure to cigarette smoke **(Figure 4A)**. Of note, no aneurysm formation or rupture were observed in room air control mice at any time point in male or female mice, highlighting the necessity of cigarette smoke exposure in this model **(Figure 2-4)**.

To determine whether continuous exposure to cigarette smoke was required for aneurysm formation, we next assessed the impact of smoking cessation in our model. To do so, male *Apoe*$^{-/-}$ mice were exposed to cigarette smoke for 8 weeks followed by a cessation period consisting of 4 weeks of room air exposure, whereas control mice were continuously exposed to cigarette smoke for 12 weeks. As expected, we observed that smoking cessation resulted in significantly reduced aneurysm incidence compared to continuous smoke exposure in males **(Figure 4B-C)**.

3.1.4. Impact of cigarette smoke on circulating lipids in hyperlipidemic mice.

Given that hypercholesterolemia is critical to atherosclerosis, we assessed the impact of cigarette smoke on circulating lipids at both early and late time points of exposure using clinical chemistry analysis of plasma samples. In male *Apoe*$^{-/-}$ mice, we observed increased triglycerides, total cholesterol, and LDL cholesterol after 4 weeks of smoke exposure compared to room air controls **(Figure 5A-D).** No differences were observed between the two groups after 12 weeks of exposure **(Figure 5E-H)**. HDL cholesterol did not differ between room air and smoke exposed mice at either time point **(Figure 5 C, G)**.

3.1.5. Cigarette smoke induces aortic aneurysms in hyperlipidemic mice.

To assess whether the impact of smoke exposure on arterial pathologies was consistent in other models of hypercholesterolemia, we also assessed *Apoe*$^{-/-}$ mice on a non-atherogenic standard chow diet and low density lipoprotein receptor

deficient (*Ldlr*$^{-/-}$) mice fed a HCD. Both hypercholesterolemic models were exposed to cigarette smoke for 12 weeks and atherosclerosis lesions in the aortic arch and abdominal aneurysm formation were assessed. We observed that smoke exposure similarly increased lesion size in the aortic arch and induced aortic aneurysms in both models of hypercholesterolemia **(Figure 6)**. Importantly, no atherosclerosis or aneurysm formation was observed in C57BL/6J mice on a HCD following smoke exposure, suggesting that hyperlipidemia resulting from perturbation of the APOE-LDLR axis of lipoprotein clearance is critical to cigarette smoke induced arterial pathologies **(Figure 6)**.

3.1.6. Increased elastin damage in aortas of smoke exposed *Apoe*$^{-/-}$ mice.

A critical feature of aortic aneurysms is damage of the elastic lamina within the medial layer of the arterial wall. To assess elastin fragmentation throughout the abdominal aorta, at least six serial cross-sections of aortic tissue stained with EVG were assessed for each sample. Elastin damage was quantified based on a 4 point scoring system; no damage (1), single elastin break (2), multiple elastin breaks (3), breaks in all layers of elastic lamina (4) **(Figure 7A)**. We observed increased elastin fragmentation in the supra-renal aorta of smoke exposed mice compared to room air controls, with more damage occurring with prolonged exposure demonstrating a dose-dependent effect **(Figure 7B)**.

3.1.7. Atherosclerosis is associated with elastin damage in the aorta of *Apoe*$^{-/-}$ mice.

To quantify whether elastin damage was specifically associated with regions of atherosclerosis, we assessed 58 histological cross-sections of abdominal aortas with elastin damage and stained adjacent cross-sections with oil red O to visualize atherosclerotic plaques **(Figure 8A)**. We observed that elastin damage occurred in regions with atherosclerosis in 91% of samples **(Figure 8B)**. Notably, regions of severe elastin damage (score 3) were more frequently observed in areas with larger atherosclerotic lesions **(Figure 8C)**. Lastly, atherosclerotic lesion size correlated with increased arterial diameter in smoke exposed mice **(Figure 8D)**. This data strongly suggests that elastin damage associated with aneurysm formation specifically co-localizes with atherosclerotic lesions.

3.1.8. Summary of results

In summary, data presented in chapter 3.1 demonstrates that exposure to cigarette smoke increases atherosclerosis and induces aneurysm formation in hyperlipidemic mice. Furthermore, we show cigarette smoke and hyperlipidemia are both critical to aneurysm formation in our model, and that smoking cessation impacts aneurysm incidence. Lastly, our data provide evidence that atherosclerosis is strongly associated with regions of elastin damage and arterial dilation, suggesting a potential mechanistic role in abdominal aortic aneurysm formation.

3.2: HYPERCHOLESTEROLEMIA INDUCED MACROPHAGES ARE INCREASED BY SMOKE EXPOSURE AND MEDIATE ELASTIN DAMAGE

The data presented in this chapter focuses on the heterogeneity and function of macrophages in arterial disease. This study is, to our knowledge, the first to present single cell RNA sequencing analysis of monocyte and macrophage populations in smoking-induced aneurysmal tissue. We also present evidence that atherosclerosis-associated macrophages directly contribute to elastin damage in the abdominal aorta. These findings highlight the capacity for atherosclerosis-associated macrophages to directly contribute to aneurysm formation, addressing a controversial question in the field.

3.2.1. Increased accumulation of monocytes and macrophage in aortas of smoke exposed mice

Since myeloid cells are critical to the development of atherosclerosis, we next focused our investigation on the presence of macrophages and monocytes within aortas of cigarette smoke exposed *Apoe*$^{-/-}$ mice. As expected, we observed an increase in monocyte populations ($CD45^{+}Ly6G^{-}CD11b^{+}CD64^{lo}Ly6C^{hi\text{-}int\text{-}neg}$) within the aortic tissue of smoke exposed mice compared to room air controls at 16 weeks by flow cytometry **(Figure 9A).** We also observed a significant increase in aortic tissue monocytes and macrophages by flow cytometry ($CD45^{+}Ly6G^{-}CD11b^{+}F480^{+}$) in smoke exposed mice compared to room air controls at 12 weeks, with a further increase observed in mice with aneurysms **(Figure 9B)**. Notably, *en*

face $CD68^+$ staining within the abdominal region of the aorta showed increased macrophage accumulation specifically at sites of pathology in smoke exposed mice compared to room air controls **(Figure 9C-D)**. Overall, exposure to cigarette smoke resulted in increased macrophage accumulation in aortic tissue compared to room air controls.

3.2.2. Single cell RNA sequencing reveals leukocyte composition of abdominal aortas

To identify leukocyte populations at sites of arterial pathology, we performed single cell RNA sequencing of $CD45^+$ immune cells and $CD31^+$ endothelial cells isolated from supra-renal aortas of naïve C57BL/6J mice (control), HCD-fed room air exposed *Apoe*$^{-/-}$ mice (room air) and HCD-fed cigarette smoke exposed *Apoe*$^{-/-}$ mice with measurable aneurysm (aneurysm) at a 16 week time point **(Figure 10A-B)**. After filtering data through quality controls, we were able to analyze the gene expression profiles of 5460 single cells. These gene expression data were aligned and visualized using uniform manifold approximation and projection (UMAP) which allows for dimensionality reduction while maintaining global structure and inter-cluster relationships **(Figure 10C)**.[214] Using Seurat based clustering we were able to identify 20 distinct clusters, which were assigned putative biological identities based on expression patterns of canonical immune cell markers **(Figure 10C-D and Table 1)**. This included identification of major immune cell populations such as neutrophils (*S100a9*), T cells (*Cd3d*), B cells (*Cd79a*), and

dendritic cells (*Flt3*) **(Figure 10C-D)**. Heatmap visualization of single cell expression of the top 20 differentially expressed genes per cluster further confirms unique cluster identities consistent with major immune cell profiles **(Figure 11 and Table 1)**. Overall, these data provide insight into the immune cell composition of smoking-induced aneurysmal tissue and can be used as a benchmark reference in further investigations.

3.2.3. Macrophage populations in abdominal aortas of hypercholesterolemic mice.

To assess whether the increased accumulation of monocytes and macrophages within aortas was accompanied by an increase in macrophage heterogeneity, we analyzed sub-clusters of monocytes and macrophages identified by single cell RNA sequencing. This analysis revealed 2 monocyte clusters consistent with classical $Ly6C^{hi}$ monocytes and non-classical $Ly6C^{lo\text{-}neg}$ monocytes as well as five unique macrophage clusters with significant differences in gene expression **(Figure 12A,C and Table 2)**. We observed naïve, non-hypercholesterolemic control aortas were primarily populated with monocytes and resident macrophages expressing transcripts consistent with those described in self-renewing adventitial macrophages (*Folr*, *Pf4*, *Lyve1*, and *Fcna*) as well as in resident arterial macrophages (*Retnla*, *Ear2*, *Fn1*, *Clec4b1*) **(Figure 12C)**.[43,109,215] In hypercholesterolemic mice resident macrophage populations were reduced, and we observed the expansion of inflammatory, interferon-inducible (IFNIC), and Trem2

foamy macrophages, which is in agreement with recently published single cell datasets in experimental atherosclerosis **(Figure 12B, Table 3)**.[109] Gene set enrichment analysis of these macrophage populations revealed increased expression of transcripts with annotated biological functions in inflammation and tissue remodelling pathways including leukocyte migration, antigen presentation, production and response to reactive oxygen species, interferon and cytokine signalling, and extracellular matrix degradation **(Figure 13, Table 4).** Of note, the transcriptional profile of monocytes and macrophages in hypercholesterolemic aortas did not differ significantly in the context of aneurysm formation with only 34 differentially expressed genes across all seven clusters **(Table 5)**. However, the proportion of cells differed with a significant increase in Ly6C^{hi} monocytes in aneurysmal tissue, which is consistent with our flow cytometric data **(Figure 12B, Table 3, and Figure 9A)**. Thus, hypercholesterolemia drives macrophage heterogeneity in arterial disease with an increase in populations with putative functions in inflammation and tissue remodelling. Of note, exposure to cigarette smoke increases the overall abundance of macrophages and their precursor, Ly6C^{hi} monocytes, in aneurysmal tissue.

3.2.4. Trajectory analysis predicts Ly6C^{hi} monocyte differentiation to protease enriched Trem2 foamy macrophages.

To investigate the relationship between monocyte differentiation and the identified macrophage populations, we used single cell transcriptomic analyses. The first

approach consisted of a restricted Monocle 3 analysis which consists of ordering single cell transcriptomic profiles in pseudo-time in order to model their progress through differentiation.[209–212] This analysis identified two major trajectories for Ly6C^{hi} monocytes comprising differentiation into either Ly6C^{lo} monocytes or Trem2 foamy macrophages **(Figure 14A)**. A second independent analysis tool was leveraged in order to verify the differentiation potential predicted by Monocle 3. This RNA velocity model consists of predicting future cell states based on the balance of unspliced nascent mRNA and spliced mature mRNA expression in each cell.[213] RNA velocity modelling also predicted Ly6C^{hi} monocyte differentiation towards Ly6C^{lo} monocytes or Trem2 foamy macrophages based on transcriptional dynamics **(Figure 14B)**. Of note, Trem2 foamy macrophages are associated with increased expression of transcripts with annotated functions in tissue remodelling including osteopontin, matrix metalloproteinases, and cathepsins **(Figure 15A)**. To visualize dynamic changes across cell states, single cell gene expression was plotted as a function of pseudo-time which highlights that loss of Ly6C^{hi} monocyte markers, such as *Ly6c2* and *Ccr2*, was associated with an increased expression of *Spp1*, *Mmp12*, *Ctsb*, and *Trem2* in Trem2 foamy macrophages or *Cebpd* and *Nr4a1* in Ly6C^{lo} monocytes **(Figure 15B)**. Overall, single cell transcriptomic-based dynamic modelling predict differentiation of Ly6C^{hi} monocytes to Ly6C^{lo} monocytes or protease-expressing Trem2 foamy macrophages in arterial tissue of hypercholesterolemic mice.

3.2.5. Aneurysmal macrophages express Trem2, osteopontin, and increased cathepsin activity *in vivo*.

To investigate the in vivo presence of monocyte derived Trem2 macrophages, we used a parabiotic model. This model of surgically joined parabionts congenic for CD45 allows for establishment of shared circulating cells and distinction between host and partner-derived leukocytes. Within aneurysmal tissue of cigarette smoke exposed mice CD45.1 mice, we detected co-expression of CD45.2 and TREM2 in $CD68^{+}$ cells, validating the presence of partner-derived Trem2 expressing macrophages which can only arise from differentiation of circulating monocytes **(Figure 16A)**. We also detected osteopontin expression in aneurysmal macrophages, which is consistent with the profile of Trem2 macrophages **(Figure 16B)**. Lastly, to assess *in vivo* proteolytic activity, we measured intracellular cathepsin activity using ProSense680, an agent that fluoresces upon being cleaved by cathepsin B, -L, or -S. Since these cathepsins are only active at the low pH found in organelles such as lysosomes, this technique largely measures intracellular cathepsin activity within cells such as macrophages. Using this approach, we observed increased cathepsin activity in smoke exposed mice with aneurysm, particularly in the supra-renal region of the aorta, compared to room air controls **(Figure 16C)**. Thus, in accordance with our transcriptomics-based observations, we were further able to confirm the presence of monocyte-derived Trem2 macrophages as well as the expression of Trem2 associated proteins and cathepsin activity in aneurysmal tissue.

3.2.6. Macrophages play a critical role in elastin damage in aortas of smoke-exposed mice.

Given the strong correlation of atherosclerosis and aneurysm observed in our model, in addition to the identification of macrophage populations with putative functions in inflammation and tissue remodelling, we next investigated the role of arterial macrophages in mediating elastin damage. To assess whether arterial macrophages are specifically associated with areas of elastin damage, we quantified $CD68^+$ cells overlaying areas of elastin damage within aortic arch cross-sections. We observed that the majority of elastin damage localized to regions overlaid with $CD68^+$ cells **(Figure 17A-B)**. To determine whether macrophages are critical to the formation of elastin damage in the aorta, we treated smoke exposed mice with an anti-mCSF1 (colony stimulating factor 1 receptor) neutralizing antibody or a non-specific isotype control antibody for 3 weeks. Since mCSF1 is a critical factor for macrophage differentiation and survival, blocking it leads to depletion of monocytes and tissue macrophages *in vivo*. We observed a significant decrease of blood monocytes in anti-CSF1 treated mice, with no differences observed in other major leukocyte populations including neutrophils, B cells, and T cells **(Figure 17C)**. Anti-mCSF1-treated mice had less accumulation of macrophages in aortic tissue as shown through $CD68^+$ staining in abdominal aorta cross-sections **(Figure 17D)**. This reduction in arterial macrophages was also associated with significant reductions in areas with elastin damage as well as the incidence of severe elastin fragmentation defined as any area with 3 or more strand breaks **(Figure 17E-F)**.

These data suggest that macrophages within atherosclerotic lesions of smoke exposed mice contribute to arterial elastin damage which is critical for subsequent aneurysm formation.

3.2.7. Summary of results

In summary, these data provide novel insight into the heterogeneity and function of macrophages in smoking induced aneurysmal disease. Here we show cigarette smoke exposure increases the abundance of arterial monocytes and macrophages, and hypercholesterolemia drives arterial macrophage diversity. Specifically, hypercholesterolemia is associated with an increase in macrophage populations with putative functions in inflammation and tissue remodelling. Notably, we observe that recruited monocytes can differentiate into Trem2 foamy macrophages in aneurysmal tissue, and that Trem2 macrophages have increased expression of proteolytic enzymes implicated in extracellular matrix degradation. Lastly, we demonstrate that macrophages play a critical role in elastin fragmentation within the arterial wall of smoke exposed mice. Together these data highlight the capacity of atherosclerosis-associated macrophages to damage the arterial wall and directly contribute to aneurysm pathology. Importantly, this study addresses a contentious question in the field and provides evidence that atherogenesis can contribute to abdominal aneurysm formation.

3.3: CIGARETTE SMOKE INCREASES ARTERIAL MONOCYTE RECRUITMENT DESPITE SUPPRESSED MONOPOIESIS

The study presented in chapter 3.3 investigated the kinetics underlying arterial macrophage accumulation following exposure to cigarette smoke. Here we show that smoking suppresses monopoiesis but increases monocyte recruitment to sites of arterial pathology. Furthermore, we provide evidence that this increased recruitment is likely due to increased endothelial dysfunction. These findings provide novel evidence regarding the impact of cigarette smoke on immune cell dynamics leading to more comprehensive insight into smoking-attributable risk in arterial disease.

3.3.1. Decreased circulating leukocytes and cytokines in cigarette smoke exposed *Apoe*$^{-/-}$ mice

Hypercholesterolemia is known to induce monocytosis and Ly6C^{hi} monocytes, in particular, have been shown to be increased and correlate with atherosclerotic disease severity.[81,90] Therefore, we next assessed circulating leukocytes in the blood of smoke exposed mice by flow cytometry **(Figure 18A)**. Surprisingly, we observed a significant decrease in Ly6C^{hi} and Ly6C$^{lo\text{-}neg}$ monocytes in the blood of smoke exposed mice compared to room air controls at 12 weeks of exposure **(Figure 18B)**. We also observed a significant decrease in neutrophils and B cells with no differences in T cell populations. Moreover, we observed reduced levels of circulating inflammatory cytokines and chemokines including CCL2, CCL4, and IL-6, despite increased atherosclerosis at this time point **(Figure 19 and Figure 1)**.

3.3.2. Cigarette smoke exposure suppresses monopoiesis in the bone marrow

To assess whether reduced monocyte levels in the blood were the result of decreased monopoiesis, we next assessed the impact of smoke exposure on hematopoietic stem and progenitor cells (HSPCs) in the bone marrow. Using flow cytometry, we assessed hematopoietic stem cells (HSCs, $Lin^-cKit^+Sca1^+CD48^-CD150^+$), hematopoietic progenitor cell 1 (HPC1, $Lin^-cKit^+Sca1^+CD48^+CD150^-$), HPC2 ($Lin^-cKit^+Sca1^+CD48^+CD150^+$), and multipotent progenitor cells (MPP, $Lin^-cKit^+Sca1^+CD48^-CD150^-$) in the bone marrow **(Figure 20)**. We also assessed monocyte-restricted progenitors including common monocyte progenitors (cMoP, $Lin^-cKit^+CD115^+CD135^-CD11b^-Ly6C^+$), transitional pre-monocyte ($CxCR4^{hi}$, $Lin^-cKit^-CD115^+CD135^-CD11b^+Ly6C^+CxCR4^{hi}$), as well as mature monocytes ($CxCR4^{lo}$, $Lin^-cKit^-CD115^+CD135^-CD11b^+Ly6C^+CxCR4^{lo}$) in the bone marrow **(Figure 21)**. We observed a significant decrease in all populations except HPC2 and MDP cells in smoke exposed mice compared to room air controls **(Figure 22)**. These data indicate that smoke exposure impacts early stages of hematopoiesis which likely contributes to the observed leukopenia in the blood.

3.3.3. Cigarette smoke increases monocyte progenitor cell death in the bone marrow but does not impact monocyte kinetics in the blood.

Since both proliferation and cell death contribute to population kinetics in the bone marrow, we next assessed whether the observed decrease in monocytes was the result of reduced proliferation or increased cell death following exposure to

cigarette smoke. We observed increased annexin V^+ staining in $CxCR4^{hi}$ pre-monocytes as well as $CxCR4^{lo}$ mature monocytes by flow cytometry indicating increased apoptosis of these cells within the bone marrow **(Figure 23A)**. Notably, this increase in cell death was not accompanied by an increase in cell proliferation as assessed by *in vivo* BrdU incorporation, which contributes to an overall decrease in all monocyte subsets in the bone marrow **(Figure 23B-C)**.

Next, we examined the kinetics of circulating monocytes, since bone marrow egress, transition to $Ly6C^{int\text{-}neg}$ monocytes, and survival may all also impact levels of $Ly6C^{hi}$ monocytes in the blood. To do so, we pulse labelled cells with BrdU, and then assessed monocyte egress and turnover kinetics in the blood over the course of 14 days.[104,216] Using this approach we observed similar proportions of newly egressed $BrdU^+$ monocytes indicating that smoke exposure did not impact monocyte egress **(Figure 23D, left panel)**. We also observed similar emergence of $Ly6C^{int}$ and $Ly6C^{neg}$ $BrdU^+$ monocytes indicating similar rates of $Ly6C^{hi}$ differentiation in smoke exposed mice compared to room air controls **(Figure 23D, middle and right panels)**. Lastly, we observe similar decay of the BrdU signal, indicating no difference in monocyte lifespan in smoke exposed mice compared to controls **(Figure 23D)**. Overall, these data suggest that decreased output from the bone marrow, not differential kinetics in the blood, contribute to the unexpected decrease of circulating monocytes following smoke exposure.

3.3.4. Increase in total but not proportion of proliferating cells in abdominal aortas of cigarette smoke exposed mice

To investigate how arterial macrophages accumulate following smoke exposure, despite decreased circulating levels of $Ly6C^{hi}$ monocytes, we next assessed local proliferation of macrophages. Since proliferation has been shown to play a dominant role in maintenance of macrophage populations in established atherosclerotic lesions, we quantified BrdU incorporation and Ki67 expression in $CD68^+$ cells in the abdominal aorta after 12 weeks of exposure. We observed a significant increase in total proliferating macrophages by both $BrdU^+$ and $Ki67^+$ co-staining in $CD68^+$ cells in *en face* abdominal aortas of smoke exposed mice; however, this increase was not proportional to the overall increase in lesion size **(Figure 24A-E)**. Furthermore, cell cycle analysis using the intercalating dye, 4',6-diamidino 2-phenylindole (DAPI), showed no difference in the percentage of macrophages in S or G2/M mitotic phases, again indicating no difference in the proportion of locally proliferating macrophages **(Figure 24F)**. Overall, these data show that there are more proliferating $CD68^+$ cells in the aortas of smoke exposed mice which contributes to the accumulation of arterial macrophages. However, given this increase is not proportional to lesion size, local proliferation of macrophages is likely not the dominant process driving increased arterial macrophage accumulation following exposure to cigarette smoke.

3.3.5. Recruited monocytes likely contribute to macrophage accumulation in cigarette smoke exposed *Apoe*$^{-/-}$ mice

In order to investigate whether recruited monocytes contribute to the accumulation of macrophages within atherosclerotic lesions of cigarette smoke-exposed mice, we used an approach that involved timed BrdU labelling of cells *in vivo*. Briefly, 3 hours following BrdU administration proliferating cells within their respective tissue compartments are labelled; however, BrdU-labelled monocytes are not detected in the circulation yet. This is because monocytes do not typically proliferate within the bloodstream, and 3 hours is not sufficient time to allow for recently proliferated monocytes to egress from the bone marrow.[83,217,218] However, 24 hours after BrdU administration, BrdU-labelled monocytes are readily detectable in the blood as well as at sites where recruitment of these labelled cells has occurred. This allows us to assess newly acquired arterial macrophages in the absence of labelled monocyte recruitment (3h) and in the presence of labelled monocyte recruitment (24h) with labelling of local proliferation occurring at both time points.

Using this approach, we observed BrdU^{+} monocytes in the blood at 24h but not at 3h in both room air and smoke exposed mice, as expected (**Figure 25A)**. At 3h, in the absence of monocyte recruitment, we observed no difference in BrdU^{+} CD68^{+} co-stained cells **(Figure 25B-C)**. However, at 24h when labelled monocytes are detected in the blood, we also observe an increase in BrdU^{+} CD68^{+} co-stained cells

in the aortas of smoke exposed mice compared to the 3h time point **(Figure 25B-C)**. This would suggest that recruitment of labelled monocytes may contribute to the accumulation of newly acquired arterial macrophages in smoke exposed mice. However, this approach does not allow for clear distinction between increased local proliferation at 24h or increased recruitment of labelled monocytes.

3.3.6. Cigarette smoke exposure increases monocyte recruitment into the aorta.

Therefore, to specifically assess Ly6C^{hi} monocyte recruitment into atherosclerotic lesions of smoke exposed mice, we used a parabiosis model. The surgical joining of mice in parabiosis allows for the establishment of a shared circulation, meaning that circulating immune cells from one mouse can enter the circulation as well as the tissues of the adjoined second mouse, and vice versa. By pairing a CD45.1-expressing *Ldlr-/-* mouse to a second, CD45.2-expressing congenic *Ldlr*$^{-/-}$ mouse, we can determine whether identified leukocytes originated in the host or partner parabiont **(Figure 26A)**. To assess the impact of cigarette smoke on monocyte recruitment to aortic tissue, *Ldlr*$^{-/-}$ parabionts were placed on an atherogenic diet and exposed to either room air or cigarette smoke for 5 weeks **(Figure 26A)**. Parabionts exhibited comparable levels of leukocyte chimerism in the blood or room air and smoke exposed mice **(Figure 26A)**. In particular, no difference was observed in Ly6C^{hi} monocyte chimerism in the blood as assessed by flow cytometry **(Figure 26B)**. There was also no difference in arterial macrophage chimerism as assessed by *en face* immunofluorescent co-staining staining of CD68 and either

CD45.1 or CD45.2 in aortic arches **(Figure 26C)**. As expected, we observed an increase in total $CD68^+$ area in smoke exposed parabionts compared to room air controls **(Figure 26D-E)**. Most importantly, we observed the $CD68^+$ area from partner-derived cells was increased in smoke exposed parabionts, indicating increased monocyte derived arterial macrophages in smoke exposed mice compared to room air controls **(Figure 26F-G)**. Overall, this data provides evidence that monocyte recruitment and differentiation into arterial macrophages is increased in smoke exposed mice, and likely drives the increased accumulation of arterial macrophages.

3.3.7. Endothelial dysfunction is implicated in increased monocyte recruitment, macrophage accumulation, and aneurysm formation in smoke exposed mice

Since monocyte recruitment is dependent on interactions between leukocytes and endothelial cells, we next examined adhesion receptor expression in smoke exposed mice. VCAM-1 has been identified as a key adhesion molecule in atherogenesis, thus we evaluated both VCAM-1 expression is aortas as well as its cognate ligand, VLA-4, on circulating monocytes. Surprisingly, we observed no difference in the total numbers, and a decrease in the proportion, of VLA-4^+ $Ly6C^{hi}$ monocytes in the blood of smoke exposed mice compared to room air controls **(Figure 27A-B)**. However, in contrast, we observed a significant increase in the expression of *Vcam1* mRNA in aortas of smoke exposed mice compared to room air controls **(Figure**

27C). This data suggests that increased recruitment may be due to the impact of cigarette smoke on endothelial cells rather than on circulating monocytes since endothelial dysfunction is characterized by increased adhesion receptor expression.

Given the critical role of nitric oxide in maintaining endothelial function and homeostasis, we next examined endothelial nitric oxide synthase (eNOS) which is major source of endothelial NO. Interestingly, eNOS levels do not differ at 2 weeks, a time point prior to significant changes in macrophage accumulation in smoke exposed mice **(Figure 28A-B)**. However, after 4 weeks of exposure, when arterial macrophages are significantly increased, we observed a significant decrease in eNOS in aortas of smoke exposed mice **(Figure 28D-E)**. This data suggests that macrophage accumulation is specifically increased in the context of endothelial dysfunction.

To determine whether eNOS inhibition can contribute to increased development of arterial disease, we used the nitric oxide synthase inhibitor Nω-Nitro-L-arginine methyl ester hydrochloride (L-NAME). We observed that L-NAME treatment of smoke exposed mice significantly increased accumulation of arterial macrophages in the aortic arch after 2 weeks **(Figure 29A-B)**. Moreover, long term treatment of smoke exposed mice with L-NAME induced abdominal aneurysm in all mice and significantly increased mortality due to aneurysm rupture **(Figure 29C-E)**. These striking observations provide proof of concept that eNOS inhibition can significantly increase arterial pathology and provides evidence that

smoking-associated loss of eNOS likely contributes to increased risk of arterial disease.

3.3.8. Summary of results

In summary, the data presented here demonstrates that cigarette smoke significantly impacts hematopoiesis and is associated with an overall suppression of circulating monocytes and pro-inflammatory cytokines, despite increased development of arterial disease. Furthermore, we show monocyte recruitment in significantly increased following exposure to cigarette smoke and is likely a key kinetic factor underlying the increased accumulation of arterial macrophages. Lastly, we demonstrate eNOS inhibition significantly contributes to arterial pathology which suggests that loss of eNOS following exposure to cigarette smoke likely contributes to smoking-attributed risk of arterial disease development.

CHAPTER 4: DISCUSSION

4.1 SUMMARY OF MAIN FINDINGS

The aim of this thesis is to better understand the pathogenesis of arterial disease with a particular focus on investigating the function and kinetics of monocytes and macrophages following exposure to key risk factors. The data presented here demonstrate that atherogenesis is associated with direct injury to the arterial wall providing experimental evidence for the interrelated pathogenesis of atherosclerosis and aortic aneurysm. Furthermore, we identify arterial macrophage heterogeneity is primarily driven by hypercholesterolemia with cigarette smoke exposure increasing the overall abundance of monocytes and macrophages at sites of arterial disease. Finally, we observe that monocyte-derived arterial macrophages are increased following exposure to cigarette smoke and propose endothelial dysfunction as a likely mechanism contributing to this increased recruitment. Taken together, these data provide novel insight into mechanisms that contribute to smoking-related arterial disease.

4.2 ATHEROSCLEROSIS AND ABDOMINAL AORTIC ANEURYSMS

4.2.1 Model of smoking-dependent aneurysm

Several challenges exist with current experimental models of abdominal aortic aneurysm. One of the commonly highlighted issues is that these models require acute injury of the aorta with clinically irrelevant interventions, which is followed by a resolution phase that is not observed in clinical disease progression.[142,174] Models that do engage relevant risk factors, like hypertension, induce pathology

that is sometimes inconsistent with clinically observed abdominal aneurysms including aortic dissection or aneurysm formation in multiple regions.[174,177]

Here we show that hypercholesterolemia or cigarette smoke alone are insufficient to induce aneurysm formation, but by engaging both of these clinically relevant risk factors, we observe spontaneous formation and rupture of abdominal aortic aneurysm. Importantly, the aneurysms in our model are characterized by increases in both gross and luminal diameters indicating involvement of all three arterial layers. This is a necessary feature of true aneurysms as opposed to pseudoaneurysms that are characterized by aortic dissection or adventitial remodelling alone.[142] Our model also recapitulates several clinically observed features of abdominal aortic aneurysm, including a reduced incidence of aneurysm following smoking cessation.[140,141,151] Furthermore, the incidence of elastin damage, aneurysm formation, and mortality due to rupture increases gradually over the course of smoke exposure highlighting a dose dependent progressive increase in smoking-related risk.[152–155] This is in sharp contrast to current models of aneurysm which feature aneurysm development in most, if not all, treated animals within hours to days of induction and do not show chronic progression.[172–174] Of note, previous models of cigarette smoke-associated aneurysm also do not show progression to rupture.[183,196,197,200] Taken together, these data suggest that our model of smoke-induced aneurysm in hypercholesterolemic mice recapitulates features of clinical epidemiology and disease progression and may provide clearer insight into disease pathogenesis compared to current models.

4.2.2 Atherosclerosis promotes arterial damage

Using this model of smoking induced aneurysm in hypercholesterolemic mice, we observed that atherosclerosis closely associates with regions of aneurysm formation. Specifically, elastin damage predominantly occurred in regions overlaid with atherosclerosis and that the size of atherosclerotic lesions correlated with severity of elastin damage and luminal diameter. Notably, we observed that elastin damage proceeds from the lumen into the media, suggesting elastin degradation proceeds from the interface of the lesion and arterial wall. This is in contrast to other proposed mechanisms suggesting that adventitial macrophages or smooth muscle cells may initiate elastin damage in the earliest stages of aneurysm pathogenesis.[163–165]

To be clear, we do not dispute that other mechanisms may also contribute to abdominal aneurysm formation, including smooth muscle cell apoptosis and production of proinflammatory mediators and proteases by other leukocytes and structural cells. Indeed, the occurrence of abdominal aneurysm in the absence of atherosclerosis or smoking history indisputably verifies the occurrence of alternative pathogenic mechanisms.[142,149,157] We do, however, propose our data provide strong evidence that in the context of abdominal atherosclerosis, components of the atherosclerotic plaque, particularly macrophages, can directly contribute to arterial wall injury and promote the formation of abdominal aortic aneurysms. This data significantly builds upon previous observations of small

abdominal aneurysms in aged hyperlipidemic mice with extensive atherosclerosis.[219] This finding is also particularly relevant given previous observations of increased atherosclerosis in the abdominal aortas of smokers compared to non-smokers in early adulthood.[171] Thus our data support the paradigm that atherosclerosis can directly increase the risk of abdominal aortic aneurysms and provides novel insight into an outstanding question in the field.

4.3 MACROPHAGE POPULATIONS AND KINETICS

4.3.1 Macrophage population insights from scRNA-seq

To date, there have been three scRNA-seq datasets published in experimental models of abdominal aortic aneurysm. One study has been conducted in each of the three major models of aneurysm including elastase-induced and $CaCl_2$-induced aneurysms in C57BL/6J mice and angiotensin II-induced aneurysm in *Apoe*$^{-/-}$ mice.[220–222] All three studies observed an overall increase in macrophages in aneurysmal tissue and identified multiple macrophage populations with distinct transcriptomic profiles. However, similar to earlier studies in atherosclerosis, the number of identified macrophage subsets differ between studies with unclear putative functions for each population. These datasets have not yet been formally compared, thus there is currently no consensus on macrophage populations in aneurysm.

Elastase Model

In the study by Zhao *et al*., aneurysm was induced in C57BL/6J mice by peri-adventitial elastase exposure and scRNA-seq analysis was performed specifically on infra-renal aortas.[220] In this model, macrophages were the largest population of cells in aneurysmal tissue with five distinct monocyte/macrophage clusters. The authors identified two resident-like macrophage populations expressing *Cx3cr1* and *Pfa*, with the smaller cluster also expressing proliferation-associated genes which is consistent with the phenotype of self-renewing arterial resident macrophages.[43,220,223] Interestingly, the authors observed the non-proliferating resident macrophage cluster was decreased in aneurysmal tissue compared to healthy controls, whereas the proliferating resident macrophages were increased. Since elastase-induced aneurysms involve acute injury, this may indicate a pro-resolution mechanism of resident arterial macrophage repopulation following injury as observed in other models of acute inflammation.[43,174]

Another two clusters were identified as monocyte-derived macrophages (*Ccr2*^{hi}, *Ly6c2*^{hi}, *Adgre1*^{hi}, *Itgam, H2-Aa*^{hi}), with one cluster identified as M1 inflammatory (*Ccl2, Ccl3, Cxcl10,* and *Il1b*) and the other as M2 reparative (*Arg1* and *Il10)*. However, the authors recognized that this distinction was not clear as both populations contained cells exhibiting overlapping expression of M1 and M2 markers and acknowledged the need for an improved framework to describe *in vivo* macrophage phenotypes.

Lastly, proinflammatory and proteolytic gene expression (*Ccl2*, *Il1b,* *Mmp14*, *Ctsd,* and *Ctss*) were observed in all macrophage clusters with most clusters exhibiting increased expression in aneurysmal tissue. This observation may indicate involvement of all macrophage clusters in aneurysm pathogenesis or may reflect suboptimal cell clustering. It should be noted that this study primarily used differential gene expression-based analyses and did not employ gene set enrichment tools, which may have contributed to the ambiguous functional profile of some clusters. Overall, Zhao *et al.*, observed the expansion of macrophages in elastase-induced aneurysm with an increase in inflammatory and proteolytic gene expression, as well as the novel identification of proliferating resident arterial macrophages by scRNA-seq.[220]

Calcium Chloride ($CaCl_2$) Model

A recently published brief report also examined macrophage populations by scRNA-seq analysis, but in a model of $CaCl_2$-induced aneurysms in C57BL/6J mice.[221] Yang *et al.*, also report multiple macrophage subsets in aneurysmal tissue; however, this study only identifies three distinct macrophage populations comprising non-inflammatory, proliferating, and inflammatory macrophages. Although overall macrophages were observed to increase in aneurysmal tissue, inflammatory macrophages (*Il1b* and *H2-Ab1*) were the only macrophage subpopulation observed to increase compared to healthy controls. Non-inflammatory (*Pf4* and *Mrc1*) and proliferating (*Mki67*) macrophages were

unchanged but present in both healthy and aneurysmal tissue. KEGG pathway enrichment revealed upregulation of inflammatory and extracellular matrix-degradation pathways in inflammatory macrophages, phagocytosis and efferocytosis pathways in non-inflammatory macrophages, and cell cycle pathways in proliferating macrophages. Similar to Zhao *et al.*, this study also suggests that the cluster of proliferating macrophages are a subset of the non-inflammatory macrophages and are likely representative of resident arterial macrophages.[220,221] Furthermore, histological analysis of aneurysmal tissue confirmed the increase in total macrophages, as well as a 1.5 fold increase in proliferating macrophages, validating the transcriptomic findings.

Of note, the authors identify an atherosclerosis-associated gene expression profile in $CaCl_2$-induced aneurysms despite this model being non-hypercholesterolemic. This may indicate a role for atherosclerosis-associated pathogenic mechanisms in aneurysm induction, even in the absence of defined atherogenesis, which supports finding in our model. Moreover, of the 155 differentially expressed genes in $CaCl_2$-induced aneurysm, osteopontin (*Spp1*) exhibited the largest fold increase in aneurysmal tissue compared to sham, which is consistent with clinical reports of increased osteopontin in the plasma and aortas of abdominal aneurysm patients.[224] Interestingly, we also identified macrophage-associated osteopontin expression in regions of arterial disease in our model of smoking-induced aneurysm. Overall, Yang *et al.*, broadly identified two primary macrophage populations that likely correspond to unchanged resident arterial

macrophages and increased inflammatory macrophages, with an additional cluster representing proliferating resident macrophages in $CaCl_2$-induced aneurysm.

Angiotensin II Model

Unlike the studies in elastase- and $CaCl_2$-induced abdominal aneurysm, the focus of Hadi *et al*., was not on characterizing cellular heterogeneity in aneurysmal tissue.[222] Instead, this study leveraged scRNA-seq analysis of angiotensin II-induced aneurysms in *Apoe*$^{-/-}$ mice, to identify the source of netrin-1 in abdominal aneurysms. In this model, netrin-1 is shown to promote aneurysm formation by stimulating MMP3 activity in vascular smooth muscle cells. Using scRNA-seq, the authors report that macrophages are the predominant source of netrin-1, and further identify that netrin-1 expressing macrophages display a proinflammatory gene expression profile whereas netrin-1 negative macrophages display an anti-inflammatory profile. Of note, the authors show that netrin-1 deficiency in leukocytes, including macrophages, protects against angiotensin II-induced aneurysms. Interestingly, earlier work from this group also demonstrated that netrin-1 deficiency is athero-protective and promotes macrophage egress from atherosclerotic lesions in *Ldlr*$^{-/-}$ mice.[129] In agreement with this finding, Hadi *et al.*, also report netrin-1 deficiency in hematopoietic cells results in reduced accumulation of arterial macrophages following PCSK9-AAV induced hypercholesterolemia. Thus, it is plausible that, in addition to the specific role of netrin-1 in provoking MMP3 activity in vascular smooth muscle cells, the loss of

arterial macrophage accumulation itself may be protective against aneurysm formation in this model. This would be in accordance with our observation of CSF1-dependent arterial macrophage accumulation contributing to elastin damage in the abdominal aorta of smoke exposed mice.

Importantly, although Hadi *et al.*, did not specifically characterize macrophage populations in aneurysm, this study identified both proinflammatory and anti-inflammatory macrophage populations, and demonstrated that loss of a specific molecule expressed by proinflammatory macrophages is associated with improved disease outcomes. Similar to our work, this study provides evidence of the functional contribution of arterial macrophages to the development of aneurysm and highlights the utility of scRNA-seq tools in identifying cellular sources of key pathogenic molecules.

Cigarette Smoke Dependent Model

In our study, we approached characterizing macrophages in cigarette smoke-induced aneurysm in hypercholesterolemic mice using an established framework of arterial macrophage populations. The profiles of these macrophages are based on a consolidated review of high dimensional datasets from *in vivo* models of atherosclerosis.[109] In agreement with other recently published scRNA-seq datasets in murine models of atherosclerosis, we observe increased diversity in macrophage populations in hypercholesterolemic aortas compared to aortas from mice with normal cholesterol levels.[109] Specifically, we observe a decrease in resident like

macrophages and an increase in Trem2 foamy macrophages, inflammatory macrophages, and IFN-inducible macrophages which are associated with inflammation and tissue remodelling. In our model of cigarette smoke induced aneurysm, we do not observe a significant difference in these macrophage populations, although we do observe an overall increase in the abundance of Ly6C^{hi} monocytes and total arterial macrophages. Thus, exposure to cigarette smoke does not alter the types of macrophages present in hypercholesterolemic aortas but does increase their accumulation. Extending these observations, we show that CSF1-dependent accumulation of arterial macrophages plays a critical role in mediating elastin damage in the abdominal aorta of smoke exposed mice. Therefore, we report for the first time, consensus-defined, arterial macrophage populations in a model of smoking-induced abdominal aortic aneurysm providing clearer insight into the diversity of macrophages in aneurysmal tissue and their putative functions.

Insights from Atherosclerosis Models

Investigating the diversity of macrophages in arterial disease is a complex task that will require revision and refinement as more data and increasingly powerful analytical tools become available. This is evidenced by the recent meta-analysis of scRNA-seq and CyTOF datasets from multiple models of atherosclerosis.[109] Individually, these studies generated high dimensional datasets clearly identifying multiple macrophage populations in hypercholesterolemic aortas. However, the number of populations and annotated functional roles varied between studies with

inconsistencies in nomenclature and gene signatures.[110–112,114–116] By combining and reanalyzing these datasets together and individually, Zernecke *et al*., were able to identify five 5 macrophage populations by scRNA-seq, three of which map to CyTOF-defined populations.[109] Together, these studies provide strong evidence for the presence of resident macrophages, Trem2 foamy macrophages, and inflammatory macrophages in atherosclerosis, which we also identified in aneurysmal tissue. Going forward, this meta-analysis provides a clearer framework to build further investigations into the contribution of these subsets to protective or pathogenic processes in atherosclerosis and potentially other arterial diseases.

Summary

Including data presented in this thesis, four studies to date have examined arterial macrophage populations in models of abdominal aortic aneurysm using scRNA-seq based tools. However, each study used a distinct model of aneurysm induction and different approaches to identify unique macrophage clusters.[220–222] Despite these dissimilar parameters, a few consistent findings have been reported including the general increase of arterial macrophages in aneurysmal tissue, as well as the presence of multiple macrophage subsets comprising at least one non-inflammatory or resident-like population and one inflammatory population. Two studies have also identified a cluster of proliferating resident-like macrophages that are increased in aneurysmal tissue. However, both these studies employ acute injury models of aneurysm induction, so this population may represent a pro-resolution response that

is uncharacteristic of chronic disease progression. Our study is the first to report on aneurysmal macrophage populations based on a consolidated framework of unique cellular profiles identified across multiple high dimensional datasets in arterial disease. Of note, our model of smoking induced aneurysms is dependent on atherosclerosis and did not differ significantly from non-aneurysmal hypercholesterolemic aortas. Going forward, it will be of interest to systematically compare macrophage populations across aneurysm models and in human disease to better delineate conserved macrophage populations and support future functional and mechanistic investigations.

4.3.2 Kinetics of systemic versus local inflammation

Cigarette smoking is associated with a number of acute and chronic inflammatory diseases and, as such, is often thought of as a pro-inflammatory stimulus.[188] However, a more accurate description is that exposure to cigarette smoke has immunomodulatory properties including both proinflammatory and immunosuppressive effects.[225] Our group has published several studies reporting on this multifaceted impact of cigarette smoke on respiratory immune responses, and here we report for the first time the impact of cigarette smoke on systemic and local inflammation in arterial disease.[226–232]

Suppressed monopoiesis

Hypercholesterolemia is known to induce monocytosis with the increase in Ly6C^{hi} monocytes being progressive and proportional to the extent of atherosclerosis.[81,90]

In fact, hypercholesterolemia has specifically been shown to activate hematopoietic stem and progenitor cells and skew them towards a Ly6C^{hi} monocyte-biased differentiation, contributing to monocytosis.[233,234] Thus our observation that cigarette smoke exposure is associated with a general decrease in most bone marrow progenitor cells, as well as circulating leukocytes, was unexpected. In particular, the reduction in circulating Ly6C^{hi} monocytes in the context of significantly more arterial disease was surprising.

To better understand the cellular kinetics underlying this decrease in monocytes, we assessed the kinetics of monocyte progenitor cells in the bone marrow. In particular, we quantified cell death and proliferation in bone marrow hematopoietic cells, as well as newly generated monocyte egress and turnover in the blood. Overall, we observed similar rates of proliferation, egress, and monocyte turnover in smoke exposed mice compared to room air controls, suggesting that cigarette smoke does not significantly impact these factors. However, we did observe increased apoptosis in monocyte precursors in the bone marrow, which likely contributes to the overall decrease in mature monocyte production.

An interesting avenue for future investigations will be to determine whether, in addition to survival, exposure to cigarette smoke can impact the differentiation potential of progenitor cells, or even prime progenitor cells in a manner that influences the downstream function of mature myeloid cells in arterial disease. There is evidence that cigarette smoke exposure can impact engraftment of HSPCs

and stem cell niche cells; however, there is much that remains unknown regarding the impact of cigarette smoke on hematopoiesis.[235] Pursuit of these questions may provide further insight into the apparent discrepancy between suppressed monopoiesis and reduction in circulating proinflammatory mediators with concurrent enhanced arterial tissue inflammation observed following exposure to cigarette smoke.

Local proliferation

Another major factor that can contribute to macrophage accumulation in arterial tissue is local proliferation.[43,79] Given the observed decrease in both circulating monocytes and proinflammatory cytokines, we initially hypothesized that arterial macrophage accumulation was driven by local proliferation. At early time points we observed no difference in proliferating macrophages within atherosclerotic lesions, but at later time points we observe a significant increase in the total number of proliferating macrophages in atherosclerotic lesions. However, at this time point, we also observe a significant increase in the total size of lesions in cigarette smoke exposed mice, which may account for the observed difference in proliferating cells. Therefore, we also assessed proliferating cells as a proportion of total macrophages and observed either no difference or a significant reduction of proliferating cells in smoke exposed aortas. If proliferation was the driving factor for the accumulation of arterial macrophages, we would expect the proportion of proliferating cells in atherosclerotic lesions to be increased following smoke exposure. Furthermore,

given that we begin the see increased lesions at early time points, we would also expect to see differential proliferation at this point. Therefore, our data suggests that although proliferation may contribute to the accumulation of cells following exposure to cigarette smoke, it is likely not the dominant factor for smoking-induced accumulation of arterial macrophages.

Monocyte recruitment

Since monocyte recruitment is critical for early atherogenesis and is another factor that can contribute to a decrease in circulating monocytes, we assessed the impact of smoke exposure on monocyte recruitment. Using a model of parabiosis we were able to investigate the contribution of partner-derived (recruited) cells to lesional macrophages following exposure to cigarette smoke. In this model, we observed similar levels of chimerism in blood leukocytes and arterial macrophages, indicating rapid cellular turnover that is dependent on recruitment which is consistent with previous studies during early atherogenesis.[79,83,218] Importantly, we observed a significant increase in total partner-derived macrophages in smoke exposed mice demonstrating that monocyte recruitment to the aorta is increased following exposure to cigarette smoke. Interestingly, other models of aneurysm have also identified a critical role for monocyte recruitment, but with a focus on adventitial macrophages.[215,236,237] Here we show monocyte recruitment to intimal lesions can also drive arterial macrophage accumulation leading to subsequent elastin damage and increased risk of aneurysm.

Our next focus was to investigate mechanisms underlying increased monocyte recruitment in the context of smoke exposure. Since adhesion receptor interactions are critical to immune cell extravasation, we first assessed the expression of VLA-4 on circulating monocytes and its cognate adhesion molecule, *Vcam1* in arterial tissue. Although many receptor ligand interactions can be involved in leukocyte extravasation, VCAM-1 has been identified as a key adhesion molecule in atherogenesis.[85] We found that smoke exposure did not increase adhesion receptor expression on circulating monocytes, but did increase *Vcam1* expression in aortas suggesting increased expression of VCAM-1 on endothelial cells may be contributing to increased monocyte recruitment to sites of arterial disease.

Of note, increased adhesion receptor expression on endothelial cells is a marker of endothelial dysfunction and has been shown to be induced by cigarette smoke components *in vitro*.[67–69,238] A major regulator of endothelial homeostasis is NO which is mainly produced by eNOS in healthy vasculature and has been shown to be dysregulated in the context of endothelial dysfunction.[239–241] Cigarette smoke has been shown to dysregulate eNOS function *in vitro* and was recently reported to do so *in vivo* as well.[193–195] Thus, we assessed eNOS expression in aortas and found that eNOS was decreased in smoke exposed mice specifically at time points where increased arterial macrophage accumulation is observed. Furthermore, we observed that *in vivo* inhibition of nitric oxide synthases resulted in increased accumulation of arterial macrophages at early time points, with prolonged inhibition resulting in

aneurysm formation and rupture. These observations provide a proof-of-concept that loss of eNOS contributes to arterial pathologies associated with smoke exposure in our model. Of note, although we used a pan nitric oxide synthase inhibitor in our study, previous studies have shown that genetic deletion or dysregulated expression of eNOS specifically is associated with increased atherosclerosis and aneurysm formation.[242–244] Therefore, smoking-associated loss of eNOS is a plausible mechanism contributing to endothelial dysfunction, increased adhesion receptor expression, and immune cell recruitment in arterial disease.

Summary

Here we show hypercholesterolemia determines the heterogeneity of macrophages with smoke exposure increasing abundance of arterial macrophages through increased monocyte recruitment. Alternative models of aneurysm have identified varying populations of macrophages; however, most models consistently identify a resident-like non-inflammatory population and an inflammatory macrophage population in aneurysmal tissue. Similar to our observations, resident populations appear to be reduced or unchanged following induction of arterial pathology, with an increase in inflammatory and/or proteolytic populations. We show that, despite suppressed monopoiesis, smoke exposure is associated with increased local inflammation characterized by increased monocyte recruitment. Importantly, in contrast to current paradigms focused on adventitial macrophages in aneurysm, our

data suggest accumulation of intimal macrophages can also promote aneurysm formation.[142,215,236,237] Lastly, we provide evidence that endothelial dysfunction likely contributes to smoking-attributed risk of arterial pathologies. Overall, better understanding macrophage population and kinetics can help identify specific pathogenic and protective functions and may ultimately provide refined targets for therapeutic intervention.

4.3 LIMITATIONS AND FUTURE DIRECTIONS

One of the major limitations of our experimental approach was focusing on a single model of smoking induced aneurysm in hypercholesterolemic mice. Although this model has the potential to better model certain aspects of abdominal aortic aneurysm pathogenesis, it also likely fails to recapitulate all aspects of human disease. This pitfall is common to all current models of abdominal aortic aneurysm, and could potentially be improved by pursuing investigations in multiple aneurysm models.[142,174] This would allow for identification of phenotypes that are conserved and reproducible across models, such as the influx of immune cells and degradation of extracellular matrix common in all aneurysm models as well as human disease.

An avenue of exploration that would significantly extend our findings presented here, is a meta-analysis of scRNA-seq-defined arterial macrophage populations in aneurysm models. Given the framework provided by Zernecke *et al.*, this analysis has the potential to improve our understanding of macrophage heterogeneity in aneurysmal disease as well as facilitating comparisons to those in

atherosclerosis. This would provide insight into potentially conserved macrophage populations in arterial disease and improve the likelihood of accurately translating these profiles to human disease. Although, it should also be acknowledged that a major limitation of our study was the reliance on transcriptomic approaches to identify macrophage heterogeneity and putative function in arterial disease. Although scRNA-seq provides an unparalleled tool for unbiased identification of unique cell clusters, gene expression data does not always translate to differences in protein expression or cell function. Thus, complementary approaches leveraging protein-based tools, such as CyTOF or multiplexed ion beam imaging (MIBI), would help validate our findings and provide a stronger foundation for future mechanistic research and functional studies.

Notably, our work identified the capacity for atherosclerotic lesions to directly promote arterial injury thus increasing the risk for abdominal aortic aneurysms. Given that smokers have been observed to develop increased abdominal atherosclerosis in early adulthood, this may provide insight into one aspect of smoking-associated risk of abdominal aortic aneurysms.[171] Currently, treatment options for abdominal aneurysms are limited to surgical intervention and screening at risk populations.[136–139] Notably, the efficacy of proactive population screening has been questioned given the large scope of individuals defined as at-risk compared to the incidence of disease.[245,246] Thus, refining the parameters defining at risk individuals may help improve the efficiency and cost of these screening programs and address a current clinical challenge. Our data suggest that identifying

whether the presence of abdominal atherosclerosis can better predict aneurysm outcomes in smokers would help address this unmet clinical need.

4.4 CONCLUDING REMARKS

The work presented in this thesis has furthered our understanding of the impact of cigarette smoke on the development of arterial disease with specific insight into the kinetics and function of arterial macrophages. Data presented in chapter 3.1 establish a model of smoking-induced abdominal aortic aneurysm and illustrate a significant association between atherogenesis and aneurysm pathology. The clinical relevance of atherosclerosis to the development of abdominal aneurysms is currently debated, and our study provides evidence that atherosclerosis significantly increases the risk of developing abdominal aortic aneurysm in the context of exposure to cigarette smoke. This study supports the utility of clinical investigation focused on identifying aneurysm outcomes specifically in smokers exhibiting abdominal atherosclerosis. In chapter 3.2 we identified hypercholesterolemia drives macrophage heterogeneity with an increase in macrophages associated with inflammation and tissue remodelling. Of note, we observe that exposure to cigarette smoke does not change the composition of these macrophages but, instead, increases their overall abundance. These data suggest that cigarette smoke does not impact macrophage function, but rather influences the kinetics contributing to increased tissue inflammation and disease progression. We addressed this question in chapter 3.3 where we identify that exposure to cigarette smoke increases monocyte recruitment despite suppressed monopoiesis and reduced systemic

mediators of inflammation. We suggest that endothelial dysfunction induced through loss of eNOS-mediated regulation likely contributes to the increased local inflammation observed in arterial tissue following exposure to cigarette smoke. These findings emphasize the differential impact of cigarette smoke on systemic and local tissue inflammatory processes and provide the foundation for several interesting avenues of further investigation. Overall, this study highlights the impact of cigarette smoke on macrophage function and kinetics and advances our understanding of smoking-attributed increased risk of arterial disease.

CHAPTER 5: REFERENCES

1. Lozano, R. *et al.* Global and regional mortality from 235 causes of death for 20 age groups in 1990 and 2010: a systematic analysis for the Global Burden of Disease Study 2010. *Lancet* **380**, 2095–128 (2012).

2. Thomas, H. *et al.* Global Atlas of Cardiovascular Disease 2000-2016: The Path to Prevention and Control. *Glob. Heart* **13**, 143–163 (2018).

3. Moran, A. E. *et al.* The global burden of ischemic heart disease in 1990 and 2010: The global burden of disease 2010 study. *Circulation* **129**, 1493–1501 (2014).

4. Kuivaniemi, H., Ryer, E. J., Elmore, J. R. & Tromp, G. Understanding the pathogenesis of abdominal aortic aneurysms. *Expert Rev. Cardiovasc. Ther.* **13**, 975–87 (2015).

5. Libby, P. *et al.* Atherosclerosis. *Nat. Rev. Dis. Prim.* **5**, 1–18 (2019).

6. Libby, P., Lichtman, A. H. & Hansson, G. K. Immune effector mechanisms implicated in atherosclerosis: from mice to humans. *Immunity* **38**, 1092–104 (2013).

7. Weber, C. & Noels, H. Atherosclerosis: current pathogenesis and therapeutic options. *Nat. Med.* **17**, 1410–22 (2011).

8. Fayad, Z. A. *et al.* Monocyte and Macrophage Dynamics in the Cardiovascular System. *J. Am. Coll. Cardiol.* **72**, 2198–2212 (2018).

9. Arnett, D. K. *et al.* 2019 ACC/AHA Guideline on the Primary Prevention of Cardiovascular Disease: A Report of the American College of Cardiology/American Heart Association Task Force on Clinical Practice Guidelines. *Circulation* **140**, e596–e646 (2019).

10. Ference, B. A. *et al.* Low-density lipoproteins cause atherosclerotic cardiovascular disease. 1. Evidence from genetic, epidemiologic, and clinical studies. A consensus statement fromthe European Atherosclerosis Society Consensus Panel. *Eur. Heart J.* **38**, 2459–2472 (2017).

11. Moran, A. E., Roth, G. A., Narula, J. & Mensah, G. A. 1990-2010 Global Cardiovascular Disease Atlas. *Glob. Heart* **9**, 3–16 (2014).

12. Carmena, R., Duriez, P. & Fruchart, J. C. Atherogenic lipoprotein particles in atherosclerosis. *Circulation* **109**, (2004).

13. Ouimet, M., Barrett, T. J. & Fisher, E. A. HDL and reverse cholesterol transport: Basic mechanisms and their roles in vascular health and disease.

Circ. Res. **124**, 1505–1518 (2019).

14. Goldstein, J. L. & Brown, M. S. A century of cholesterol and coronaries: From plaques to genes to statins. *Cell* **161**, 161–172 (2015).

15. Baigent, C. *et al.* Efficacy and safety of more intensive lowering of LDL cholesterol: A meta-analysis of data from 170 000 participants in 26 randomised trials. *Lancet* **376**, 1670–1681 (2010).

16. Bucher, N. L. R., Overath, P. & Lynen, F. β-hydroxy-β-methylglutaryl coenzyme a reductase, cleavage and condensing enzymes in relation to cholesterol formation in rat liver. *BBA - Biochim. Biophys. Acta* **40**, 491–501 (1960).

17. Endo, A., Kuroda, M. & Tanzawa, K. Competitive inhibition of 3-hydroxy-3-methylglutaryl coenzyme a reductase by ML-236A and ML-236B fungal metabolites, having hypocholesterolemic activity. *FEBS Lett.* **72**, 323–326 (1976).

18. Vega, G. L. & Grundy, S. M. Influence of lovastatin therapy on metabolism of low density lipoproteins in mixed hyperlipidaemia. *J. Intern. Med.* **230**, 341–350 (1991).

19. Mabuchi, H. *et al.* Effects of an Inhibitor of 3-Hydroxy-3-Methylglutaryl Coenzyme a Reductase on Serum Lipoproteins and Ubiquinone-10 Levels in Patients with Familial Hypercholesterolemia. *N. Engl. J. Med.* **305**, 478–482 (1981).

20. Uauy, R., Vega, G. L., Grundy, S. M. & Bilheimer, D. M. Lovastatin therapy in receptor-negative homozygous familial hypercholesterolemia: Lack of effect on low-density lipoprotein concentrations or turnover. *J. Pediatr.* **113**, 387–392 (1988).

21. Cannon, C. P. *et al.* Ezetimibe Added to Statin Therapy after Acute Coronary Syndromes. *N. Engl. J. Med.* **372**, 2387–2397 (2015).

22. Cohen, J. C., Boerwinkle, E., Mosley, T. H. & Hobbs, H. H. Sequence Variations in PCSK9, Low LDL, and Protection against Coronary Heart Disease . *N. Engl. J. Med.* **354**, 1264–1272 (2006).

23. Abifadel, M. *et al.* Mutations in PCSK9 cause autosomal dominant hypercholesterolemia. *Nat. Genet.* **34**, 154–156 (2003).

24. Nicholls, S. J. *et al.* Effect of evolocumab on progression of coronary disease in statin-treated patients: The GLAGOV randomized clinical trial. *JAMA - J. Am. Med. Assoc.* **316**, 2373–2384 (2016).

25. Sabatine, M. S. *et al.* Evolocumab and Clinical Outcomes in Patients with Cardiovascular Disease. *N. Engl. J. Med.* **376**, 1713–1722 (2017).

26. Robinson, J. G. *et al.* Efficacy and Safety of Alirocumab in Reducing Lipids and Cardiovascular Events. *N. Engl. J. Med.* **372**, 1489–1499 (2015).

27. Ridker, P. M., Hennekens, C. H., Buring, J. E. & Rifai, N. C-Reactive Protein and Other Markers of Inflammation in the Prediction of Cardiovascular Disease in Women. *N. Engl. J. Med.* **342**, 836–843 (2000).

28. Ridker, P. M., Cushman, M., Stampfer, M. J., Tracy, R. P. & Hennekens, C. H. Inflammation, Aspirin, and the Risk of Cardiovascular Disease in Apparently Healthy Men. *N. Engl. J. Med.* **336**, 973–979 (1997).

29. Ridker, P. M. *et al.* Inflammation, Pravastatin, and the Risk of Coronary Events After Myocardial Infarction in Patients With Average Cholesterol Levels. *Circulation* **98**, 839–844 (1998).

30. Geovanini, G. R. & Libby, P. Atherosclerosis and inflammation: overview and updates. *Clin. Sci.* **132**, 1243–1252 (2018).

31. Ridker, P. M., Kastelein, J. J. P., Genest, J. & Koenig, W. C-reactive protein and cholesterol are equally strong predictors of cardiovascular risk and both are important for quality clinical care. *Eur. Heart J.* **34**, 1258–1261 (2013).

32. Ridker, P. M. *et al.* Rosuvastatin to Prevent Vascular Events in Men and Women with Elevated C-Reactive Protein. *N. Engl. J. Med.* **359**, 2195–2207 (2008).

33. Ridker, P. M. *et al.* Antiinflammatory Therapy with Canakinumab for Atherosclerotic Disease. *N. Engl. J. Med.* **377**, 1119–1131 (2017).

34. Ridker, P. M. *et al.* Relationship of C-reactive protein reduction to cardiovascular event reduction following treatment with canakinumab: a secondary analysis from the CANTOS randomised controlled trial. *Lancet* **391**, 319–328 (2018).

35. Ridker, P. M. *et al.* Modulation of the interleukin-6 signalling pathway and incidence rates of atherosclerotic events and all-cause mortality: Analyses from the Canakinumab Anti-Inflammatory Thrombosis Outcomes Study (CANTOS). *Eur. Heart J.* **39**, 3499–3507 (2018).

36. Ridker, P. M. *et al.* Low-Dose Methotrexate for the Prevention of Atherosclerotic Events. *N. Engl. J. Med.* **380**, 752–762 (2019).

37. Mons, U. *et al.* Impact of smoking and smoking cessation on cardiovascular events and mortality among older adults: Meta-analysis of Individual participant data from prospective cohort studies of the CHANCES consortium. *BMJ* **350**, (2015).

38. Dawber, T. R. *et al.* Some factors associated with the development of coronary heart disease: six years' follow-up experience in the Framingham study. *Am. J. Public Health* **49**, 1349–1356 (1959).

39. Hammond, E. C. & Horn, D. The relationship between human smoking habits and death rates: A follow-up study of 187,766 men. *J. Am. Med. Assoc.* **155**, 1316–1328 (1954).

40. Burke, G. M., Genuardi, M., Shappell, H., D'Agostino, R. B. & Magnani, J. W. Temporal Associations Between Smoking and Cardiovascular Disease, 1971 to 2006 (from the Framingham Heart Study). *Am. J. Cardiol.* **120**, 1787–1791 (2017).

41. Tsamis, A., Krawiec, J. T. & Vorp, D. A. Elastin and collagen fibre microstructure of the human aorta in ageing and disease: a review. *J. R. Soc. Interface* **10**, 20121004 (2013).

42. Williams, J. W. *et al.* Limited proliferation capacity of aortic intima resident macrophages requires monocyte recruitment for atherosclerotic plaque progression. *Nat. Immunol.* **21**, 1194–1204 (2020).

43. Ensan, S. *et al.* Self-renewing resident arterial macrophages arise from embryonic CX3CR1(+) precursors and circulating monocytes immediately after birth. *Nat. Immunol.* **17**, 159–68 (2016).

44. Bennett, M. R., Sinha, S. & Owens, G. K. Vascular Smooth Muscle Cells in Atherosclerosis. *Circ. Res.* **118**, 692–702 (2016).

45. Plump, A. S. *et al.* Severe hypercholesterolemia and atherosclerosis in apolipoprotein E-deficient mice created by homologous recombination in ES cells. *Cell* **71**, 343–353 (1992).

46. Getz, G. S. & Reardon, C. A. Animal Models of Atherosclerosis. *Arterioscler. Thromb. Vasc. Biol.* **32**, 1104–1115 (2012).

47. Dansky, H. M., Charlton, S. A., Harper, M. M. & Smith, J. D. T and B lymphocytes play a minor role in atherosclerotic plaque formation in the apolipoprotein E-deficient mouse. *Proc. Natl. Acad. Sci. U. S. A.* **94**, 4642–6 (1997).

48. Nakashima, Y., Plump, A. S., Raines, E. W., Breslow, J. L. & Ross, R. ApoE-deficient mice develop lesions of all phases of atherosclerosis

throughout the arterial tree. *Arterioscler. Thromb. a J. Vasc. Biol.* **14**, 133–40 (1994).

49. Borén, J. & Williams, K. J. The central role of arterial retention of cholesterol-rich apolipoprotein-B-containing lipoproteins in the pathogenesis of atherosclerosis: a triumph of simplicity. *Curr. Opin. Lipidol.* **27**, 473–483 (2016).

50. Williams, K. J. & Tabas, I. The response-to-retention hypothesis of early atherogenesis. *Arteriosclerosis, Thrombosis, and Vascular Biology* **15**, 551–562 (1995).

51. Ross, R. & Glomset, J. A. The pathogenesis of atherosclerosis (first of two parts). *N. Engl. J. Med.* **295**, 369–77 (1976).

52. Ross, R. & Glomset, J. A. The pathogenesis of atherosclerosis (second of two parts). *N. Engl. J. Med.* **295**, 420–5 (1976).

53. Stary, H. C. *et al.* A definition of initial, fatty streak, and intermediate lesions of atherosclerosis: A report from the committee on vascular lesions of the council on arteriosclerosis, American Heart Association. *Arterioscler. Thromb.* **14**, 840–856 (1994).

54. Stary, H. C. *et al.* A definition of advanced types of atherosclerotic lesions and a histological classification of atherosclerosis: A report from the Committee on Vascular Lesions of the council on arteriosclerosis, American heart association. *Circulation* **92**, 1355–1374 (1995).

55. Gimbrone, M. A. & García-Cardeña, G. Endothelial Cell Dysfunction and the Pathobiology of Atherosclerosis. *Circ. Res.* **118**, 620–636 (2016).

56. Kwon, G. P., Schroeder, J. L., Amar, M. J., Remaley, A. T. & Balaban, R. S. Contribution of macromolecular structure to the retention of low-density lipoprotein at arterial branch points. *Circulation* **117**, 2919–27 (2008).

57. Skålén, K. *et al.* Subendothelial retention of atherogenic lipoproteins in early atherosclerosis. *Nature* **417**, 750–754 (2002).

58. Schwenke, D. C. & Carew, T. E. Initiation of atherosclerotic lesions in cholesterol-fed rabbits. II. Selective retention of LDL vs. selective increases in LDL permeability in susceptible sites of arteries. *Arteriosclerosis* **9**, 908–918 (1989).

59. Paulson, K. E. *et al.* Resident intimal dendritic cells accumulate lipid and contribute to the initiation of atherosclerosis. *Circ. Res.* **106**, 383–90 (2010).

60. Cybulsky, M. I., Cheong, C. & Robbins, C. S. Macrophages and Dendritic Cells: Partners in Atherogenesis. *Circ. Res.* **118**, 637–652 (2016).

61. Bochkov, V. N. *et al.* Generation and biological activities of oxidized phospholipids. *Antioxid. Redox Signal.* **12**, 1009–59 (2010).

62. Miller, Y. I. *et al.* Oxidation-specific epitopes are danger-associated molecular patterns recognized by pattern recognition receptors of innate immunity. *Circ. Res.* **108**, 235–48 (2011).

63. Dai, G. *et al.* Distinct endothelial phenotypes evoked by arterial waveforms derived from atherosclerosis-susceptible and -resistant regions of human vasculature. *Proc. Natl. Acad. Sci. U. S. A.* **101**, 14871–14876 (2004).

64. Chatzizisis, Y. S. *et al.* Role of Endothelial Shear Stress in the Natural History of Coronary Atherosclerosis and Vascular Remodeling. Molecular, Cellular, and Vascular Behavior. *Journal of the American College of Cardiology* **49**, 2379–2393 (2007).

65. Lee, S. *et al.* A role for NADPH oxidase 4 in the activation of vascular endothelial cells by oxidized phospholipids. *Free Radic. Biol. Med.* **47**, 145–151 (2009).

66. Huber, J. *et al.* Oxidized Membrane Vesicles and Blebs From Apoptotic Cells Contain Biologically Active Oxidized Phospholipids That Induce Monocyte-Endothelial Interactions. *Arterioscler. Thromb. Vasc. Biol.* **22**, 101–107 (2002).

67. Makwana, O. *et al.* Impact of cigarette versus electronic cigarette aerosol conditioned media on aortic endothelial cells in a microfluidic cardiovascular model. *Sci. Rep.* **11**, 4747 (2021).

68. Shen, Y., Rattan, V., Sultana, C. & Kalra, V. K. Cigarette smoke condensate-induced adhesion molecule expression and transendothelial migration of monocytes. *Am. J. Physiol. - Hear. Circ. Physiol.* **270**, (1996).

69. Ueno, H., Pradhan, S., Schlessel, D., Hirasawa, H. & Sumpio, B. Nicotine Enhances Human Vascular Endothelial Cell Expression of ICAM-1 and VCAM-1 via Protein Kinase C, p38 Mitogen-Activated Protein Kinase, NF-kappaB, and AP-1. *Cardiovasc. Toxicol.* **6**, (2006).

70. Moore, K. J., Sheedy, F. J. & Fisher, E. A. Macrophages in atherosclerosis: a dynamic balance. *Nat. Rev. Immunol.* **13**, 709–21 (2013).

71. Hilgendorf, I., Swirski, F. K. & Robbins, C. S. Monocyte Fate in Atherosclerosis. *Arterioscler. Thromb. Vasc. Biol.* **35**, 272–280 (2015).

72. Tabas, I. & Bornfeldt, K. E. Macrophage Phenotype and Function in Different Stages of Atherosclerosis. *Circ. Res.* **118**, 653–667 (2016).

73. Goo, Y.-H., Son, S.-H., Kreienberg, P. B. & Paul, A. Novel Lipid Droplet-Associated Serine Hydrolase Regulates Macrophage Cholesterol Mobilization. *Arterioscler. Thromb. Vasc. Biol.* **34**, 386–396 (2014).

74. Fisher, E. A., Feig, J. E., Hewing, B., Hazen, S. L. & Smith, J. D. High-density lipoprotein function, dysfunction, and reverse cholesterol transport. *Arterioscler. Thromb. Vasc. Biol.* **32**, 2813–20 (2012).

75. Duewell, P. *et al.* NLRP3 inflammasomes are required for atherogenesis and activated by cholesterol crystals. *Nature* **464**, 1357–1361 (2010).

76. Kellner-Weibel, G. *et al.* Crystallization of free cholesterol in model macrophage foam cells. *Arterioscler. Thromb. Vasc. Biol.* **19**, 1891–1898 (1999).

77. Freigang, S. *et al.* Fatty acid-induced mitochondrial uncoupling elicits inflammasome-independent IL-1α and sterile vascular inflammation in atherosclerosis. *Nat. Immunol.* **14**, 1045–53 (2013).

78. Westerterp, M. *et al.* Cholesterol efflux pathways suppress inflammasome activation, NETosis, and atherogenesis. *Circulation* **138**, 898–912 (2018).

79. Robbins, C. S. *et al.* Local proliferation dominates lesional macrophage accumulation in atherosclerosis. *Nat. Med.* **19**, 1166–1172 (2013).

80. Combadière, C. *et al.* Combined inhibition of CCL2, CX3CR1, and CCR5 abrogates Ly6C(hi) and Ly6C(lo) monocytosis and almost abolishes atherosclerosis in hypercholesterolemic mice. *Circulation* **117**, 1649–57 (2008).

81. Swirski, F. K. *et al.* Monocyte accumulation in mouse atherogenesis is progressive and proportional to extent of disease. *Proc. Natl. Acad. Sci.* **103**, 10340–10345 (2006).

82. Nakashima, Y., Raines, E. W., Plump, A. S., Breslow, J. L. & Ross, R. Upregulation of VCAM-1 and ICAM-1 at atherosclerosis-prone sites on the endothelium in the ApoE-deficient mouse. *Arterioscler. Thromb. Vasc. Biol.* **18**, 842–51 (1998).

83. Jongstra-Bilen, J. *et al.* Low-grade chronic inflammation in regions of the normal mouse arterial intima predisposed to atherosclerosis. *J. Exp. Med.* **203**, 2073–2083 (2006).

84. Iiyama, K. *et al.* Patterns of vascular cell adhesion molecule-1 and

intercellular adhesion molecule-1 expression in rabbit and mouse atherosclerotic lesions and at sites predisposed to lesion formation. *Circ. Res.* **85**, 199–207 (1999).

85. Galkina, E. & Ley, K. Vascular Adhesion Molecules in Atherosclerosis. *Arterioscler. Thromb. Vasc. Biol.* **27**, 2292–2301 (2007).

86. Tacke, F. *et al.* Monocyte subsets differentially employ CCR2, CCR5, and CX3CR1 to accumulate within atherosclerotic plaques. *J. Clin. Invest.* **117**, 185–194 (2007).

87. Soehnlein, O. *et al.* Distinct functions of chemokine receptor axes in the atherogenic mobilization and recruitment of classical monocytes. *EMBO Mol. Med.* **5**, 471–81 (2013).

88. Guo, J. *et al.* Repopulation of Apolipoprotein E Knockout Mice With CCR2-Deficient Bone Marrow Progenitor Cells Does Not Inhibit Ongoing Atherosclerotic Lesion Development. *Arterioscler. Thromb. Vasc. Biol.* **25**, 1014–1019 (2005).

89. Boring, L., Gosling, J., Cleary, M. & Charo, I. F. Decreased lesion formation in CCR2-/- mice reveals a role for chemokines in the initiation of atherosclerosis. *Nature* **394**, 894–7 (1998).

90. Swirski, F. K. *et al.* Ly-6Chi monocytes dominate hypercholesterolemia-associated monocytosis and give rise to macrophages in atheromata. *J. Clin. Invest.* **117**, 195–205 (2007).

91. Gautier, E. L. *et al.* Macrophage apoptosis exerts divergent effects on atherogenesis as a function of lesion stage. *Circulation* **119**, 1795–804 (2009).

92. Akhtar, S., Gremse, F., Kiessling, F., Weber, C. & Schober, A. CXCL12 promotes the stabilization of atherosclerotic lesions mediated by smooth muscle progenitor cells in Apoe-deficient mice. *Arterioscler. Thromb. Vasc. Biol.* **33**, 679–86 (2013).

93. Feil, S. *et al.* Transdifferentiation of vascular smooth muscle cells to macrophage-like cells during atherogenesis. *Circ. Res.* **115**, 662–667 (2014).

94. Shankman, L. S. *et al.* KLF4-dependent phenotypic modulation of smooth muscle cells has a key role in atherosclerotic plaque pathogenesis. *Nat. Med.* **21**, 628–637 (2015).

95. Aikawa, E. *et al.* Osteogenesis associates with inflammation in early-stage atherosclerosis evaluated by molecular imaging in vivo. *Circulation* **116**,

2841–2850 (2007).

96. Abdelbaky, A. *et al.* Focal arterial inflammation precedes subsequent calcification in the same location: A longitudinal FDG-PET/CT study. *Circ. Cardiovasc. Imaging* **6**, 747–754 (2013).

97. Sage, A. P., Tintut, Y. & Demer, L. L. Regulatory mechanisms in vascular calcification. *Nature Reviews Cardiology* **7**, 528–536 (2010).

98. Rattazzi, M. *et al.* Calcification of Advanced Atherosclerotic Lesions in the Innominate Arteries of ApoE-Deficient Mice. *Arterioscler. Thromb. Vasc. Biol.* **25**, (2005).

99. Johnson, R. C., Leopold, J. A. & Loscalzo, J. Vascular Calcification: Pathobiological Mechanisms and Clinical Implications. *Circ. Res.* **99**, 1044–1059 (2006).

100. Rosenfeld, M. E. *et al.* Advanced atherosclerotic lesions in the innominate artery of the ApoE knockout mouse. *Arterioscler. Thromb. Vasc. Biol.* **20**, 2587–92 (2000).

101. Virmani, R., Kolodgie, F. D., Burke, A. P., Farb, A. & Schwartz, S. M. Lessons from sudden coronary death: A comprehensive morphological classification scheme for atherosclerotic lesions. *Arterioscler. Thromb. Vasc. Biol.* **20**, 1262–1275 (2000).

102. Newby, A. C. Metalloproteinase production from macrophages - a perfect storm leading to atherosclerotic plaque rupture and myocardial infarction. *Exp. Physiol.* **101**, 1327–1337 (2016).

103. Lavin, Y. *et al.* Tissue-resident macrophage enhancer landscapes are shaped by the local microenvironment. *Cell* **159**, 1312–1326 (2014).

104. Yona, S. *et al.* Fate Mapping Reveals Origins and Dynamics of Monocytes and Tissue Macrophages under Homeostasis. *Immunity* **38**, 79–91 (2013).

105. Swirski, F. K., Robbins, C. S. & Nahrendorf, M. Development and Function of Arterial and Cardiac Macrophages. *Trends in Immunology* **37**, 32–40 (2016).

106. Stöger, J. L. *et al.* Distribution of macrophage polarization markers in human atherosclerosis. *Atherosclerosis* **225**, 461–468 (2012).

107. Chinetti-Gbaguidi, G., Colin, S. & Staels, B. Macrophage subsets in atherosclerosis. *Nat. Rev. Cardiol.* **12**, 10–17 (2015).

108. Nahrendorf, M. & Swirski, F. K. Abandoning M1/M2 for a network model

of macrophage function. *Circulation Research* **119**, 414–417 (2016).

109. Zernecke, A. *et al.* Meta-Analysis of Leukocyte Diversity in Atherosclerotic Mouse Aortas. *Circ. Res.* 402–426 (2020). doi:10.1161/CIRCRESAHA.120.316903

110. Lin, J. Da *et al.* Single-cell analysis of fate-mapped macrophages reveals heterogeneity, including stem-like properties, during atherosclerosis progression and regression. *JCI insight* **4**, (2019).

111. Winkels, H. *et al.* Atlas of the Immune Cell Repertoire in Mouse Atherosclerosis Defined by Single-Cell RNA-Sequencing and Mass Cytometry. *Circ. Res.* **122**, 1675–1688 (2018).

112. Cochain, C. *et al.* Single-Cell RNA-Seq Reveals the Transcriptional Landscape and Heterogeneity of Aortic Macrophages in Murine Atherosclerosis. *Circ. Res.* **122**, 1661–1674 (2018).

113. Dick, S. A. *et al.* Self-renewing resident cardiac macrophages limit adverse remodeling following myocardial infarction. *Nat. Immunol.* **20**, 29–39 (2019).

114. Kim, K. *et al.* Transcriptome Analysis Reveals Nonfoamy Rather Than Foamy Plaque Macrophages Are Proinflammatory in Atherosclerotic Murine Models. *Circ. Res.* **123**, 1127–1142 (2018).

115. Cole, J. E. *et al.* Immune cell census in murine atherosclerosis: Cytometry by time of flight illuminates vascular myeloid cell diversity. *Cardiovasc. Res.* **114**, 1360–1371 (2018).

116. McArdle, S. *et al.* Migratory and dancing macrophage subsets in atherosclerotic lesions. *Circulation Research* **125**, 1038–1051 (2019).

117. Schulz, C. *et al.* A lineage of myeloid cells independent of myb and hematopoietic stem cells. *Science (80-.).* **335**, 86–90 (2012).

118. Gomez Perdiguero, E. *et al.* Tissue-resident macrophages originate from yolk-sac-derived erythro-myeloid progenitors. *Nature* **518**, 547–551 (2015).

119. Hoeffel, G. *et al.* C-Myb+ Erythro-Myeloid Progenitor-Derived Fetal Monocytes Give Rise to Adult Tissue-Resident Macrophages. *Immunity* **42**, 665–678 (2015).

120. Mucenski, M. L. *et al.* A functional c-myb gene is required for normal murine fetal hepatic hematopoiesis. *Cell* **65**, 677–689 (1991).

121. Bain, C. C. *et al.* Constant replenishment from circulating monocytes maintains the macrophage pool in the intestine of adult mice. *Nat. Immunol.* **15**, 929–937 (2014).

122. Tabas, I. Macrophage death and defective inflammation resolution in atherosclerosis. *Nature Reviews Immunology* **10**, 36–46 (2010).

123. Liu, J. *et al.* Reduced macrophage apoptosis is associated with accelerated atherosclerosis in low-density lipoprotein receptor-null mice. *Arterioscler. Thromb. Vasc. Biol.* **25**, 174–179 (2005).

124. Arai, S. *et al.* A role for the apoptosis inhibitory factor AIM/Spα/Api6 in atherosclerosis development. *Cell Metab.* **1**, 201–213 (2005).

125. Boesten, L. S. M. *et al.* Macrophage p53 controls macrophage death in atherosclerotic lesions of apolipoprotein E deficient mice. *Atherosclerosis* **207**, 399–404 (2009).

126. Reis, E. D. *et al.* Dramatic remodeling of advanced atherosclerotic plaques of the apolipoprotein e-deficient mouse in a novel transplantation model. *J. Vasc. Surg.* **34**, 541–547 (2001).

127. Llodrá, J. *et al.* Emigration of monocyte-derived cells from atherosclerotic lesions characterizes regressive, but not progressive, plaques. *Proc. Natl. Acad. Sci. U. S. A.* **101**, 11779–11784 (2004).

128. Trogan, E. *et al.* Gene expression changes in foam cells and the role of chemokine receptor CCR7 during atherosclerosis regression in ApoE-deficient mice. *Proc. Natl. Acad. Sci. U. S. A.* **103**, 3781–3786 (2006).

129. Van Gils, J. M. *et al.* The neuroimmune guidance cue netrin-1 promotes atherosclerosis by inhibiting the emigration of macrophages from plaques. *Nat. Immunol.* **13**, 136–143 (2012).

130. Lavine, K. J. *et al.* Distinct macrophage lineages contribute to disparate patterns of cardiac recovery and remodeling in the neonatal and adult heart. *Proc. Natl. Acad. Sci. U. S. A.* **111**, 16029–16034 (2014).

131. Hashimoto, D. *et al.* Tissue-Resident Macrophages Self-Maintain Locally throughout Adult Life with Minimal Contribution from Circulating Monocytes. *Immunity* **38**, 792–804 (2013).

132. Erbel, R. *et al.* 2014 ESC Guidelines on the diagnosis and treatment of aortic diseases: Document covering acute and chronic aortic diseases of the thoracic and abdominal aorta of the adult. The Task Force for the Diagnosis and Treatment of Aortic Diseases of the European . *Eur. Heart J.* **35**, 2873–926 (2014).

133. Filardo, G., Powell, J. T., Martinez, M. A.-M. & Ballard, D. J. Surgery for small asymptomatic abdominal aortic aneurysms. *Cochrane database Syst. Rev.* **2**, CD001835 (2015).

134. Ashton, H. A. *et al.* The Multicentre Aneurysm Screening Study (MASS) into the effect of abdominal aortic aneurysm screening on mortality in men: a randomised controlled trial. *Lancet (London, England)* **360**, 1531–9 (2002).

135. Parkinson, F., Ferguson, S., Lewis, P., Williams, I. M. & Twine, C. P. Rupture rates of untreated large abdominal aortic aneurysms in patients unfit for elective repair. *J. Vasc. Surg.* **61**, 1606–12 (2015).

136. Brown, L. C. & Powell, J. T. Risk factors for aneurysm rupture in patients kept under ultrasound surveillance. in *Annals of Surgery* **230**, 289–297 (Ann Surg, 1999).

137. Mastracci, T. M. & Cinà, C. S. Screening for abdominal aortic aneurysm in Canada: Review and position statement of the Canadian Society for Vascular Surgery. *Journal of Vascular Surgery* **45**, (2007).

138. Chaikof, E. L. *et al.* The Society for Vascular Surgery practice guidelines on the care of patients with an abdominal aortic aneurysm. *J. Vasc. Surg.* **67**, 2-77.e2 (2018).

139. Owens, D. K. *et al.* Screening for Abdominal Aortic Aneurysm: US Preventive Services Task Force Recommendation Statement. *JAMA - Journal of the American Medical Association* **322**, 2211–2218 (2019).

140. Cosford, P. & Leng, G. C. Screening for abdominal aortic aneurysm. *Cochrane Database of Systematic Reviews* (2007). doi:10.1002/14651858.CD002945.pub2

141. Moll, F. L. *et al.* Management of abdominal aortic aneurysms clinical practice guidelines of the European society for vascular surgery. *Eur. J. Vasc. Endovasc. Surg.* **41 Suppl 1**, S1–S58 (2011).

142. Sakalihasan, N. *et al.* Abdominal aortic aneurysms. *Nature Reviews Disease Primers* **4**, (2018).

143. Verloes, A., Sakalihasan, N., Koulischer, L. & Limet, R. Aneurysms of the abdominal aorta: familial and genetic aspects in three hundred thirteen pedigrees. *J. Vasc. Surg.* **21**, 646–655 (1995).

144. Majumder, P. P., St. Jean, P. L., Ferrell, R. E., Webster, M. W. & Steed, D. L. On the inheritance of abdominal aortic aneurysm. *Am. J. Hum. Genet.* **48**, 164–170 (1991).

145. Rolph, R. C., Waltham, M., Smith, A. & Kuivaniemi, H. Expanding Horizons for Abdominal Aortic Aneurysms. *Aorta* **3**, 9–15 (2015).

146. Joergensen, T. M. M. *et al.* High Heritability of Liability to Abdominal Aortic Aneurysms: A Population Based Twin Study. *J. Vasc. Surg.* **64**, 537 (2016).

147. Wahlgren, C. M., Larsson, E., Magnusson, P. K. E., Hultgren, R. & Swedenborg, J. Genetic and environmental contributions to abdominal aortic aneurysm development in a twin population. *J. Vasc. Surg.* **51**, 3–7 (2010).

148. Tang, W. *et al.* Lifetime Risk and Risk Factors for Abdominal Aortic Aneurysm in a 24-Year Prospective Study: The ARIC Study (Atherosclerosis Risk in Communities). *Arterioscler. Thromb. Vasc. Biol.* **36**, 2468–2477 (2016).

149. Forsdahl, S. H., Singh, K., Solberg, S. & Jacobsen, B. K. Risk Factors for Abdominal Aortic Aneurysms: A 7-Year Prospective Study: The Tromso Study, 1994-2001. *Circulation* **119**, 2202–2208 (2009).

150. Kent, K. C. *et al.* Analysis of risk factors for abdominal aortic aneurysm in a cohort of more than 3 million individuals. *J. Vasc. Surg.* **52**, 539–548 (2010).

151. Wilmink, T. B. M. The association between cigarette smoking and abdominal aortic aneurysms. *J. Vasc. Surg.* **30**, 1099–1105 (1999).

152. Jahangir, E. *et al.* Smoking, sex, risk factors and abdominal aortic aneurysms: a prospective study of 18 782 persons aged above 65 years in the Southern Community Cohort Study. *J. Epidemiol. Community Health* **69**, 481–8 (2015).

153. Lee, A. J., Fowkes, F. G., Carson, M. N., Leng, G. C. & Allan, P. L. Smoking, atherosclerosis and risk of abdominal aortic aneurysm. *Eur. Heart J.* **18**, 671–6 (1997).

154. Lindquist Liljeqvist, M., Hultgren, R., Siika, A., Gasser, T. C. & Roy, J. Gender, smoking, body size, and aneurysm geometry influence the biomechanical rupture risk of abdominal aortic aneurysms as estimated by finite element analysis. *J. Vasc. Surg.* **65**, 1014-1021.e4 (2017).

155. Sweeting, M. J., Thompson, S. G., Brown, L. C. & Powell, J. T. Meta-analysis of individual patient data to examine factors affecting growth and rupture of small abdominal aortic aneurysms. *Br. J. Surg.* **99**, 655–665 (2012).

156. Lindeman, J. H. N. The pathophysiologic basis of abdominal aortic aneurysm progression: a critical appraisal. *Expert Rev. Cardiovasc. Ther.* **13**, 839–51 (2015).

157. Toghill, B. J., Saratzis, A. & Bown, M. J. Abdominal aortic aneurysm—an independent disease to atherosclerosis? *Cardiovascular Pathology* **27**, 71–75 (2017).

158. Biros, E. *et al.* Differential gene expression in human abdominal aortic aneurysm and aortic occlusive disease. *Oncotarget* **6**, 12984–96 (2015).

159. Johnsen, S. H., Forsdahl, S. H., Singh, K. & Jacobsen, B. K. Atherosclerosis in abdominal aortic aneurysms: a causal event or a process running in parallel? The Tromsø study. *Arterioscler. Thromb. Vasc. Biol.* **30**, 1263–8 (2010).

160. Hernesniemi, J. A., Vänni, V. & Hakala, T. The prevalence of abdominal aortic aneurysm is consistently high among patients with coronary artery disease. *Journal of Vascular Surgery* **62**, 232-240.e3 (2015).

161. Lederle, F. A. The strange relationship between diabetes and abdominal aortic aneurysm. *European Journal of Vascular and Endovascular Surgery* **43**, 254–256 (2012).

162. Peshkova, I. O., Schaefer, G. & Koltsova, E. K. Atherosclerosis and Aortic Aneurysm: is inflammation a common denominator? *FEBS J.* (2015). doi:10.1111/febs.13634

163. Turner, G. H. *et al.* Assessment of macrophage infiltration in a murine model of abdominal aortic aneurysm. *J. Magn. Reson. Imaging* **30**, 455–460 (2009).

164. Tieu, B. C. *et al.* An adventitial IL-6/MCP1 amplification loop accelerates macrophage-mediated vascular inflammation leading to aortic dissection in mice. *J. Clin. Invest.* **119**, 3637–3651 (2009).

165. Tieu, B. C. *et al.* Aortic adventitial fibroblasts participate in angiotensin-induced vascular wall inflammation and remodeling. *J. Vasc. Res.* **48**, 261–272 (2011).

166. Martinez-Pinna, R. *et al.* Increased levels of thioredoxin in patients with abdominal aortic aneurysms (AAAs). A potential link of oxidative stress with AAA evolution. *Atherosclerosis* **212**, 333–8 (2010).

167. López-Candales, A. *et al.* Decreased vascular smooth muscle cell density in medial degeneration of human abdominal aortic aneurysms. *Am. J. Pathol.* **150**, 993–1007 (1997).

168. Wilson, W. R. W. *et al.* Matrix metalloproteinase-8 and -9 are increased at the site of abdominal aortic aneurysm rupture. *Circulation* **113**, 438–45 (2006).

169. Emeto, T. I., Moxon, J. V, Au, M. & Golledge, J. Oxidative stress and abdominal aortic aneurysm: potential treatment targets. *Clin. Sci.* **130**, 301–15 (2016).

170. Wolinsky, H. & Glagov, S. Comparison of abdominal and thoracic aortic medial structure in mammals. Deviation of man from the usual pattern. *Circ. Res.* **25**, 677–86 (1969).

171. McGill, H. C. *et al.* Effects of Coronary Heart Disease Risk Factors on Atherosclerosis of Selected Regions of the Aorta and Right Coronary Artery. *Arterioscler. Thromb. Vasc. Biol.* **20**, 836–845 (2000).

172. Thompson, R. W. *et al.* Pathophysiology of abdominal aortic aneurysms: insights from the elastase-induced model in mice with different genetic backgrounds. *Ann. N. Y. Acad. Sci.* **1085**, 59–73 (2006).

173. Wang, Y., Krishna, S. & Golledge, J. The calcium chloride-induced rodent model of abdominal aortic aneurysm. *Atherosclerosis* **226**, 29–39 (2013).

174. Golledge, J. Abdominal aortic aneurysm: update on pathogenesis and medical treatments. *Nature Reviews Cardiology* **16**, 225–242 (2019).

175. Daugherty, A., Manning, M. W. & Cassis, L. A. Angiotensin II promotes atherosclerotic lesions and aneurysms in apolipoprotein E-deficient mice. *J. Clin. Invest.* **105**, 1605–1612 (2000).

176. Daugherty, A. & Cassis, L. Chronic angiotensin II infusion promotes atherogenesis in low density lipoprotein receptor -/- mice. in *Annals of the New York Academy of Sciences* **892**, 108–118 (New York Academy of Sciences, 1999).

177. Saraff, K., Babamusta, F., Cassis, L. A. & Daugherty, A. Aortic dissection precedes formation of aneurysms and atherosclerosis in angiotensin II-infused, apolipoprotein E-deficient mice. *Arterioscler. Thromb. Vasc. Biol.* **23**, 1621–6 (2003).

178. Dale, M. A., Ruhlman, M. K. & Baxter, B. T. Inflammatory cell phenotypes in AAAs: Their role and potential as targets for therapy. *Arterioscler. Thromb. Vasc. Biol.* **35**, 1746–1755 (2015).

179. Koch, A. E. *et al.* Human abdominal aortic aneurysms. Immunophenotypic analysis suggesting an immune-mediated response. *Am. J. Pathol.* **137**, 1199–213 (1990).

180. Galle, C. *et al.* Predominance of type 1 CD4+ T cells in human abdominal aortic aneurysm. *Clin. Exp. Immunol.* **142**, 519–27 (2005).

181. Curci, J. A., Liao, S., Huffman, M. D., Shapiro, S. D. & Thompson, R. W. Expression and localization of macrophage elastase (matrix metalloproteinase-12) in abdominal aortic aneurysms. *J. Clin. Invest.* **102**, 1900–10 (1998).

182. Abdul-Hussien, H. *et al.* Collagen degradation in the abdominal aneurysm: a conspiracy of matrix metalloproteinase and cysteine collagenases. *Am. J. Pathol.* **170**, 809–17 (2007).

183. Wang, S. *et al.* Activation of AMP-activated protein kinase α2 by nicotine instigates formation of abdominal aortic aneurysms in mice in vivo. *Nat. Med.* **18**, 902–910 (2012).

184. Lindeman, J. H. N. *et al.* Distinct defects in collagen microarchitecture underlie vessel-wall failure in advanced abdominal aneurysms and aneurysms in Marfan syndrome. *Proc. Natl. Acad. Sci. U. S. A.* **107**, 862–5 (2010).

185. Faarvang, A.-S. A. *et al.* Smoking is associated with lower amounts of arterial type I collagen and decorin. *Atherosclerosis* **247**, 201–206 (2016).

186. Ng, M. *et al.* Smoking prevalence and cigarette consumption in 187 countries, 1980-2012. *J. Am. Med. Assoc.* **311**, 183–92 (2014).

187. Krueger, H., Krueger, J. & Koot, J. Variation across Canada in the economic burden attributable to excess weight, tobacco smoking and physical inactivity. *Can J Public Heal.* **106**, 171–177 (2015).

188. US Department of Health and Human Services. *The health consequences of smoking—50 years of progress: A report of the surgeon general*. (2014).

189. Mozaffarian, D. *et al.* Heart Disease and Stroke Statistics-2015 Update: A Report From the American Heart Association. *Circulation* **131**, e29-322 (2014).

190. Giebe, S. *et al.* Cigarette smoke extract counteracts atheroprotective effects of high laminar flow on endothelial function. *Redox Biol.* **12**, 776–786 (2017).

191. Caterina, R. De *et al.* Nitric oxide decreases cytokine-induced endothelial activation. *J. Clin. Invest.* **96**, 60–68 (1995).

192. Förstermann, U., Xia, N. & Li, H. Roles of Vascular Oxidative Stress and Nitric Oxide in the Pathogenesis of Atherosclerosis. *Circ. Res.* **120**, (2017).

193. El-mahdy, M. A. *et al.* Chronic Cigarette Smoke Exposure Triggers A Vicious Cycle of Leukocyte and Endothelial-Mediated Oxidant Stress that Results in Vascular Dysfunction. *Am. J. Physiol. Heart Circ. Physiol.* (2020). doi:10.1152/ajpheart.00657.2019

194. Abdelghany, T. M. *et al.* Cigarette Smoke Constituents Cause Endothelial Nitric Oxide Synthase Dysfunction and Uncoupling Due to Depletion of Tetrahydrobiopterin With Degradation of GTP Cyclohydrolase. *Nitric oxide Biol. Chem.* **76**, (2018).

195. Lowe, E. R. *et al.* Time-dependent Inhibition and Tetrahydrobiopterin Depletion of Endothelial Nitric-Oxide Synthase Caused by Cigarettes. *Drug Metab. Dispos.* **33**, (2005).

196. Buckley, C. *et al.* Accelerated enlargement of experimental abdominal aortic aneurysms in a mouse model of chronic cigarette smoke exposure. *J. Am. Coll. Surg.* **199**, 896–903 (2004).

197. Bergoeing, M. P. *et al.* Cigarette smoking increases aortic dilatation without affecting matrix metalloproteinase-9 and -12 expression in a modified mouse model of aneurysm formation. *J. Vasc. Surg.* **45**, 1217-1227.e2 (2007).

198. Boué, S. *et al.* Modulation of atherogenic lipidome by cigarette smoke in apolipoprotein E-deficient mice. *Atherosclerosis* **225**, 328–34 (2012).

199. Lietz, M. *et al.* Cigarette-smoke-induced atherogenic lipid profiles in plasma and vascular tissue of apolipoprotein E-deficient mice are attenuated by smoking cessation. *Atherosclerosis* **229**, 86–93 (2013).

200. Stolle, K., Berges, A., Lietz, M., Lebrun, S. & Wallerath, T. Cigarette smoke enhances abdominal aortic aneurysm formation in angiotensin II-treated apolipoprotein E-deficient mice. *Toxicol. Lett.* **199**, 403–409 (2010).

201. Botelho, F. M. F. M. *et al.* Innate immune processes are sufficient for driving cigarette smoke-induced inflammation in mice. *Am. J. Respir. Cell Mol. Biol.* **42**, 394–403 (2010).

202. Swirski, F. K. *et al.* Identification of splenic reservoir monocytes and their deployment to inflammatory sites. *Science (80-.).* **325**, 612–616 (2009).

203. HS, C. *et al.* Paradoxical Suppression of Atherosclerosis in the Absence of microRNA-146a. *Circ. Res.* **121**, 354–367 (2017).

204. Chong, S. Z. *et al.* CXCR4 identifies transitional bone marrow premonocytes that replenish the mature monocyte pool for peripheral

responses. *J. Exp. Med.* **213**, 2293 (2016).

205. Butler, A., Hoffman, P., Smibert, P., Papalexi, E. & Satija, R. Integrating single-cell transcriptomic data across different conditions , technologies , and species. *Nat. Biotechnol.* **36**, 411–420 (2018).

206. Stuart, T. *et al.* Comprehensive Integration of Single-Cell Data. *Cell* **177**, 1888-1902.e21 (2019).

207. Ritchie, M. E. *et al.* Limma powers differential expression analyses for RNA-sequencing and microarray studies. *Nucleic Acids Res.* **43**, e47 (2015).

208. Subramanian, A. *et al.* Gene set enrichment analysis: A knowledge-based approach for interpreting genome-wide expression profiles. *Proc. Natl. Acad. Sci. U. S. A.* **102**, 15545–15550 (2005).

209. Cao, J. *et al.* The single-cell transcriptional landscape of mammalian organogenesis. *Nature* **566**, 496–502 (2019).

210. Trapnell, C. *et al.* The dynamics and regulators of cell fate decisions are revealed by pseudotemporal ordering of single cells. *Nat. Biotechnol.* **32**, 381–386 (2014).

211. Qiu, X. *et al.* Reversed graph embedding resolves complex single-cell trajectories. *Nat. Methods* **14**, 979–982 (2017).

212. Traag, V. A., Waltman, L. & van Eck, N. J. From Louvain to Leiden: guaranteeing well-connected communities. *Sci. Rep.* **9**, (2019).

213. La Manno, G. *et al.* RNA velocity of single cells. *Nature* **560**, 494–498 (2018).

214. Becht, E. *et al.* Dimensionality reduction for visualizing single-cell data using UMAP. *Nat. Biotechnol.* **37**, 38–47 (2019).

215. Weinberger, T. *et al.* Ontogeny of arterial macrophages defines their functions in homeostasis and inflammation. *Nat. Commun.* **11**, (2020).

216. Hettinger, J. *et al.* Origin of monocytes and macrophages in a committed progenitor. *Nat. Immunol.* **14**, 821–830 (2013).

217. Goto, Y., Hogg, J. C., Suwa, T., Quinlan, K. B. & van Eeden, S. F. A novel method to quantify the turnover and release of monocytes from the bone marrow using the thymidine analog 5′-bromo-2′-deoxyuridine. *Am. J. Physiol. Physiol.* **285**, C253–C259 (2003).

218. Zhu, S.-N., Chen, M., Jongstra-Bilen, J. & Cybulsky, M. I. GM-CSF

regulates intimal cell proliferation in nascent atherosclerotic lesions. *J. Exp. Med.* **206**, 2141–9 (2009).

219. Tangirala, R. K., Rubin, E. M. & Palinski, W. Quantitation of atherosclerosis in murine models: Correlation between lesions in the aortic origin and in the entire aorta, and differences in the extent of lesions between sexes in LDL receptor-deficient and apolipoprotein E-deficient mice. *J. Lipid Res.* **36**, 2320–2328 (1995).

220. Zhao, G. *et al.* Single-cell RNA sequencing reveals the cellular heterogeneity of aneurysmal infrarenal abdominal aorta. *Cardiovasc. Res.* (2020). doi:10.1093/cvr/cvaa214

221. Yang, H., Zhou, T., Stranz, A., DeRoo, E. & Liu, B. Single-Cell RNA Sequencing Reveals Heterogeneity of Vascular Cells in Early Stage Murine Abdominal Aortic Aneurysm-Brief Report. *Arterioscler. Thromb. Vasc. Biol.* **41**, 1158–1166 (2021).

222. Hadi, T. *et al.* Macrophage-derived netrin-1 promotes abdominal aortic aneurysm formation by activating MMP3 in vascular smooth muscle cells. *Nat. Commun.* **9**, 5022 (2018).

223. Trumpp, A., Essers, M. & Wilson, A. Awakening dormant haematopoietic stem cells. *Nat. Rev. Immunol.* **10**, 201–209 (2010).

224. Golledge, J. *et al.* Association Between Osteopontin and Human Abdominal Aortic Aneurysm. *Arterioscler. Thromb. Vasc. Biol.* **27**, 655–660 (2007).

225. Stämpfli, M. R. & Anderson, G. P. How cigarette smoke skews immune responses to promote infection, lung disease and cancer. *Nat. Rev. Immunol.* **9**, 377–384 (2009).

226. Morissette, M. C., Shen, P., Thayaparan, D. & Stämpfli, M. R. Disruption of pulmonary lipid homeostasis drives cigarette smoke-induced lung inflammation in mice. *Eur. Respir. J.* **46**, 1451–60 (2015).

227. Cass, S. P. *et al.* Current smoking status is associated with reduced sputum immunoglobulin M and G expression in COPD. *Eur. Respir. J.* **57**, 1902338 (2021).

228. Shen, P. *et al.* Cigarette smoke attenuates the nasal host response to Streptococcus pneumoniae and predisposes to invasive pneumococcal disease in mice. *Infect. Immun.* **84**, 1536–1547 (2016).

229. Morissette, M. C., Shen, P., Thayaparan, D. & Stämpfli, M. R. Impacts of peroxisome proliferatoractivated receptor-γ activation on cigarette smoke-

induced exacerbated response to bacteria. *Eur. Respir. J.* **45**, 191–200 (2015).

230. Nikota, J. K. J. K. *et al.* Cigarette smoke primes the pulmonary environment to IL-1α/CXCR-2-dependent nontypeable Haemophilus influenzae-exacerbated neutrophilia in mice. *J. Immunol.* **193**, 3134–45 (2014).

231. Botelho, F. M. *et al.* IL-1α/IL-1R1 expression in chronic obstructive pulmonary disease and mechanistic relevance to smoke-induced neutrophilia in mice. *PLoS One* **6**, e28457 (2011).

232. Roos, A. B. *et al.* IL-17A and the Promotion of Neutrophilia in Acute Exacerbation of Chronic Obstructive Pulmonary Disease. *Am. J. Respir. Crit. Care Med.* **192**, 428–37 (2015).

233. Seijkens, T. *et al.* Hypercholesterolemia-induced priming of hematopoietic stem and progenitor cells aggravates atherosclerosis. *FASEB J.* **28**, 2202–2213 (2014).

234. van Kampen, E., Jaminon, A., van Berkel, T. J. C. & Van Eck, M. Diet-induced (epigenetic) changes in bone marrow augment atherosclerosis. *J. Leukoc. Biol.* **96**, 833–41 (2014).

235. Siggins, R. *et al.* Cigarette Smoke Alters the Hematopoietic Stem Cell Niche. *Med. Sci.* **2**, 37–50 (2014).

236. Moore, J. P. *et al.* M2 macrophage accumulation in the aortic wall during angiotensin ii infusion in mice is associated with fibrosis, elastin loss, and elevated blood pressure. *Am. J. Physiol. - Hear. Circ. Physiol.* **309**, H906–H917 (2015).

237. Ishibashi, M. *et al.* Bone marrow-derived monocyte chemoattractant protein-1 receptor CCR2 is critical in angiotensin II-induced acceleration of atherosclerosis and aneurysm formation in hypercholesterolemic mice. *Arterioscler. Thromb. Vasc. Biol.* **24**, (2004).

238. Messner, B. & Bernhard, D. Smoking and Cardiovascular Disease: Mechanisms of Endothelial Dysfunction and Early Atherogenesis. *Arterioscler. Thromb. Vasc. Biol.* **34**, 509–515 (2014).

239. Alderton, W. K., Cooper, C. E. & Knowles, R. G. Nitric oxide synthases: Structure, function and inhibition. *Biochem. J.* **357**, 593–615 (2001).

240. Schulz, E., Gori, T. & Münzel, T. Oxidative stress and endothelial dysfunction in hypertension. *Hypertens. Res.* **34**, 665–673 (2011).

241. Wang, S. *et al.* Acute inhibition of guanosine triphosphate cyclohydrolase 1 uncouples endothelial nitric oxide synthase and elevates blood pressure. *Hypertension* **52**, 484–90 (2008).

242. Kuhlencordt, P. J. *et al.* Accelerated Atherosclerosis, Aortic Aneurysm Formation, and Ischemic Heart Disease in Apolipoprotein E/Endothelial Nitric Oxide Synthase Double-Knockout Mice. *Circulation* **104**, 448–454 (2001).

243. Chen, J., Kuhlencordt, P., Astern, J., Gyurko, R. & Huang, P. Hypertension Does Not Account for the Accelerated Atherosclerosis and Development of Aneurysms in Male Apolipoprotein E/Endothelial Nitric Oxide Synthase Double Knockout Mice. *Circulation* **104**, (2001).

244. Ozaki, M. *et al.* Overexpression of endothelial nitric oxide synthase accelerates atherosclerotic lesion formation in apoE-deficient mice. *J. Clin. Invest.* **110**, 331–340 (2002).

245. Ali, M. U. *et al.* A systematic review of short-term vs long-term effectiveness of one-time abdominal aortic aneurysm screening in men with ultrasound. *Journal of Vascular Surgery* **68**, 612–623 (2018).

246. Benson, R. A., Meecham, L., Fisher, O. & Loftus, I. M. Ultrasound screening for abdominal aortic aneurysm: Current practice, challenges and controversies. *British Journal of Radiology* **91**, (2018).

CHAPTER 6: FIGURES, FIGURE LEGENDS, AND TABLES

FIGURE 1

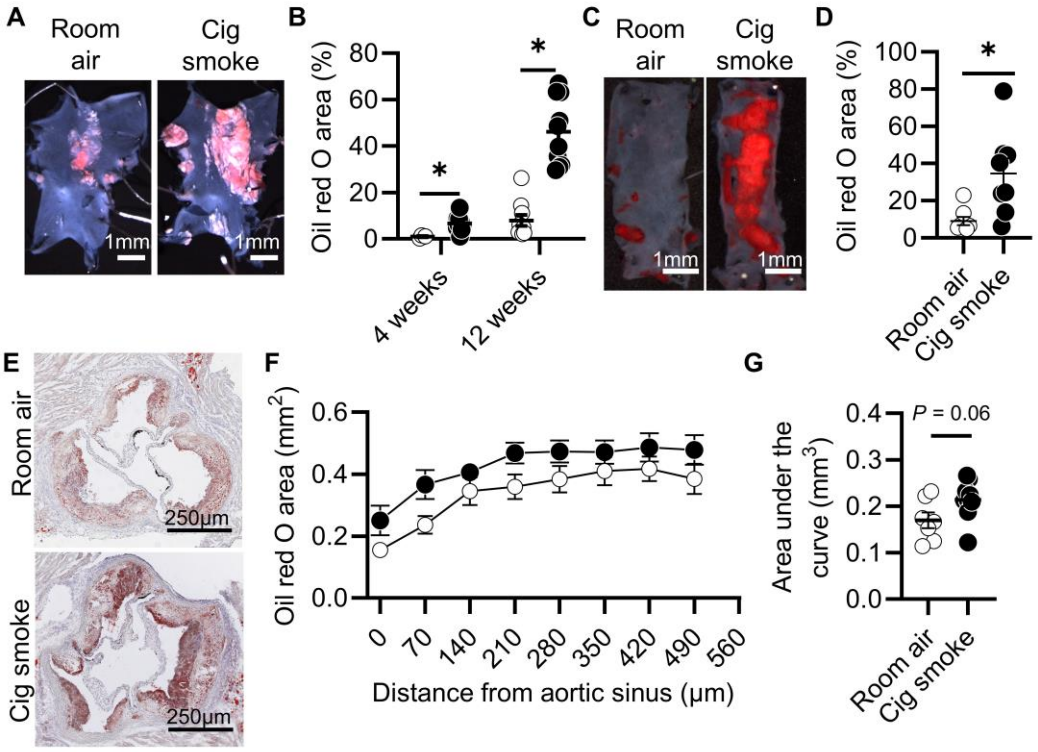

Figure 1: Cigarette smoke exposure increases atherosclerosis in *Apoe*$^{-/-}$ mice. Male *Apoe*$^{-/-}$ mice were placed on a high cholesterol diet (HCD) and exposed to room air (white) or cigarette smoke (black). **(A)** *en face* oil red O (ORO) staining of the lesser curvature of the aortic arch at 12 weeks and (**B)** quantification of ORO staining in the lesser curvature of the aortic arch at 4 and 12 weeks. Two-tailed unpaired Student's t-test **P*<0.05. **(C)** *en face* ORO staining of the abdominal aorta at 12 weeks and **(D)** quantification of ORO staining in the abdominal aorta at 12 weeks. Two-tailed Student's t-test **P*<0.05. **(E)** ORO staining of aortic root cross-sections at 12 weeks and **(F)** quantification of ORO staining in 8 consecutive cross-sections spanning the aortic root at 12 weeks and **(G)** quantification of area under the curve for data shown in (F)**.** Two-tailed Student's t-test *P*=0.0605.

FIGURE 2

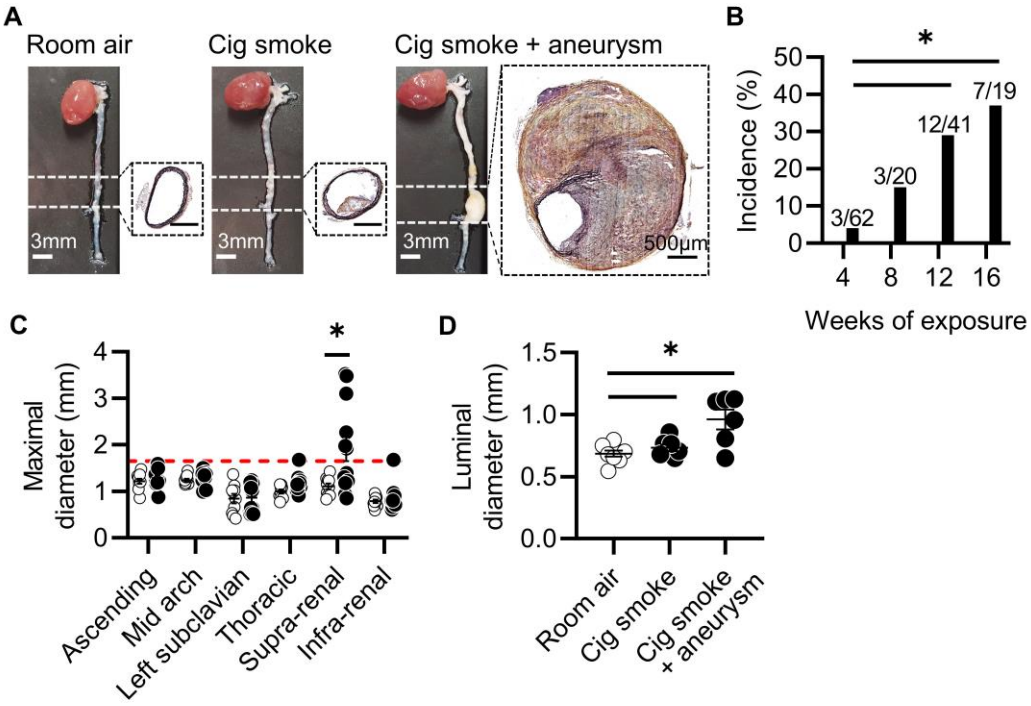

Figure 2: Cigarette smoke exposure induces aortic aneurysms in *Apoe*$^{-/-}$ mice. Male *Apoe*$^{-/-}$ mice were placed on a high cholesterol diet (HCD) and exposed to room air (white) or cigarette smoke (black). **(A)** Gross morphology of whole aortas and Movat pentachrome-stained supra-renal cross-sections at 12 weeks. **(B)** Incidence of aortic aneurysm at 4, 8, 12, and 16 weeks of exposure (room air; 4 week n= 26, 8 week n=14, 12 week n=28, 16 week n=15). Chi square test with post hoc pairwise comparisons **P*<0.05. **(C)** Maximal outer aortic diameter at 12 weeks. Red dashed line indicates a 50% increase in diameter over baseline. Ordinary one-way ANOVA, Tukey's multiple comparisons **P*<0.05. **(D)** Luminal diameter of the supra-renal aorta at 12 weeks. Ordinary one-way ANOVA, Tukey's multiple comparisons **P*<0.05

FIGURE 3

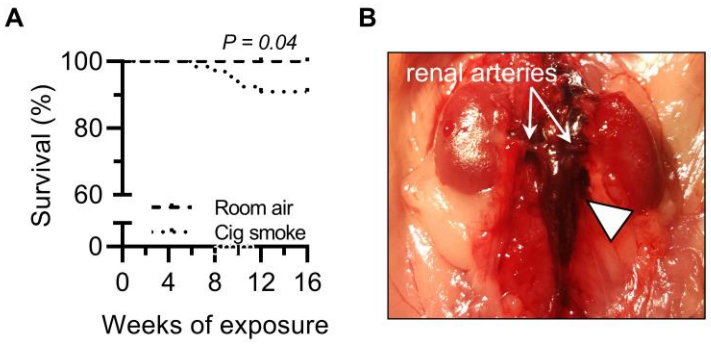

Figure 3: Aortic aneurysms proceed to spontaneous rupture in cigarette smoke exposed *Apoe*$^{-/-}$ mice. Male *Apoe*$^{-/-}$ mice were placed on a high cholesterol diet (HCD) and exposed to room air (large dash) or cigarette smoke (small dash). **(A)** Kaplan-Meier survival curve tracking death due to ruptured aneurysm (n=43 room air, n=68 cig smoke). Log-rank (Mantel-Cox) test **P*=0.04. **(B)** Representative image of ruptured abdominal aortic aneurysm indicated by white arrow.

FIGURE 4

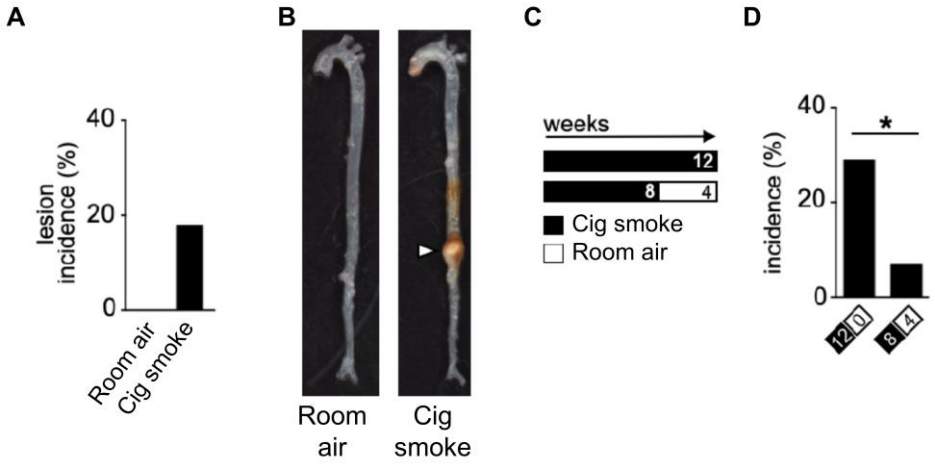

Figure 4: Cigarette smoke induced aortic aneurysm incidence is less in female *Apoe*$^{-/-}$ mice and following smoking cessation. Female *Apoe*$^{-/-}$ mice were placed on a high cholesterol diet (HCD) and exposed to room air (white) or cigarette smoke (black). **(A)** Incidence of aortic aneurysm at 12 weeks of exposure (n=22 room air, n=28 cig smoke). Two-sided Fisher's exact test *P>0.05*. **(B)** Gross morphology of whole aortas. White arrow indicates aneurysm. **(C)** Schematic outlining exposure and cessation periods for male *Apoe*$^{-/-}$ mice on HCD. **(D)** Incidence of aortic aneurysm (n=41 12 weeks, n=27 8 weeks cig smoke with 4 weeks cessation). Two-sided Fisher's exact test **P<0.05*.

FIGURE 5

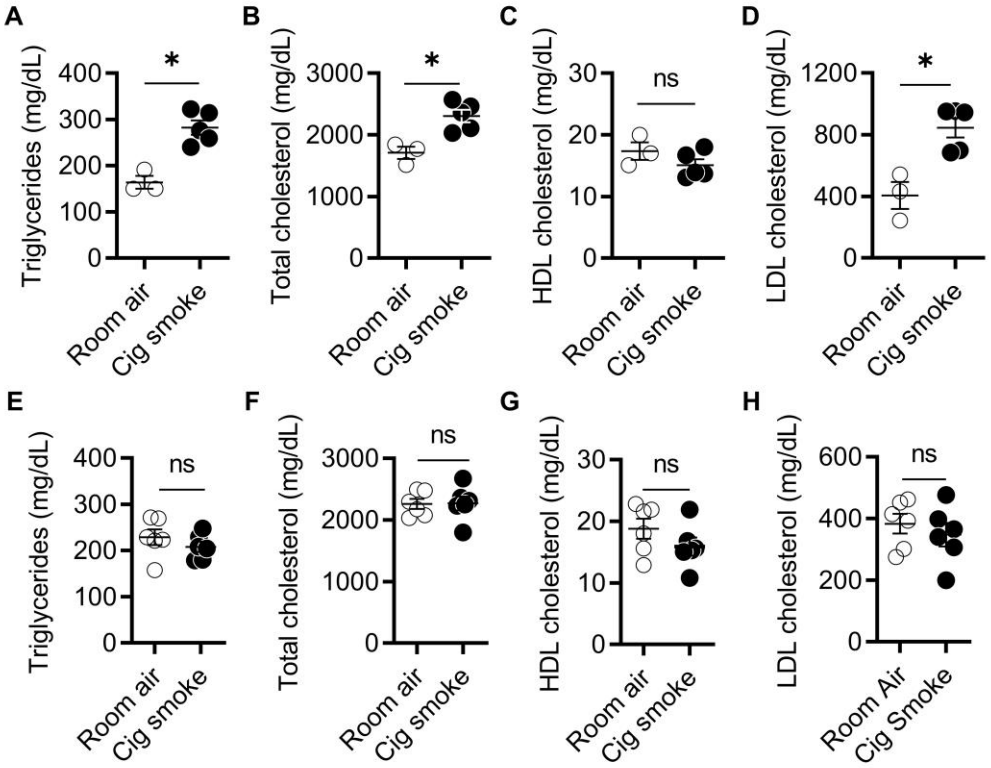

Figure 5: Cigarette smoke exposure increases plasma lipids at early time points. Male *Apoe*$^{-/-}$ mice were placed on a high cholesterol diet (HCD) and exposed to room air (white) or cigarette smoke (black) for **(A-D)** 4 weeks or **(E-H)** 12 weeks. Quantification of plasma **(A, E)** triglycerides, **(B, F)** total cholesterol, **(C, G)** high density lipoprotein (HDL) cholesterol, and **(D, H)** low density lipoprotein (LDL) cholesterol. Two-tailed unpaired Student's t-test **P*<0.05.

FIGURE 6

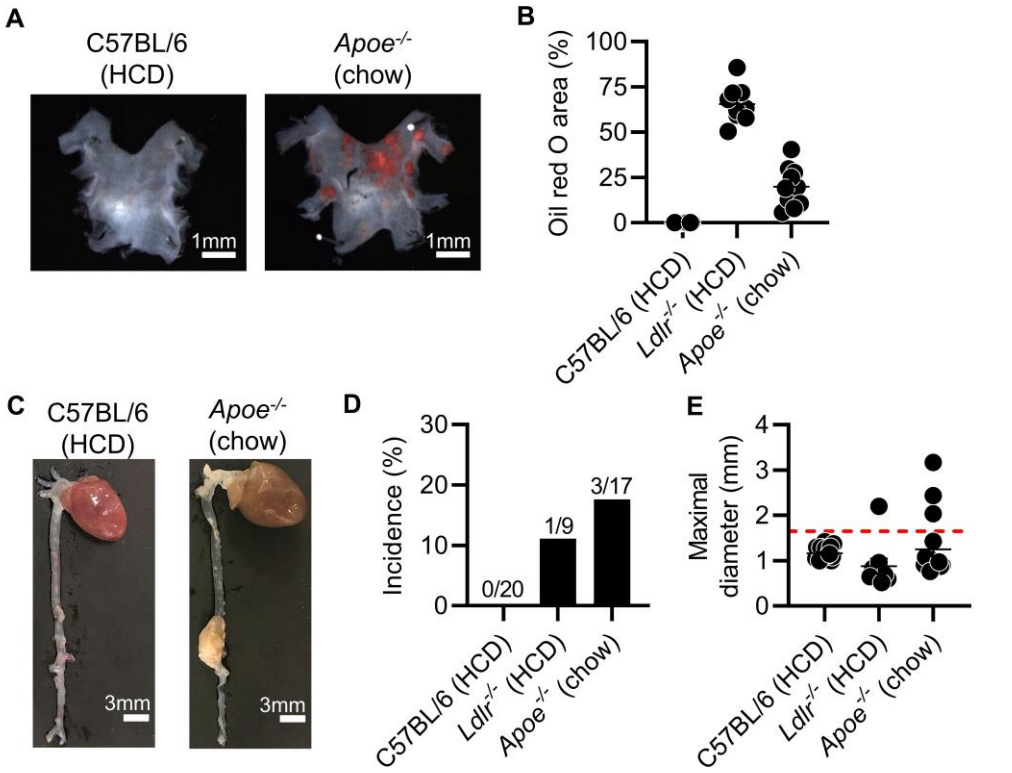

Figure 6: Cigarette smoke only induces aortic aneurysms in hyperlipidemic mice. Male *Apoe*$^{-/-}$ mice on a chow diet, low density lipoprotein receptor deficient (*Ldlr*$^{-/-}$) mice on a high cholesterol diet (HCD), and non-hyperlipidemic C57BL/6J mice on a HCD were exposed to cigarette smoke for 12 weeks. (**A)** *en face* oil red O (ORO) staining of the lesser curvature of the aortic arch **(B**) quantification of ORO in the arch (**C)** gross morphology of the whole aorta **(D)** aortic aneurysm incidence (room air; n=5 *Apoe*$^{-/-}$ (chow) and n=5 *Ldlr*$^{-/-}$) (**E)** maximal outer aortic diameter. Red dashed line indicates a 50% increase in diameter over baseline.

FIGURE 7

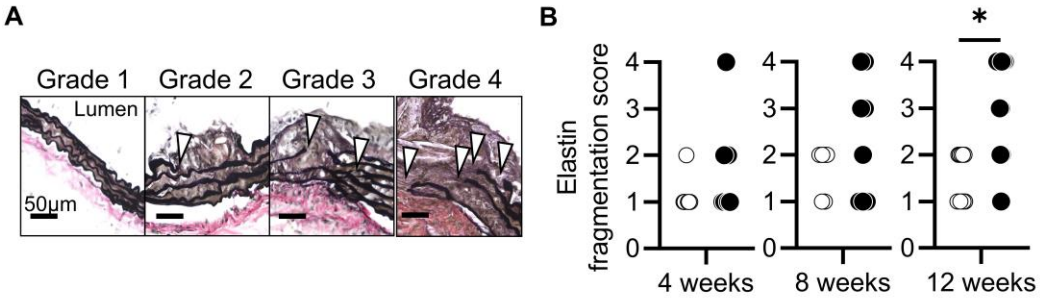

Figure 7: Cigarette smoke exposure increases elastin damage in aortas of *Apoe*$^{-/-}$ mice. Male *Apoe*$^{-/-}$ mice were placed on a HCD and exposed to room air (white) or cigarette smoke (black). **(A)** Representative images of standard elastin fragmentation scoring in EVG stained arterial cross sections (1=no damage, 2=single elastin strand break, 3=multiple elastin strand breaks, 4=breaks in all elastin layers). White arrows indicate elastin breaks. **(B)** Quantification of elastin fragmentation in the supra-renal aorta at 4, 8, and 12 weeks of exposure (n=8-12 per group). Two-tailed Mann-Whitney test *P<0.05.

FIGURE 8

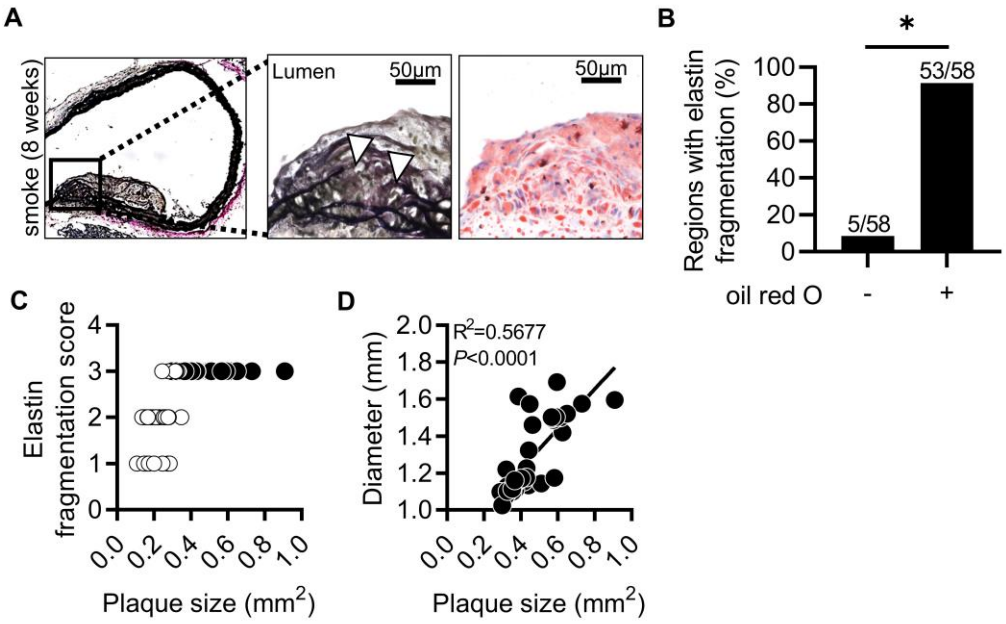

Figure 8: Atherosclerosis is associated with elastin damage in the aorta of *Apoe*$^{-/-}$ mice. Male *Apoe*$^{-/-}$ mice were placed on a HCD and exposed to room air (white) or cigarette smoke (black). **(A)** Representative Movat pentachrome (left 2 panels) and oil red O (right panel) staining in adjacent abdominal aorta cross-sections of smoke exposed mice at 8 weeks of exposure. **(B)** Quantification of abdominal aorta cross-sections with elastin damage and overlying atherosclerotic plaque in smoke exposed mice (n=21 mice). Two-sided Fisher's exact test *$P<0.05$. **(C)** Relationship between plaque size and elastin fragmentation in the aorta at 12 weeks. **(D)** Relationship between atherosclerotic plaque size and aortic luminal diameter at 12 weeks. Data represent 36 aortic cross-sections from n=6 cig smoke mice. Linear regression analysis *$P<0.05$.

FIGURE 9

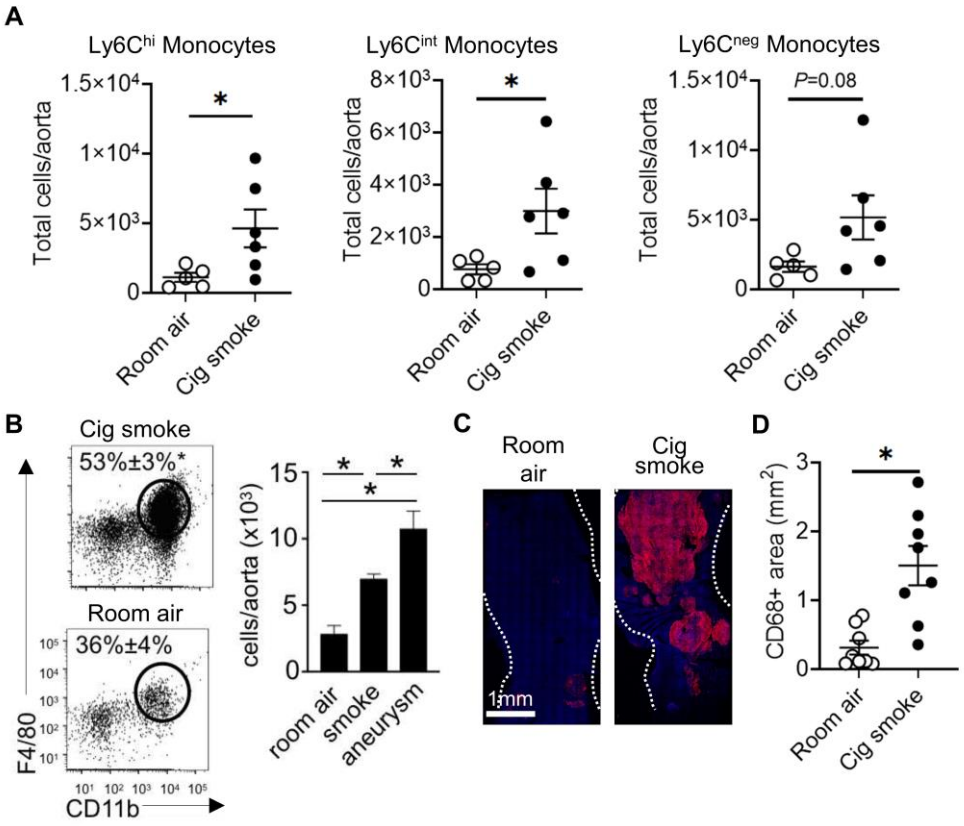

Figure 9: Cigarette smoke exposure increases accumulation of monocytes and macrophage in aortas of *Apoe*$^{-/-}$ mice. Male *Apoe*$^{-/-}$ mice were placed on a high cholesterol diet (HCD) and exposed to room air (white) or cigarette smoke (black) for 12 weeks. (**A)** Quantification of monocytes in whole aortas assessed by flow cytometry. (**B)** Quantification of CD11b^{+}F4/80^{+} monocytes/macrophages in whole aortas assessed by flow cytometry. **(C)** Representative images and **(D)** quantification of *en face* CD68^{+} staining of the abdominal aorta at 16 weeks. Two-tailed unpaired Student's t-test **P*<0.05.

FIGURE 10

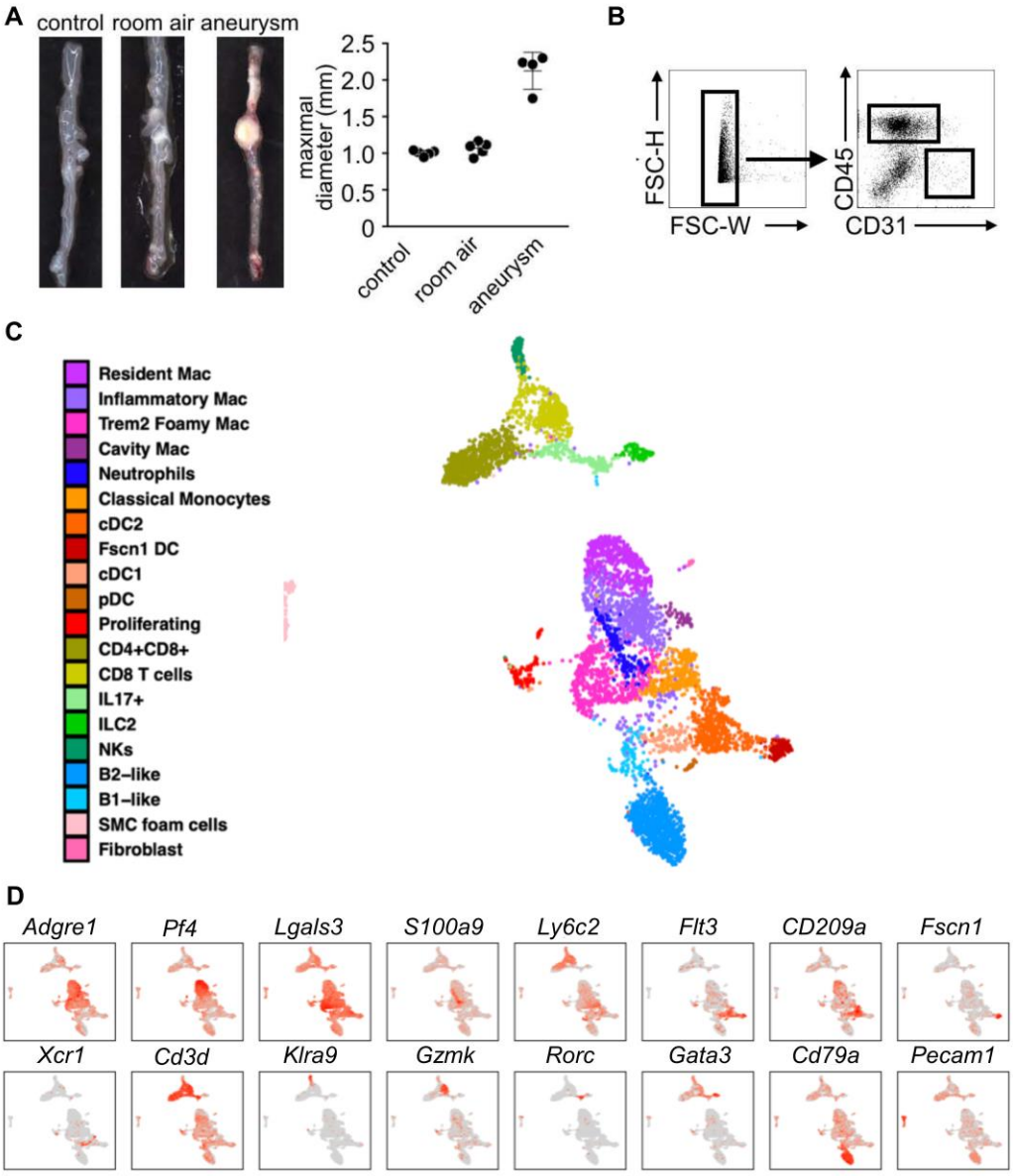

Figure 10: Immune cell populations identified by single cell RNA sequencing analysis of abdominal aortas. Abdominal aorta sections were collected from C57BL/6J mice (control), *Apoe*$^{-/-}$ mice on a high cholesterol diet (HCD) exposed to room air (room air) or cigarette smoke with aneurysm (smoke/aneurysm) at 16 weeks. (**A)** Gross morphology of abdominal aortas and quantification of maximal outer diameter (n=5 C57BL/6J, n=5 room air, n=4 smoke/aneurysm) (**B)** gating strategy to sort CD45^{+} and CD31^{+} cells from abdominal aortas for single cell RNA sequencing. **(C)** UMAP dimensionality reduction analysis identifying unique immune cell populations **(D)** Feature plots depicting single cell gene expression of canonical immune cell markers.

FIGURE 11

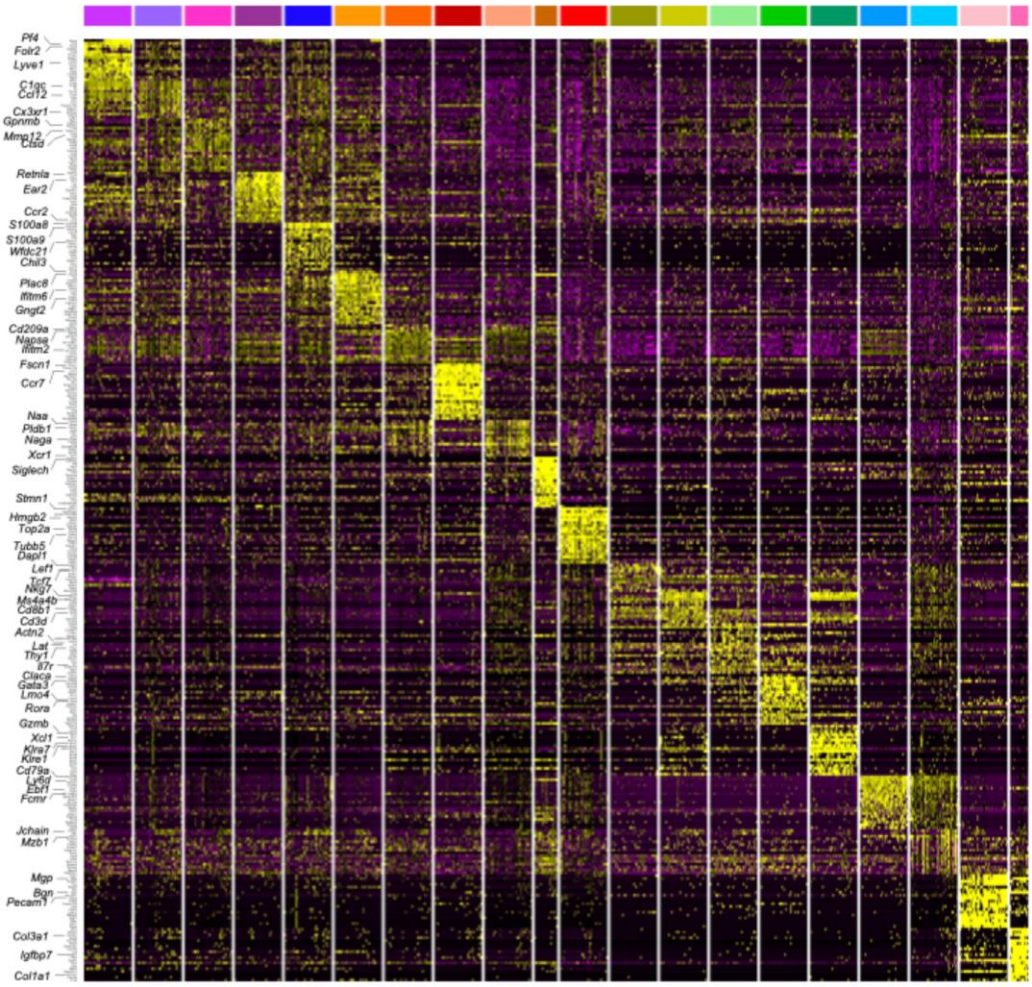

Figure 11: Differential gene expression of immune cell clusters. Heat map of the top 20 differentially expressed genes per immune cell cluster identified by single cell RNA sequencing analysis of abdominal aortas from C57BL/6 mice (control, n=5), *Apoe*$^{-/-}$ mice on a high cholesterol diet (HCD) exposed to room air (room air, n=5) or cigarette smoke with aneurysm (smoke/aneurysm, n=4) at 16 weeks.

FIGURE 12

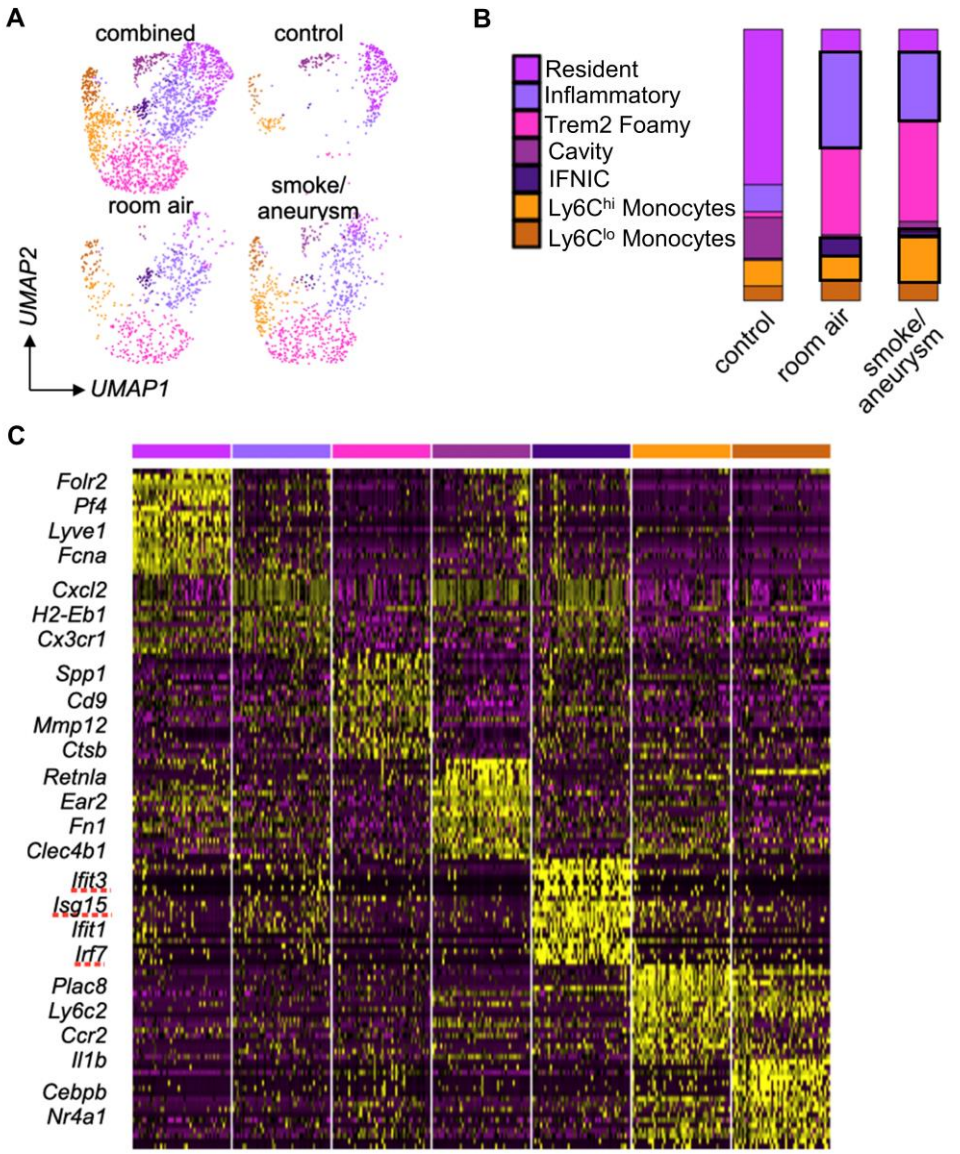

Figure 12: Hypercholesterolemia increases macrophage diversity in abdominal aortas of *Apoe*$^{-/-}$ mice. Single cell RNA sequencing of CD45^{+} cells from abdominal aortas from C57BL/6 mice (control, n=5), *Apoe*$^{-/-}$ mice on a high cholesterol diet (HCD) exposed to room air (room air, n=5) or cigarette smoke with aneurysm (smoke/aneurysm, n=4) at 16 weeks. (**A)** UMAP dimensionality reduction analysis identifying unique monocyte and macrophage populations. (**B)** Proportion of each population with significant changes outlined in black (bootstrap false discovery rate <0.01). **(C)** Heat map of the top 20 differentially expressed genes per populations identified in (A).

FIGURE 13

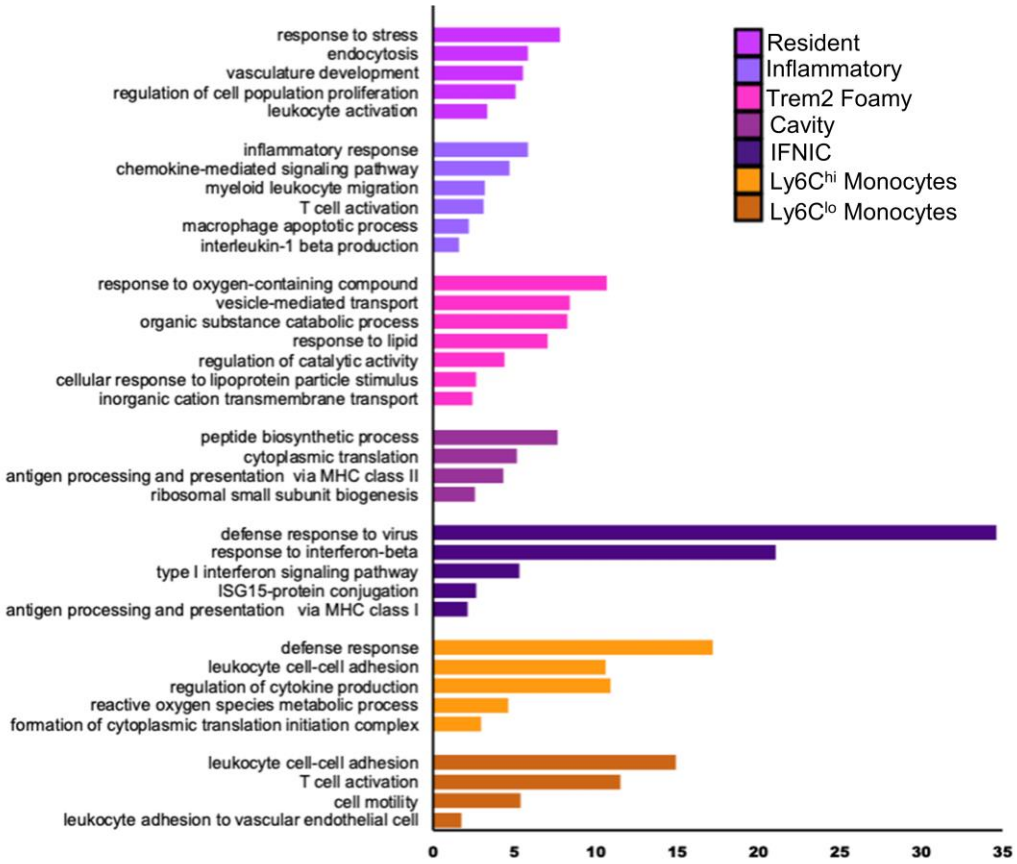

Figure 13: Functional enrichment analysis of arterial monocyte and macrophage populations. Pathway analysis (gProfiler) of significantly upregulated biological or functional processes based on differentially expressed genes in each monocyte/macrophage population identified by single cell RNA sequencing of CD45^{+} cells from abdominal aortas from C57BL/6 mice (control, n=5), *Apoe*$^{-/-}$ mice on a high cholesterol diet (HCD) exposed to room air (room air, n=5) or cigarette smoke with aneurysm (smoke/aneurysm, n=4) at 16 weeks.

FIGURE 14

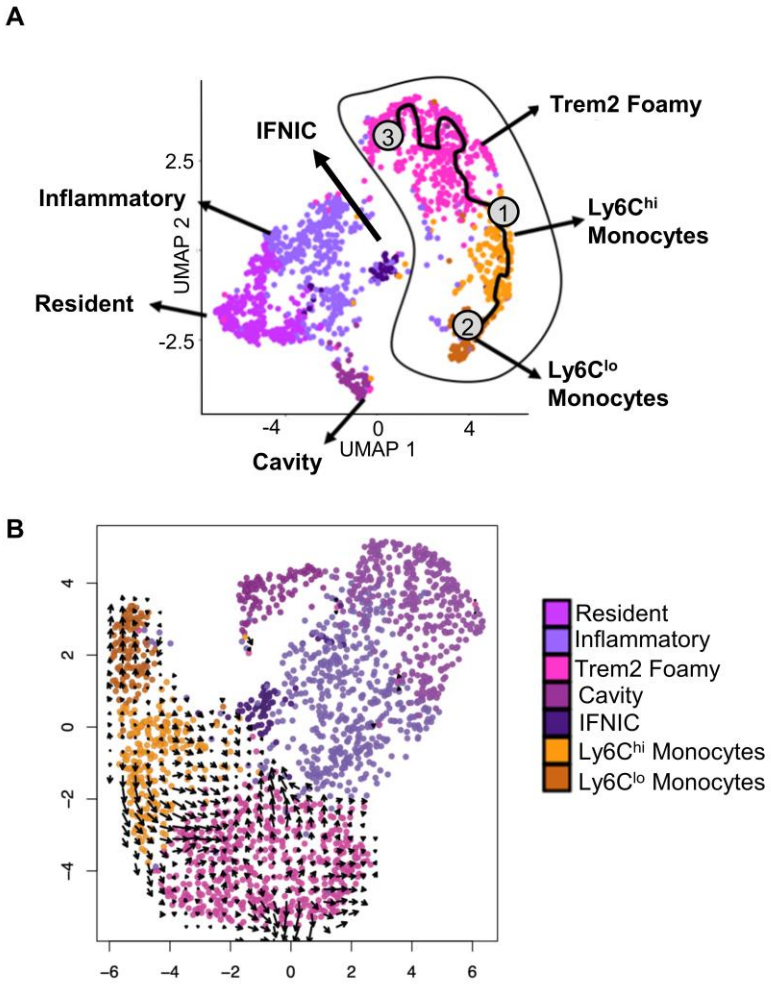

Figure 14: Trajectory analysis predicts Ly6C^{hi} monocyte differentiation to Trem2 foamy macrophages. Single cell RNA sequencing of CD45^{+} cells from abdominal aortas from C57BL/6 mice (control, n=5), *Apoe*$^{-/-}$ mice on a high cholesterol diet (HCD) exposed to room air (room air, n=5) or cigarette smoke with aneurysm (smoke/aneurysm, n=4) at 16 weeks. (**A)** UMAP dimensionality reduction using Monocle 3 visualized with Seurat cluster annotations. Solid outline indicates monocyte-derived macrophage partition as identified by trajectory analysis in Monocle 3. Numbered line indicates trajectory of (1) Ly6C^{hi} monocytes towards (2) Ly6C^{lo} monocytes or (3) Trem2 foamy macrophages. (**B)** Velocity field projected onto UMAP plot of unique monocyte and macrophage populations.

FIGURE 15

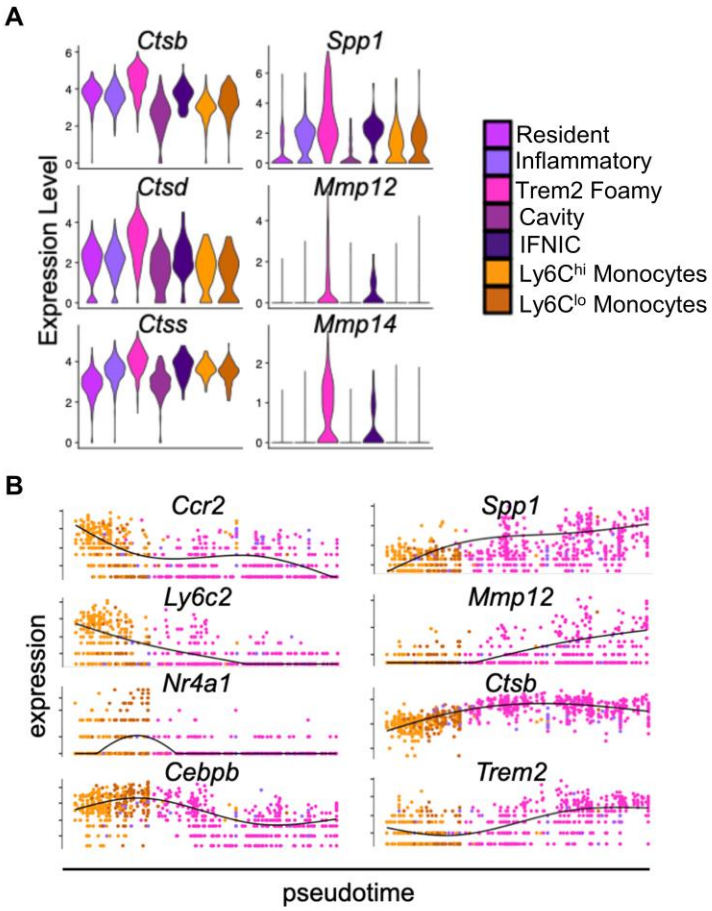

Figure 15: Trem2 foamy macrophages have enriched expression of genes implicated in extracellular matrix degradation. Single cell RNA sequencing of CD45^{+} cells from abdominal aortas from C57BL/6 mice (control, n=5), *Apoe*$^{-/-}$ mice on a high cholesterol diet (HCD) exposed to room air (room air, n=5) or cigarette smoke with aneurysm (smoke/aneurysm, n=4) at 16 weeks. (**A)** Violin plots of single cell gene expression per population for genes implicated in degeneration of the extracellular matrix. (**B)** Change in gene expression across pseudo-time from Ly6C^{hi} monocytes to Trem2 foamy macrophages.

FIGURE 16

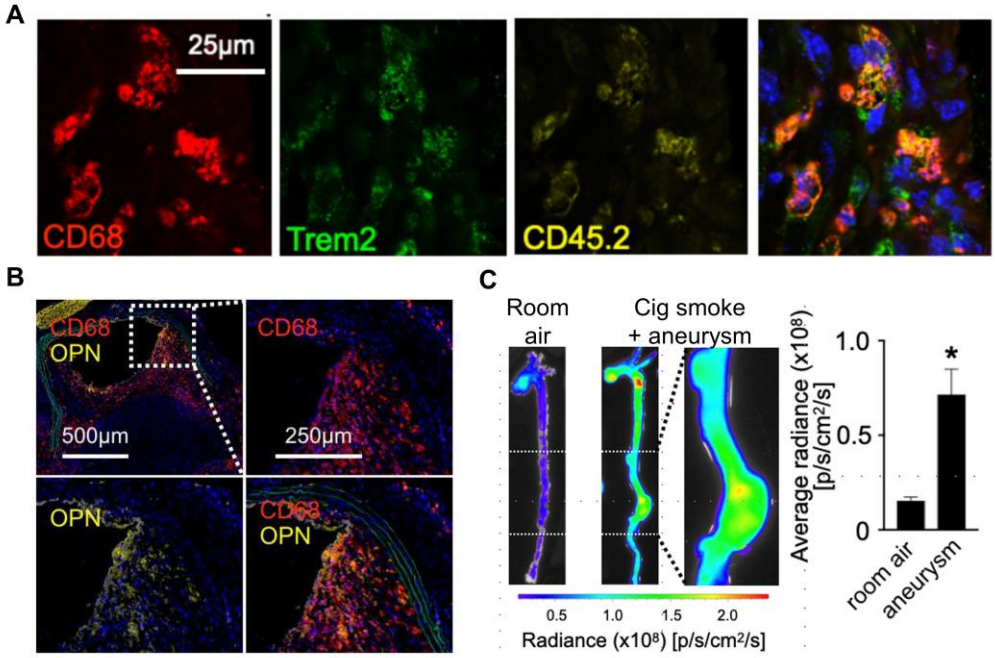

Figure 16: *in vivo* protein expression of Trem2 macrophage associated genes. *Apoe*$^{-/-}$ mice were placed on a high cholesterol diet (HCD) and exposed to room air or cigarette smoke for 16 weeks. **(A)** Immunofluorescence showing co-localization of TREM2 (triggering receptor expressed on myeloid cells 2) and partner (monocyte)-derived CD45.2^{+}CD68^{+} macrophages in cross-sections of aneurysmal tissue of CD45.1 parabionts. **(B)** Immunofluorescence showing co-localization of CD68^{+} cells with osteopontin (OPN) in aneurysmal cross-sections. **(C)** Detection of intracellular cathepsin activity using near infrared protease-sensing (lys-lys cleavage of Prosense-680) *in vivo* (n=8 room air, n=3 cig smoke with aneurysm). Two-tailed unpaired Student's t-test **P*<0.05.

FIGURE 17

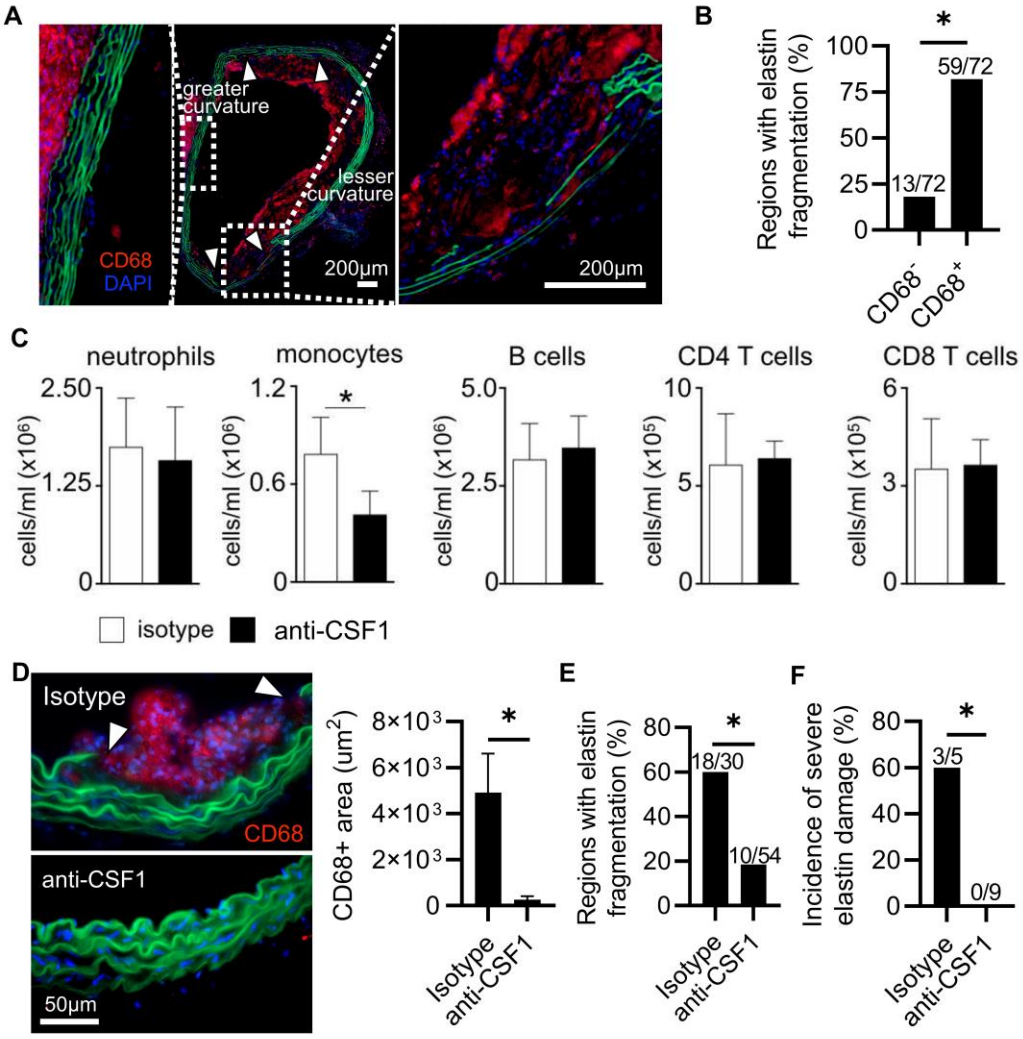

Figure 17: Macrophages play a critical role in elastin damage in aortas of smoke-exposed mice. (A) Representative images of CD68⁺ cells (red) penetrating and disrupting elastin fibres (green) in aortic arch cross-sections of smoke-exposed *Apoe*$^{-/-}$ mice at 16 weeks. **(B)** Quantification of the association between elastin fragmentation and overlying CD68⁺ cells in the aortic arch. Data obtained from serial cross-sections of 11 aortas with elastin damage. Two-sided Fisher's exact test **P<0.05.* **(C-F)** *Apoe*$^{-/-}$ mice exposed to cigarette smoke for 4 weeks were treated with isotype or anti-colony stimulating factor 1 (anti-CSF1) antibody for the last 3 weeks of exposure (n=5 isotype and n=9 anti-CSF1). Data represent analysis of 6 abdominal aorta cross-sections per mouse. **(D)** Representative images and quantification of CD68⁺ staining (red) in the abdominal aorta. Two-tailed unpaired Student's t-test **P*<0.05. **(E)** Quantification of elastin fragmentation in abdominal aorta. Two-sided Fisher's exact contingency test **P*<0.05. **(F)** Incidence of severe elastin fragmentation in abdominal aortas. Two-sided Fisher's exact contingency test **P*<0.05.

FIGURE 18

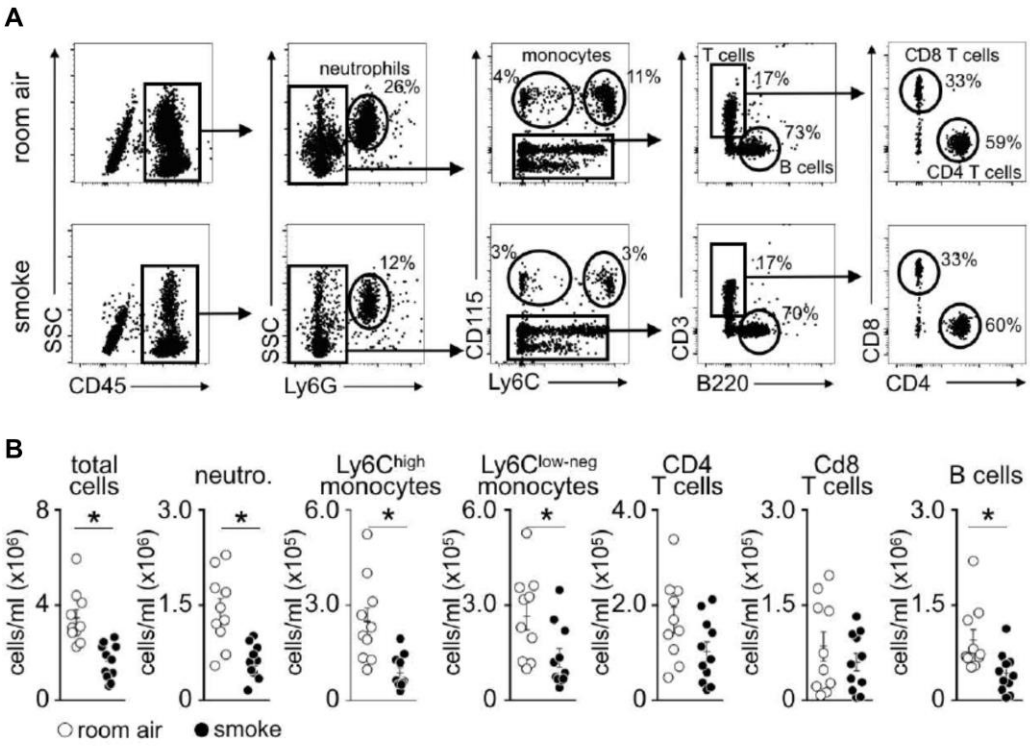

Figure 18: Cigarette smoke exposure decreases circulating leukocytes in *Apoe*$^{-/-}$ mice. Male *Apoe*$^{-/-}$ mice were placed on a high cholesterol diet (HCD) and exposed to room air (white) or cigarette smoke (black) for 12 weeks. **(A)** Cell proportions and representative gating strategy to identify major blood leukocyte populations by flow cytometry. **(B)** Quantification of major blood leukocyte populations. Two-tailed unpaired Student's t-test *P<0.05.

FIGURE 19

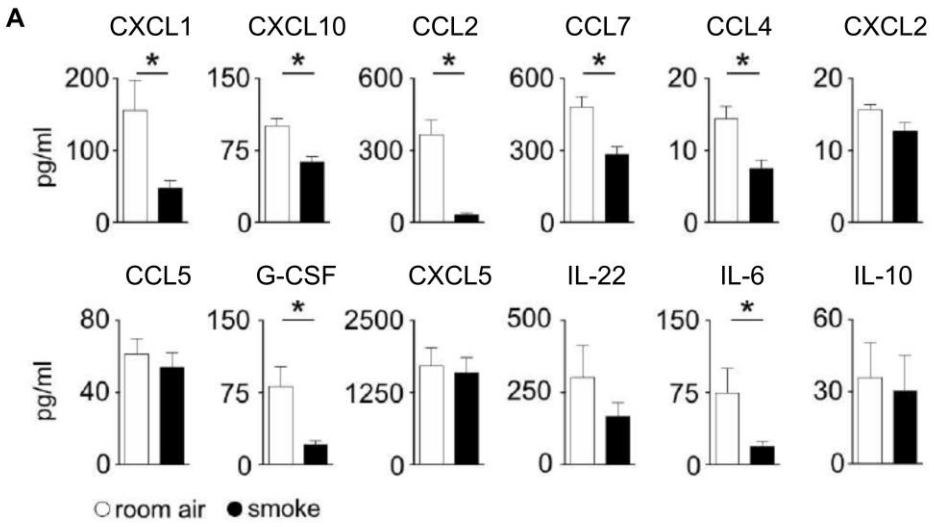

Figure 19: Cigarette smoke exposure decreases circulating chemokines and cytokines in *Apoe*$^{-/-}$ mice. (A) Quantification of cytokines by Luminex multiplex assay in the serum of male *Apoe*$^{-/-}$ mice placed on a high cholesterol diet (HCD) and exposed to room air (white) or cigarette smoke (black) for 12 weeks. Two-tailed unpaired Student's t-test *P<0.05. CXCL: C-X-C motif ligand, CCL: C-C motif ligand, G-CSF: granulocyte colony stimulating factor, and IL: interleukin.

FIGURE 20

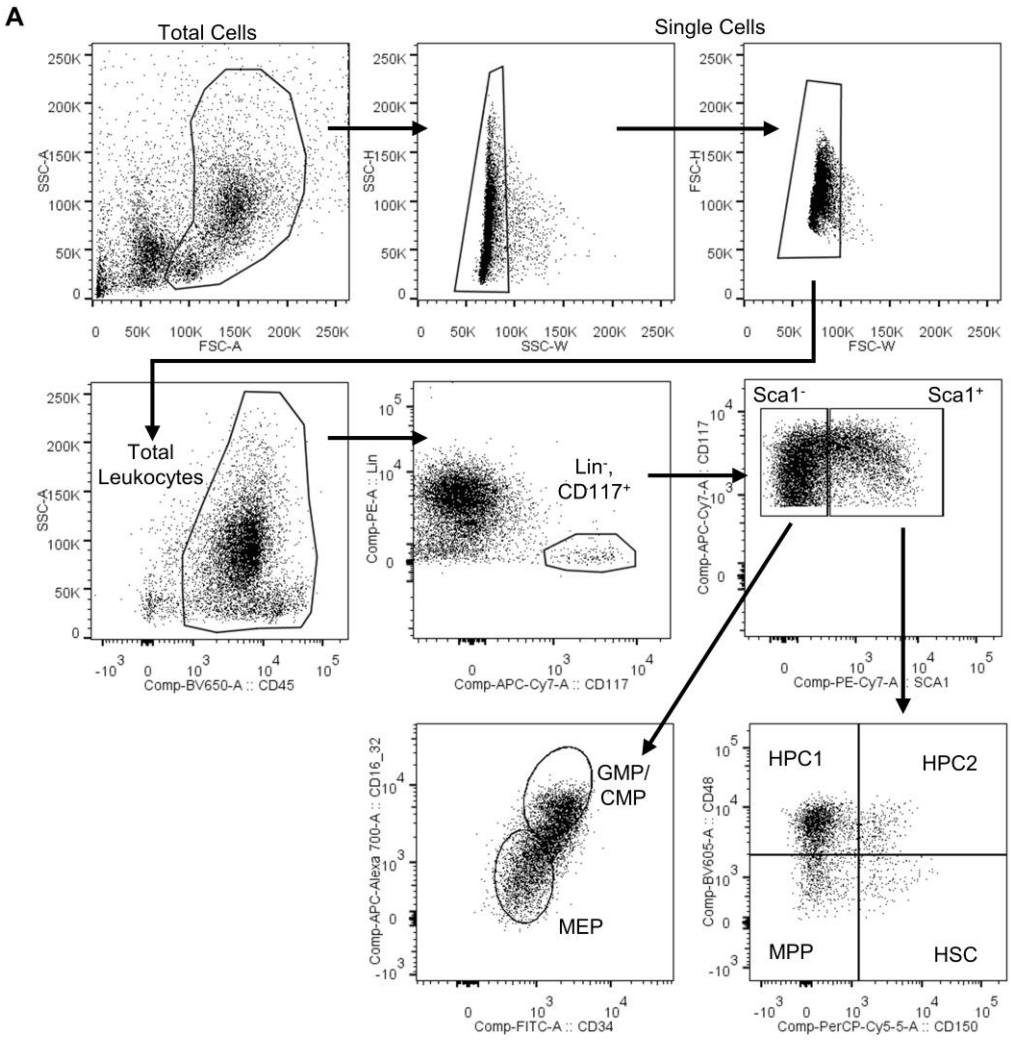

Figure 20: Gating strategy for hematopoietic stem and progenitor cell populations in the bone marrow. (A) Representative flow cytometry plots illustrating the gating strategy used to identify hematopoietic stem and progenitor cells in bone marrow of male *Apoe*$^{-/-}$ mice placed on a high cholesterol diet (HCD) for 12 weeks. Identified cell populations include hematopoietic stem cells (HSC), hematopoietic progenitor cells 1 and 2 (HPC1 and HPC2), multipotent progenitor cells (MPP), granulocyte-monocyte progenitor cells (GMP), common myeloid progenitor cells (CMP), and megakaryocyte-erythroid progenitor cells (MEP).

FIGURE 21

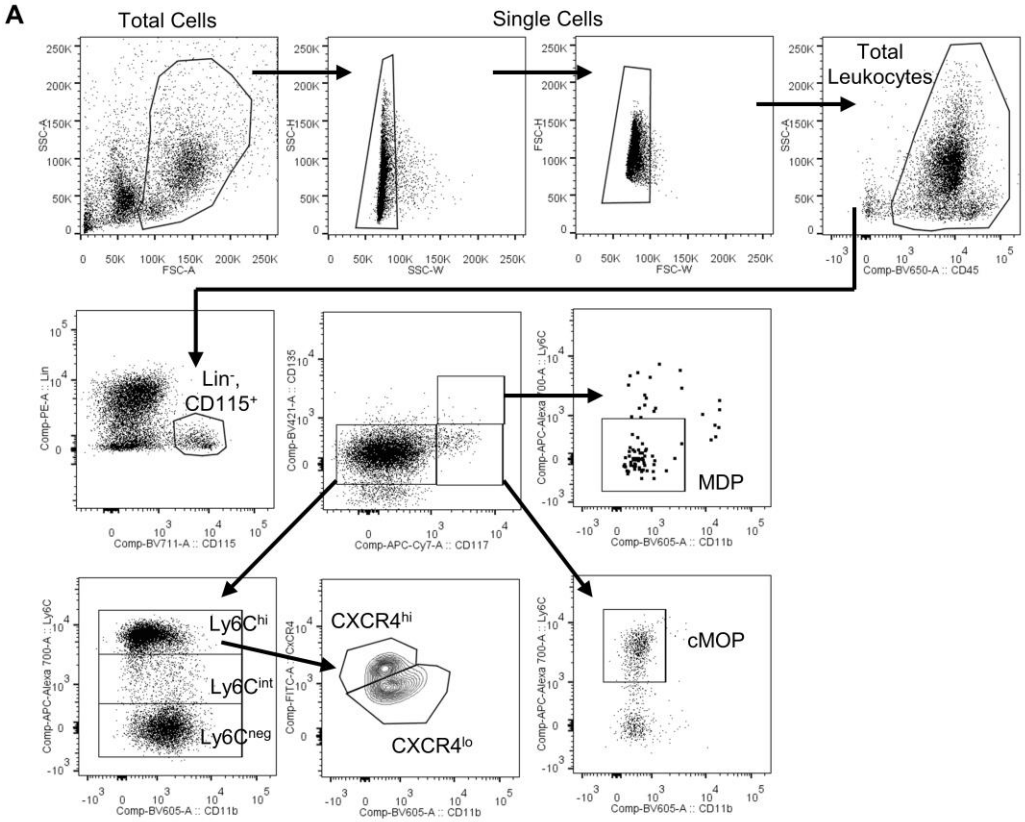

Figure 21: Gating strategy for myeloid-focused progenitor cell populations in the bone marrow. (A) Representative flow cytometry plots illustrating the gating strategy used to identify myeloid-focused progenitor cells in bone marrow of male *Apoe*$^{-/-}$ mice placed on a high cholesterol diet (HCD) for 12 weeks. Identified myeloid-focused progenitor populations include monocyte-dendritic cell progenitors (MDP), common monocyte progenitors (cMoP), transitional pre-monocyte (CxCR4^{hii}), and mature monocytes ready for egress (CxCR4^{lo}).

FIGURE 22

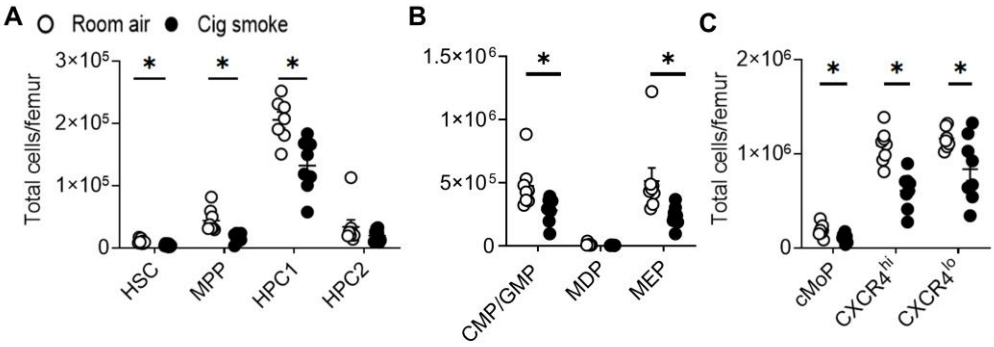

Figure 22: Cigarette smoke exposure decreases hematopoietic stem and progenitor cell populations in the bone marrow. Male *Apoe*$^{-/-}$ mice were placed on a high cholesterol diet (HCD) and exposed to room air (white) or cigarette smoke (black) for 12 weeks. Quantification of major hematopoietic stem and progenitor cell populations in the bone marrow. including **(A)** hematopoietic stem cells (HSC), hematopoietic progenitor cells 1 and 2 (HPC1 and HPC2), multipotent progenitor cells (MPP), **(B)** granulocyte-monocyte progenitor cells (GMP), common myeloid progenitor cells (CMP), and megakaryocyte-erythroid progenitor cells (MEP), monocyte-dendritic cell progenitors (MDP), **(C)** common monocyte progenitors (cMoP), transitional pre-monocyte (CxCR4^{hii}), and mature monocytes ready for egress (CxCR4^{lo}). Data analyzed by ordinary one-way ANOVA, Tukey's multiple comparisons **P*<0.05.

FIGURE 23

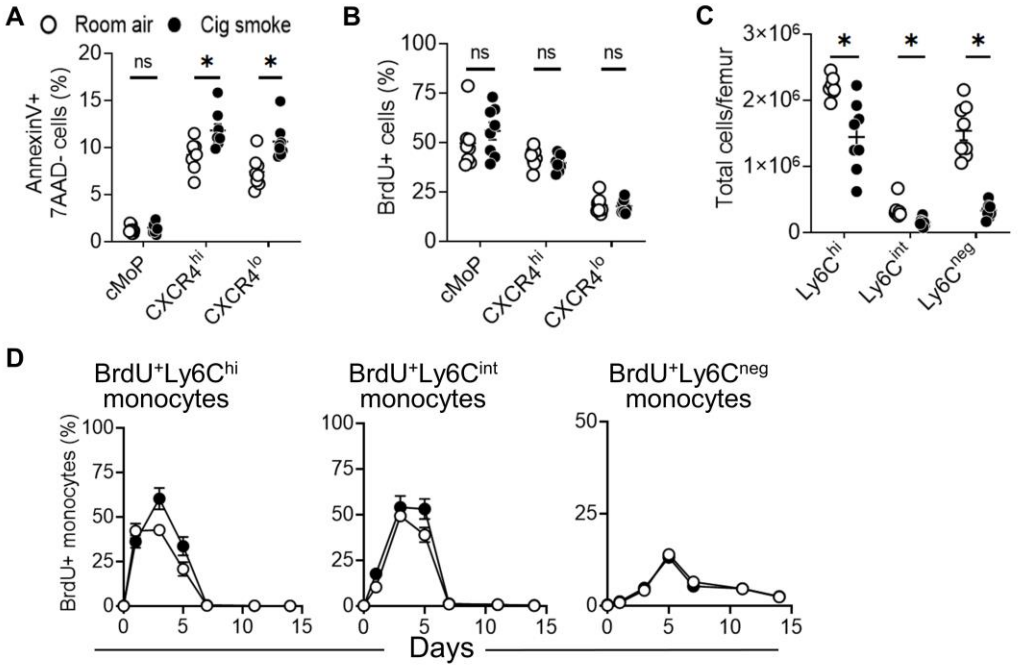

Figure 23: Cigarette smoke increases monocyte progenitor cell death in the bone marrow but does not impact monocyte kinetics in the blood. Male *Apoe*$^{-/-}$ mice were placed on a high cholesterol diet (HCD) and exposed to room air (white) or cigarette smoke (black) for 12 weeks and received injections of BrdU 3h prior to sample collection. **(A)** Percent of apoptotic cells identified as annexin V+ and 7AAD- by flow cytometry in the bone marrow. **(B)** Percent of proliferating cells identified as BrdU+ by flow cytometry. **(C)** Bone marrow monocyte numbers assessed by flow cytometry. Data in **(A-C)** analyzed by ordinary one-way ANOVA, Tukey's multiple comparisons **P*<0.05. **(G)** Kinetics of Ly6C^{hi}, Ly6C^{int}, and Ly6C^{lo} monocytes in the blood after BrdU-pulse labelling and egress from the bone marrow over 14 days. n=7 mice per group. Holm-Sidak multiple comparisons, ns *P*>0.05.

FIGURE 24

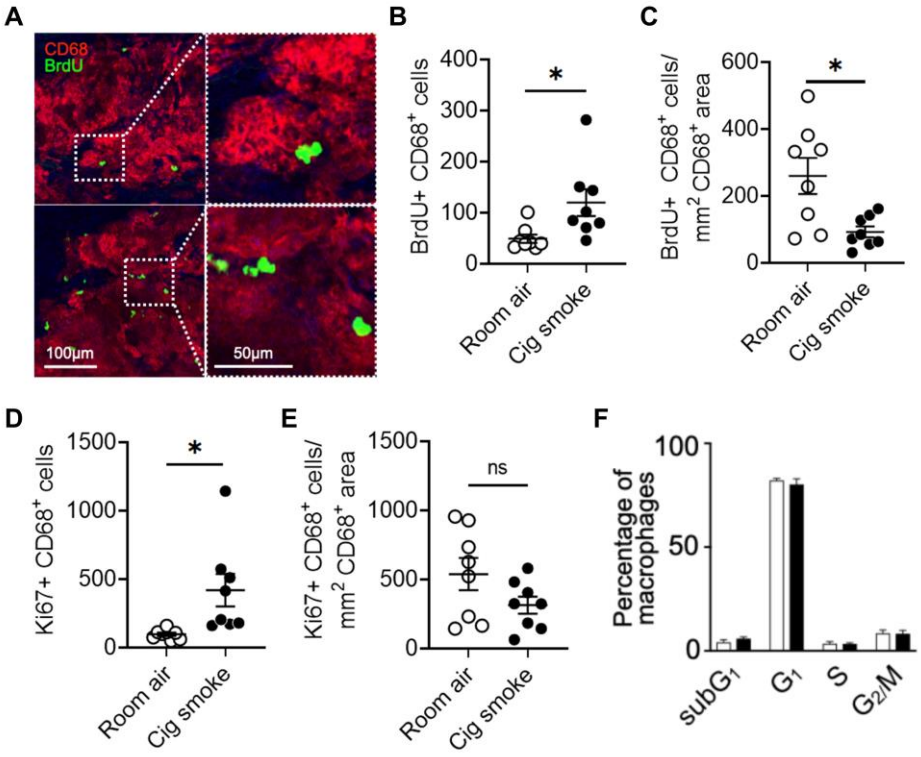

Figure 24: Increase in total but not proportion of proliferating cells in abdominal aortas of smoke exposed *Apoe*$^{-/-}$ mice. *Apoe*$^{-/-}$ mice were placed on a high cholesterol diet (HCD) and exposed to room air (white) or cigarette smoke (black) for 12 weeks. **(A)** Representative images of co-stained BrdU^{+}CD68^{+} cells in the abdominal aorta and quantification of **(B)** total and **(C)** proportion of BrdU^{+}CD68^{+} cells **(D)** Total number and **(E)** proportion of Ki67^{+}CD68^{+} cells in the abdominal aorta at 12 weeks. **(F)** Cell cycle analysis of DAPI-stained arterial macrophages by flow cytometry (n=3). Data analyzed by two-tailed unpaired Student's t-test *P<0.05, with correction for multiple comparisons in (F).

FIGURE 25

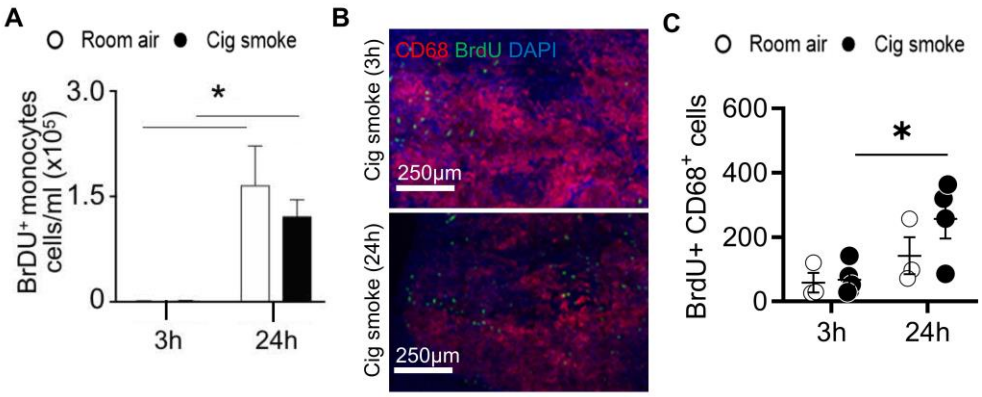

Figure 25: No increase in arterial BrdU⁺ macrophages in the absence of labelled monocyte recruitment. *Apoe*$^{-/-}$ mice were placed on a high cholesterol diet (HCD) and exposed to room air (white) or cigarette smoke (black) for 5 weeks. Mice received BrdU injections 3h or 24h before sample collection. **(A)** BrdU⁺ monocytes in the blood. **(B)** Representative images of *en face* BrdU and CD68 co-staining in the aortic arch. **(C)** Quantification of BrdU⁺CD68⁺ cells in the aortic arch. Data analyzed by ordinary one-way ANOVA, Tukey's multiple comparisons **P*<0.05.

FIGURE 26

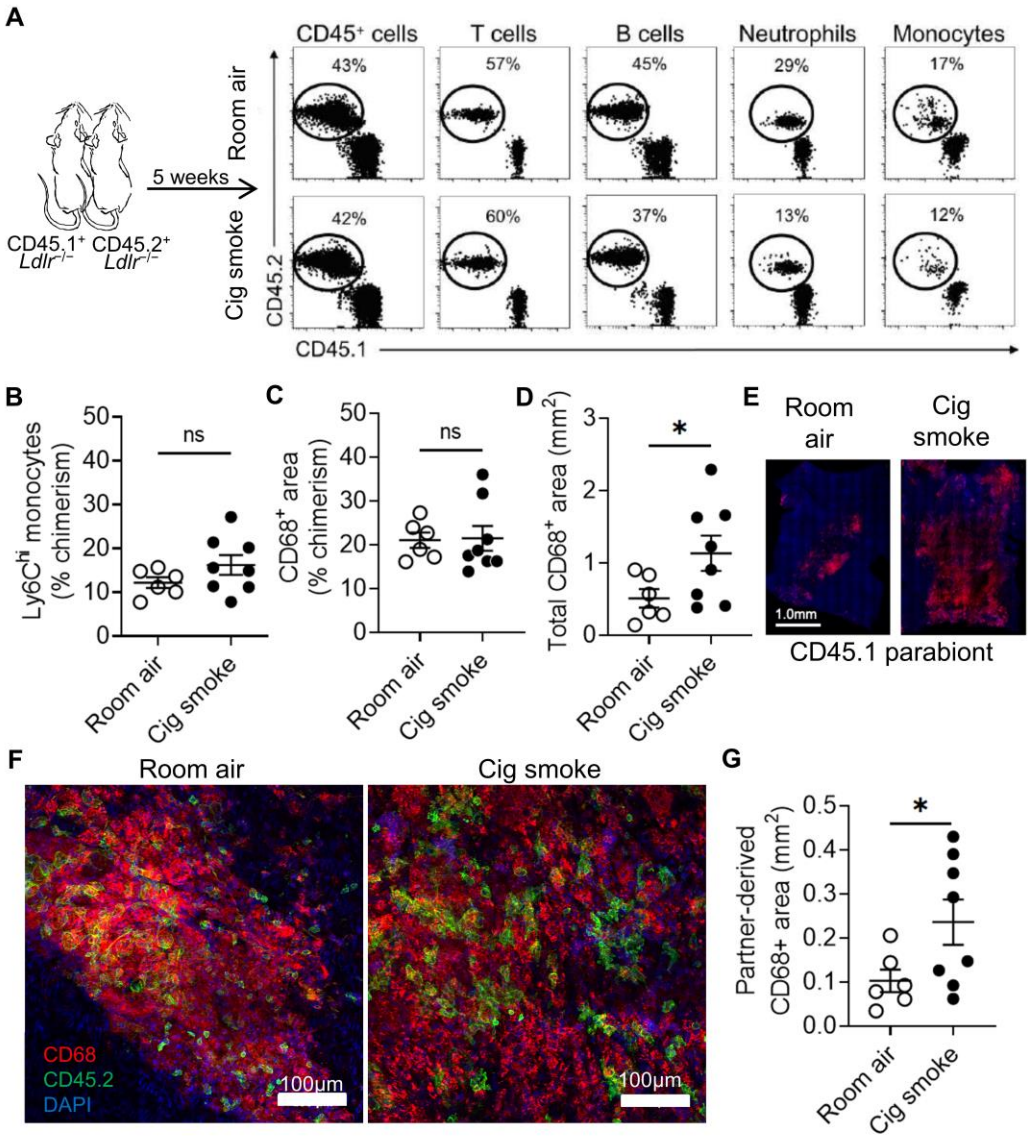

Figure 26: Cigarette smoke exposure increases monocyte recruitment into the aorta. Low density lipoprotein deficient (*Ldlr*$^{-/-}$) congenic mice expressing either CD45.1 or CD45.2 were surgically joined by parabiosis allowing for establishment of shared circulation. **(A)** Parabionts were exposed to room.air (white) or cigarette smoke (black) for 5 weeks. Chimerism of CD45.1 and CD45.2 expressing leukocytes was assessed by flow cytometry in the blood **(B)** Chimerism of Ly6C^{hi} monocytes in the blood and **(C)** Chimerism of CD68^{+} area in the aortic arch. **(D)** Total CD68^{+} area in the aortic arch. **(E)** Representative images of total CD68^{+} area in the aortic arch of CD45.1 parabionts **(F)** Representative images of *en face* CD68 and CD45.2 co-staining in the aortic arch of CD45.1 parabionts. **(G)** Total partner-derived CD68^{+} area in the aortic arch. Data are from n= 6 room air and n=8 cig smoke mice and analysed by two-tailed unpaired Student's t-test *P<0.05.

FIGURE 27

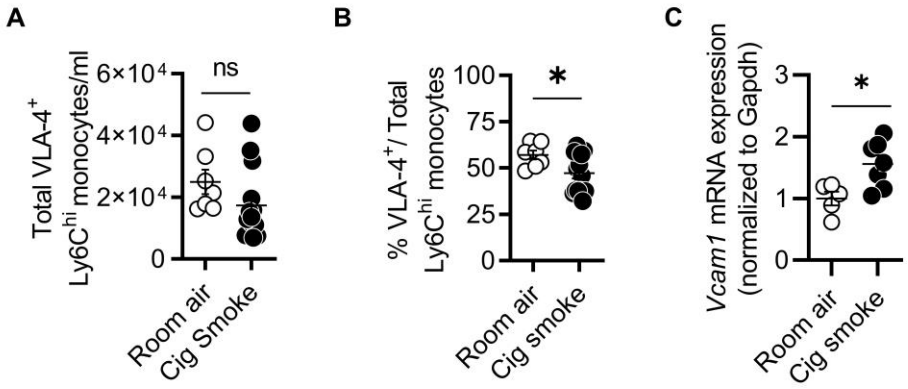

Figure 27: Cigarette smoke exposure increases expression of endothelial adhesion molecules but not cognate ligands on monocytes. *Apoe*$^{-/-}$ mice were placed on a high cholesterol diet (HCD) and exposed to room air (white) or cigarette smoke (black) for 16 weeks. **(A)** Total number and **(B)** proportion of VLA-4^{+} (CD49d^{+}CD29^{+}) Ly6C^{hi} monocytes in the blood. **(C)** *Vcam1* mRNA expression in whole aortas normalized to *Gapdh*. Data analyzed by two-tailed unpaired Student's t-test **P*<0.05.

FIGURE 28

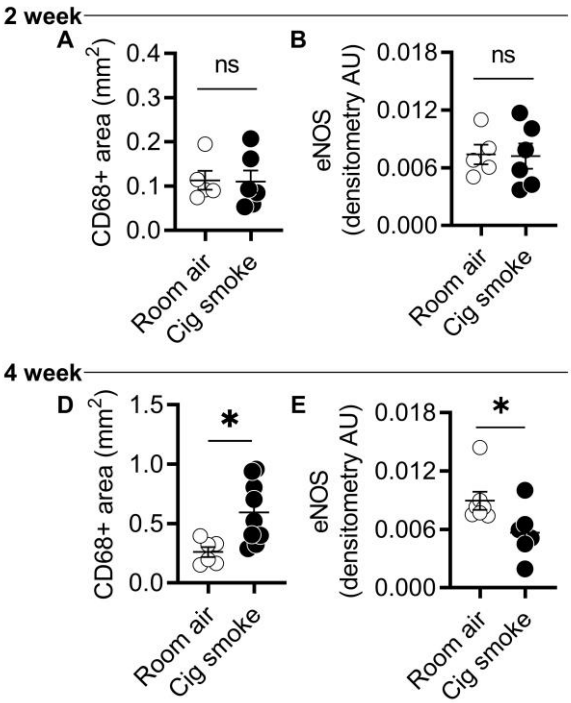

Figure 28: Reduced eNOS in aortas is associated with increased arterial macrophage accumulation in smoke exposed *Apoe*$^{-/-}$ mice. Male *Apoe*$^{-/-}$ mice on a high cholesterol diet (HCD) were exposed to room air (white) or cigarette smoke (black) for **(A-B)** 2 weeks or **(C-D)** 4 weeks. (**A, C)** *en face* CD68^{+} area in the lesser curvature of the aortic arch. **(B, D**) Quantification of eNOS protein in whole aortic tissue by Western blot. Data is normalized to total protein stain per sample. Data analyzed by Two-tailed unpaired Student's t-test **P*<0.05.

FIGURE 29

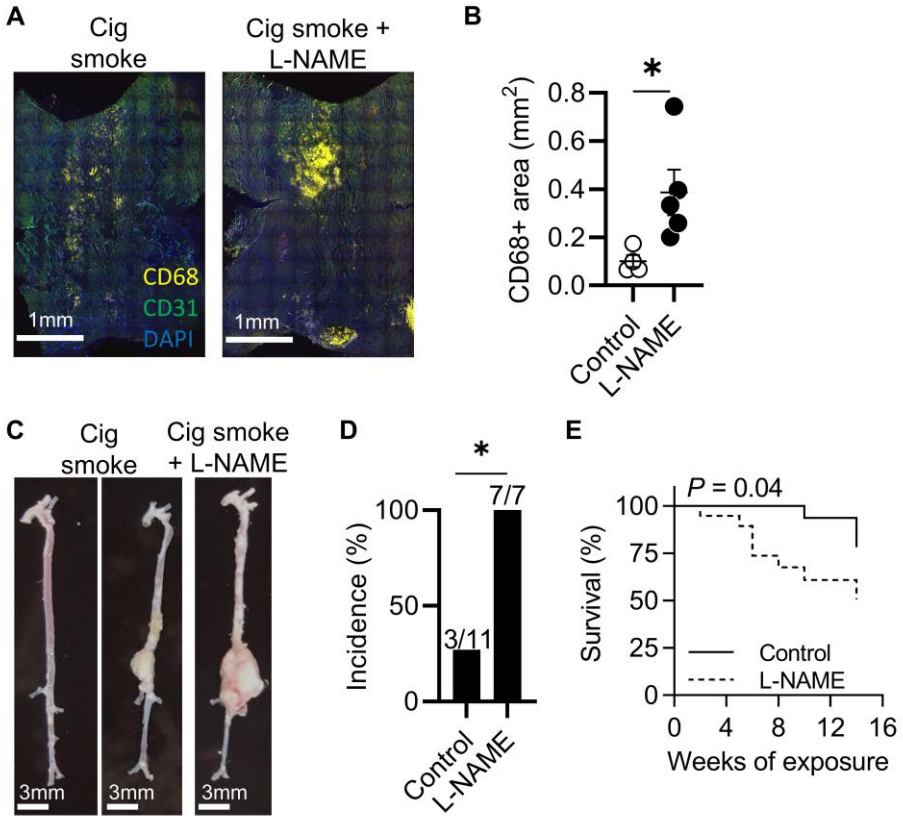

Figure 29: NOS inhibition increases arterial macrophages and induces aneurysm formation and rupture in smoke exposed *Apoe*$^{-/-}$ mice. Male *Apoe*$^{-/-}$ mice on a high cholesterol diet (HCD) were exposed to cigarette smoke and received normal water (control) or L-NAME-treated water (L-NAME). **(A)** *en face* CD68^{+} area in the lesser curvature of the aortic arch at 2 weeks. **(B)** Gross morphology of whole aortas at 14 weeks. **(C)** Aneurysm incidence at 14 weeks. **(D)** Kaplan-Meier survival curve tracking death due to ruptured aneurysm (n=16 control, n=19 L-NAME). Log-rank (Mantel-Cox) test **P*=0.04.

TABLE 1: Top 20 differentially expressed genes in each cell cluster

Gene	avg_ logFC	pct.1	pct.2	p_val_adj	Cluster Name
Fcna	1.552	0.506	0.039	4.67E-290	Resident Mac
Mgl2	1.724	0.864	0.209	6.63E-257	Resident Mac
Sepp1	2.023	1	0.667	3.15E-255	Resident Mac
Maf	1.489	0.869	0.233	1.94E-248	Resident Mac
Hpgd	1.314	0.679	0.118	1.40E-237	Resident Mac
C1qc	1.660	1	0.638	1.58E-231	Resident Mac
Apoe	3.512	0.683	0.137	3.71E-230	Resident Mac
Dab2	1.494	0.938	0.351	3.87E-229	Resident Mac
Trf	1.622	0.976	0.422	1.41E-225	Resident Mac
Cfh	1.271	0.769	0.18	2.34E-222	Resident Mac
Cd36	1.349	0.688	0.133	4.35E-222	Resident Mac
C1qa	1.671	1	0.674	2.59E-220	Resident Mac
Fcgrt	1.607	0.899	0.35	6.70E-215	Resident Mac
Ednrb	1.164	0.427	0.04	2.17E-212	Resident Mac
Cd209g	1.480	0.343	0.021	4.54E-210	Resident Mac
Itm2b	1.083	1	0.969	1.97E-204	Resident Mac
Timp2	1.406	0.916	0.381	2.13E-201	Resident Mac
Ninj1	1.689	0.892	0.377	1.21E-198	Resident Mac
Stab1	1.280	0.75	0.207	1.51E-191	Resident Mac
Pmp22	1.114	0.653	0.14	8.48E-189	Resident Mac
Ctsc1	0.980	0.994	0.658	1.03E-179	Inflammatory Mac
C1qb1	1.146	0.994	0.753	3.88E-177	Inflammatory Mac
Fcgr4	0.833	0.681	0.185	3.86E-174	Inflammatory Mac
Trf1	0.937	0.925	0.41	4.68E-174	Inflammatory Mac
C1qc1	1.081	0.982	0.628	4.54E-172	Inflammatory Mac
C1qa1	1.119	0.979	0.666	5.29E-168	Inflammatory Mac
Aif11	0.928	0.946	0.465	6.72E-167	Inflammatory Mac
Clec4a21	0.817	0.819	0.276	9.86E-166	Inflammatory Mac
Adgre11	0.889	0.859	0.313	6.42E-165	Inflammatory Mac
Ms4a71	0.991	0.907	0.418	3.80E-163	Inflammatory Mac
Clec4b1	0.836	0.625	0.159	1.19E-159	Inflammatory Mac
Sepp11	0.832	0.989	0.658	1.24E-157	Inflammatory Mac
Clec4a11	0.812	0.824	0.29	2.21E-155	Inflammatory Mac
Tmem176b1	0.895	0.963	0.533	1.04E-154	Inflammatory Mac
Cx3cr1	0.862	0.688	0.212	2.18E-149	Inflammatory Mac
Csf1r1	0.759	0.939	0.417	2.78E-149	Inflammatory Mac
Fcgr31	0.786	0.942	0.429	1.40E-148	Inflammatory Mac
Fcgr2b1	0.858	0.894	0.423	6.84E-148	Inflammatory Mac
Itm2b1	0.665	1	0.968	5.87E-144	Inflammatory Mac
Mrc11	0.658	0.745	0.235	1.13E-142	Inflammatory Mac
Syngr1	0.889	0.542	0.049	2.78E-293	Trem2 Foamy Mac
Lilr4b	1.333	0.883	0.247	1.95E-257	Trem2 Foamy Mac
Lgals3	1.952	0.996	0.744	3.92E-248	Trem2 Foamy Mac
Cd682	1.375	0.99	0.543	7.96E-229	Trem2 Foamy Mac
Mmp14	0.803	0.62	0.098	3.03E-226	Trem2 Foamy Mac
Ctsb2	1.708	1	0.861	1.53E-225	Trem2 Foamy Mac
Lilrb4a	1.353	0.928	0.365	5.37E-218	Trem2 Foamy Mac
Ctsz1	1.153	0.996	0.717	3.02E-217	Trem2 Foamy Mac
Fth12	1.210	1	0.996	6.11E-208	Trem2 Foamy Mac
Ftl12	1.215	1	0.993	6.65E-208	Trem2 Foamy Mac
Anxa51	1.168	0.981	0.649	4.31E-203	Trem2 Foamy Mac
Ctss1	1.219	1	0.872	9.98E-200	Trem2 Foamy Mac
Lgmn2	1.289	0.992	0.632	3.93E-190	Trem2 Foamy Mac
Ctsd	1.589	0.992	0.705	1.42E-188	Trem2 Foamy Mac
Mpeg11	1.086	0.943	0.391	1.77E-186	Trem2 Foamy Mac
Gusb1	1.070	0.904	0.368	3.43E-184	Trem2 Foamy Mac
Slc15a31	0.798	0.764	0.193	1.10E-182	Trem2 Foamy Mac

Gene	avg_ logFC	pct.1	pct.2	p_val_adj	Cluster Name
Cxcl161	1.184	0.92	0.39	5.15E-181	Trem2 Foamy Mac
Cstb	1.363	0.975	0.605	1.25E-176	Trem2 Foamy Mac
Trem22	1.255	0.846	0.304	6.20E-176	Trem2 Foamy Mac
Hr	0.488	0.259	0.004	1.29E-120	Cavity Mac
Ear2	2.321	0.759	0.1	1.68E-59	Cavity Mac
Aldh1a2	0.514	0.259	0.011	6.27E-51	Cavity Mac
Fn11	2.048	0.926	0.19	1.31E-50	Cavity Mac
Upb1	0.697	0.333	0.023	1.04E-42	Cavity Mac
Gfra2	0.431	0.333	0.028	1.33E-33	Cavity Mac
Lpl2	2.003	0.796	0.201	2.49E-32	Cavity Mac
Lyz11	3.187	0.722	0.159	5.06E-32	Cavity Mac
Clec4b11	1.523	0.759	0.207	3.01E-28	Cavity Mac
Ccl62	1.809	1	0.605	4.67E-27	Cavity Mac
Retnla1	3.750	0.815	0.301	2.65E-26	Cavity Mac
Crip11	1.515	1	0.924	8.92E-26	Cavity Mac
Cd226	0.481	0.407	0.051	3.29E-25	Cavity Mac
Batf31	0.970	0.722	0.191	4.37E-23	Cavity Mac
Ccl93	1.363	0.963	0.523	8.40E-23	Cavity Mac
Dok21	1.036	0.796	0.245	9.41E-22	Cavity Mac
Gda2	1.082	0.759	0.218	1.23E-21	Cavity Mac
Ccdc109b3	1.117	0.796	0.305	2.71E-19	Cavity Mac
Gpx12	1.045	1	0.76	8.33E-19	Cavity Mac
Ccr21	0.933	0.981	0.423	3.55E-18	Cavity Mac
Wfdc21	1.147	0.368	0.01	1.77E-226	Neutrophils
Slfn4	0.793	0.443	0.02	9.73E-213	Neutrophils
Stfa2l1	0.924	0.297	0.006	6.49E-212	Neutrophils
S100a9	3.651	0.973	0.219	3.56E-180	Neutrophils
Retnlg	2.496	0.541	0.043	2.71E-179	Neutrophils
G0s2	0.693	0.335	0.017	1.60E-141	Neutrophils
S100a8	3.872	0.995	0.347	4.90E-141	Neutrophils
Mxd1	1.031	0.681	0.095	1.20E-134	Neutrophils
Lcn2	0.911	0.297	0.015	2.76E-130	Neutrophils
Csf3r	0.982	0.638	0.09	9.06E-128	Neutrophils
Gm5483	0.828	0.254	0.01	6.29E-125	Neutrophils
Trem1	0.631	0.378	0.028	2.02E-123	Neutrophils
Arg2	0.637	0.411	0.034	1.61E-121	Neutrophils
Slc7a11	0.804	0.486	0.051	1.06E-119	Neutrophils
Lrg1	1.002	0.541	0.065	2.30E-119	Neutrophils
Clec4d1	1.016	0.719	0.124	2.39E-116	Neutrophils
Il1r2	0.980	0.6	0.083	6.46E-116	Neutrophils
Cxcl22	1.593	0.881	0.265	1.51E-97	Neutrophils
Clec4e1	0.840	0.595	0.096	8.90E-97	Neutrophils
Mmp91	0.749	0.503	0.068	8.22E-94	Neutrophils
Hp1	1.883	0.753	0.123	1.02E-221	Classical Monocytes
Sirpb1c2	1.513	0.837	0.173	2.02E-207	Classical Monocytes
Gm9733	1.244	0.517	0.053	3.23E-194	Classical Monocytes
Ifitm62	1.509	0.747	0.157	1.91E-169	Classical Monocytes
Gsr1	1.484	0.837	0.226	7.55E-169	Classical Monocytes
Cebpb4	1.745	0.983	0.46	4.31E-155	Classical Monocytes
Trem31	0.805	0.353	0.03	1.35E-145	Classical Monocytes
Msrb12	1.513	0.943	0.433	6.75E-145	Classical Monocytes
Plac81	2.088	0.95	0.511	1.02E-143	Classical Monocytes
Ifitm34	1.405	1	0.709	2.72E-138	Classical Monocytes
Treml4	0.930	0.36	0.036	2.32E-131	Classical Monocytes
Lst14	1.337	0.953	0.462	6.23E-125	Classical Monocytes
Tyrobp5	0.978	1	0.78	6.30E-124	Classical Monocytes
Adgre4	0.966	0.39	0.047	7.74E-124	Classical Monocytes
Sirpb1b2	1.016	0.633	0.147	3.62E-119	Classical Monocytes

Gene	avg_ logFC	pct.1	pct.2	p_val_adj	Cluster Name
Lyz25	1.495	1	0.954	3.32E-116	Classical Monocytes
Klra22	0.870	0.463	0.076	9.89E-114	Classical Monocytes
Prdx51	1.227	0.943	0.61	3.48E-109	Classical Monocytes
Ms4a6c3	1.226	0.94	0.511	6.26E-107	Classical Monocytes
Fcer1g5	0.931	1	0.827	4.48E-104	Classical Monocytes
Ffar2	0.828	0.39	0.027	1.04E-221	cDC2
Plbd12	1.138	0.952	0.365	3.05E-182	cDC2
Cd209a	1.899	0.646	0.15	2.27E-167	cDC2
Napsa1	1.220	0.945	0.433	4.27E-162	cDC2
Gm2a2	1.160	0.975	0.537	6.81E-158	cDC2
Flt3	0.770	0.477	0.074	5.84E-155	cDC2
Syngr2	1.163	0.95	0.514	1.59E-153	cDC2
H2-Ab12	1.099	1	0.96	1.02E-147	cDC2
H2-DMb12	1.050	0.963	0.52	6.72E-144	cDC2
Spint1	0.642	0.393	0.052	2.52E-143	cDC2
Ifi302	1.079	0.947	0.545	9.47E-141	cDC2
Ddr1	0.442	0.29	0.025	3.18E-140	cDC2
H2-Aa2	1.037	1	0.925	1.05E-137	cDC2
Cd742	0.929	1	0.982	5.70E-131	cDC2
Klrd1	1.107	0.703	0.218	6.36E-123	cDC2
Cbfa2t3	0.696	0.616	0.158	3.45E-121	cDC2
Ifitm11	2.254	0.71	0.278	1.42E-120	cDC2
S100a114	0.870	0.995	0.718	1.09E-116	cDC2
Lsp12	0.805	0.986	0.793	1.67E-116	cDC2
Bex6	0.457	0.265	0.026	7.96E-116	cDC2
Mreg	0.953	0.592	0.016	2.13E-303	Fscn1 DC
Socs2	1.960	0.892	0.051	7.51E-297	Fscn1 DC
Il4i1	2.077	0.942	0.065	1.02E-275	Fscn1 DC
Slco5a1	0.533	0.275	0.003	1.06E-219	Fscn1 DC
Tbc1d41	2.137	0.925	0.091	1.44E-206	Fscn1 DC
Eno31	1.842	0.842	0.075	2.05E-194	Fscn1 DC
Tnfrsf9	1.184	0.642	0.038	1.93E-192	Fscn1 DC
Stap2	0.488	0.308	0.006	1.31E-187	Fscn1 DC
Tnfrsf4	1.533	0.683	0.047	6.13E-184	Fscn1 DC
Strip2	0.472	0.275	0.005	1.28E-166	Fscn1 DC
Gadd45b	1.569	0.8	0.094	3.39E-146	Fscn1 DC
Cd274	1.065	0.667	0.059	2.12E-144	Fscn1 DC
Ccr7	2.606	0.958	0.172	1.14E-140	Fscn1 DC
Ccl221	1.888	0.508	0.034	2.46E-139	Fscn1 DC
Zmynd151	2.076	0.75	0.09	8.97E-135	Fscn1 DC
Relb1	1.928	0.95	0.176	9.96E-134	Fscn1 DC
Cd200	1.456	0.775	0.095	1.14E-126	Fscn1 DC
Vsig10	0.588	0.308	0.012	7.58E-125	Fscn1 DC
Rogdi1	2.030	0.983	0.218	2.00E-124	Fscn1 DC
Tbc1d8	0.990	0.642	0.066	8.84E-123	Fscn1 DC
Gcsam	0.642	0.473	0.014	2.17E-234	cDC1
Xcr1	0.739	0.443	0.014	7.83E-213	cDC1
Snx22	0.532	0.42	0.014	4.71E-193	cDC1
Mycl	0.410	0.397	0.015	1.52E-169	cDC1
Flt32	0.819	0.786	0.09	4.69E-137	cDC1
Ifi2051	1.772	0.618	0.076	4.64E-109	cDC1
Clec9a	0.359	0.313	0.016	4.53E-105	cDC1
Pdia5	0.327	0.321	0.022	8.56E-85	cDC1
Itgae	0.399	0.336	0.025	3.87E-82	cDC1
Naga1	0.853	0.779	0.164	4.11E-74	cDC1
Tlr3	0.278	0.275	0.019	2.53E-71	cDC1
Dbn1	0.294	0.336	0.029	2.52E-70	cDC1
Amica11	0.705	0.672	0.119	8.09E-70	cDC1

Gene	avg_ logFC	pct.1	pct.2	p_val_adj	Cluster Name
Ffar4	0.301	0.252	0.017	6.91E-68	cDC1
St3gal51	0.502	0.527	0.075	1.44E-67	cDC1
Plbd13	1.308	0.992	0.398	1.61E-67	cDC1
Cystm1	0.334	0.389	0.044	7.02E-63	cDC1
P2ry14	0.414	0.389	0.046	1.15E-60	cDC1
Casp61	0.658	0.802	0.189	2.57E-59	cDC1
Btla	0.438	0.565	0.093	1.08E-58	cDC1
Paqr5	0.899	0.583	0.004	1.82E-280	pDC
Dntt	1.279	0.667	0.006	1.79E-264	pDC
Klk1	1.124	0.417	0.002	2.92E-256	pDC
Cd300c	1.370	0.667	0.006	7.21E-245	pDC
Cox6a2	2.681	0.875	0.015	1.49E-207	pDC
Siglech	2.787	1	0.029	4.84E-160	pDC
Upb11	1.475	0.792	0.023	8.54E-123	pDC
Klk1b27	0.942	0.375	0.004	6.30E-121	pDC
Ccr9	1.589	0.833	0.025	1.52E-119	pDC
Lefty1	1.145	0.667	0.019	5.59E-100	pDC
Pacsin1	1.239	0.75	0.028	1.78E-87	pDC
Smim5	1.759	0.75	0.031	5.57E-83	pDC
Gm14161	0.503	0.292	0.004	2.08E-82	pDC
Havcr1	0.510	0.292	0.004	1.69E-76	pDC
Klra17	0.870	0.583	0.02	3.83E-75	pDC
Atp1b1	2.082	0.917	0.053	6.05E-75	pDC
Runx2	1.289	0.792	0.044	2.77E-66	pDC
Spns3	1.256	0.667	0.031	1.46E-65	pDC
Lag3	1.622	0.833	0.057	2.86E-57	pDC
Tex2	0.907	0.625	0.031	1.75E-55	pDC
Cenpm	0.622	0.545	0.012	4.15E-299	Proliferating
Rrm2	1.573	0.688	0.024	8.40E-292	Proliferating
Fbxo5	0.723	0.545	0.013	1.18E-286	Proliferating
Melk	0.452	0.429	0.006	1.31E-284	Proliferating
Spc24	0.984	0.777	0.035	5.93E-280	Proliferating
Rad51ap1	0.460	0.411	0.006	1.16E-279	Proliferating
Kif23	0.833	0.643	0.021	1.10E-276	Proliferating
Ttk	0.326	0.312	0.002	1.09E-272	Proliferating
Bub1b	0.515	0.5	0.012	1.68E-266	Proliferating
Lockd	1.067	0.83	0.042	2.87E-263	Proliferating
Hist1h2ap	2.344	0.732	0.035	4.26E-263	Proliferating
Mxd3	0.396	0.339	0.003	2.49E-262	Proliferating
Tk1	0.857	0.634	0.024	5.85E-255	Proliferating
Hist1h2ae	0.608	0.473	0.011	2.73E-249	Proliferating
Kifc1	0.431	0.42	0.008	1.43E-246	Proliferating
Cdc20	1.053	0.571	0.019	5.46E-244	Proliferating
Asf1b	1.028	0.777	0.041	2.19E-242	Proliferating
Ckap2	0.386	0.339	0.004	1.94E-239	Proliferating
Nek2	0.359	0.286	0.003	1.88E-226	Proliferating
Cdca5	0.346	0.304	0.003	4.02E-226	Proliferating
Rps18	0.871	1	0.997	3.66E-292	CD4+CD8+
Rplp0	0.857	1	0.99	4.87E-289	CD4+CD8+
Rps6	0.807	1	0.994	3.06E-273	CD4+CD8+
Rps15a	0.872	1	0.994	7.33E-273	CD4+CD8+
Cd3d	1.324	0.934	0.341	1.11E-272	CD4+CD8+
Rps14	0.661	1	1	3.76E-272	CD4+CD8+
Rps23	0.722	1	0.997	1.61E-270	CD4+CD8+
Rps16	0.768	1	0.996	3.15E-266	CD4+CD8+
Rplp1	0.799	1	0.992	1.40E-265	CD4+CD8+
Rps27	0.813	1	0.999	4.88E-262	CD4+CD8+
Cd3g	1.127	0.921	0.292	6.02E-261	CD4+CD8+

Gene	avg_ logFC	pct.1	pct.2	p_val_adj	Cluster Name
Rps19	0.764	1	0.999	1.01E-259	CD4+CD8+
Rps7	0.852	1	0.989	2.65E-258	CD4+CD8+
Rpl32	0.719	1	0.998	8.91E-255	CD4+CD8+
Rps24	0.777	1	0.995	9.77E-253	CD4+CD8+
Rpl13a	0.765	1	0.999	1.39E-249	CD4+CD8+
Rps28	0.683	1	0.996	1.05E-248	CD4+CD8+
Rpl13	0.739	1	0.998	5.20E-246	CD4+CD8+
Rps29	0.616	1	0.999	9.89E-241	CD4+CD8+
Rpl17	0.743	1	0.991	4.61E-240	CD4+CD8+
Nkg7	2.409	0.982	0.327	2.26E-276	CD8 T cells
Gzmk	1.509	0.472	0.04	1.88E-239	CD8 T cells
Ms4a4b1	1.813	0.985	0.369	5.51E-232	CD8 T cells
Ccl51	2.711	0.982	0.512	2.23E-221	CD8 T cells
Ctsw	1.390	0.665	0.118	2.13E-208	CD8 T cells
Cd3g1	1.466	0.932	0.321	1.22E-190	CD8 T cells
Cd8a1	1.525	0.645	0.124	1.77E-186	CD8 T cells
Cd3d1	1.400	0.94	0.37	2.19E-181	CD8 T cells
Lck1	1.262	0.852	0.266	2.90E-170	CD8 T cells
AW1120101	1.483	0.972	0.607	4.47E-167	CD8 T cells
Ctla2a	1.163	0.668	0.152	1.85E-162	CD8 T cells
Cxcr6	1.257	0.568	0.103	7.43E-156	CD8 T cells
Hcst1	1.327	0.892	0.439	1.07E-147	CD8 T cells
Klrc1	1.113	0.318	0.029	3.16E-143	CD8 T cells
Thy11	1.207	0.782	0.25	5.26E-143	CD8 T cells
Gimap41	1.218	0.848	0.347	7.23E-140	CD8 T cells
Xcl1	1.257	0.4	0.054	3.61E-137	CD8 T cells
Cd8b12	1.468	0.662	0.19	4.37E-130	CD8 T cells
Samd3	0.768	0.29	0.027	5.83E-126	CD8 T cells
Cd3e1	1.074	0.688	0.221	3.96E-113	CD8 T cells
Cd163l1	1.622	0.321	0.007	6.14E-222	IL17+
Ly6g5b	0.931	0.265	0.004	2.54E-218	IL17+
Actn2	1.313	0.393	0.022	2.97E-167	IL17+
5430421N21Rik	1.332	0.311	0.014	1.17E-153	IL17+
Il18r1	1.494	0.571	0.074	5.84E-133	IL17+
Cxcr61	1.968	0.663	0.117	5.46E-119	IL17+
Podnl1	0.803	0.281	0.016	1.04E-113	IL17+
Cd3g2	1.752	0.929	0.345	1.59E-105	IL17+
Icos	1.080	0.378	0.042	1.08E-92	IL17+
Rora	1.000	0.444	0.068	1.08E-81	IL17+
Lat3	1.262	0.806	0.283	7.96E-75	IL17+
F2r	0.983	0.357	0.048	3.56E-72	IL17+
Pdcd1	1.195	0.342	0.046	6.62E-69	IL17+
Cd3e2	1.201	0.714	0.238	6.81E-64	IL17+
Tnfrsf25	0.692	0.26	0.028	2.64E-63	IL17+
Thy12	1.254	0.745	0.272	7.02E-62	IL17+
Cd3d2	1.094	0.872	0.394	3.65E-58	IL17+
S100a102	1.054	0.959	0.747	3.52E-57	IL17+
Bcl11b2	0.914	0.531	0.138	1.21E-52	IL17+
Cd821	1.253	0.719	0.343	2.92E-49	IL17+
Il1rl1	1.632	0.667	0.03	4.88E-235	ILC2
Klrg1	1.656	0.59	0.023	2.22E-222	ILC2
Rab27b	0.942	0.324	0.005	1.91E-212	ILC2
Rnf128	1.769	0.657	0.036	2.09E-201	ILC2
Gata31	2.109	0.752	0.051	1.99E-197	ILC2
Calca	2.287	0.343	0.008	2.32E-181	ILC2
Arg1	1.371	0.4	0.016	1.65E-147	ILC2
Slc6a13	1.036	0.39	0.015	2.47E-142	ILC2
Hs3st11	1.401	0.524	0.042	3.21E-110	ILC2

Gene	avg_ logFC	pct.1	pct.2	p_val_adj	Cluster Name
Cxcr62	1.642	0.848	0.123	4.67E-108	ILC2
Rora1	1.430	0.61	0.072	1.50E-93	ILC2
Ltb4r13	1.639	0.781	0.15	4.77E-81	ILC2
Il2ra1	0.864	0.333	0.029	1.15E-62	ILC2
Tnfrsf183	1.773	0.724	0.182	2.58E-55	ILC2
Xlr4c1	0.873	0.343	0.037	2.99E-51	ILC2
Ctla2a2	2.049	0.695	0.179	8.19E-50	ILC2
Xlr4a	0.984	0.4	0.058	1.05E-44	ILC2
Ramp31	1.242	0.352	0.049	1.54E-40	ILC2
Id24	1.282	0.914	0.433	1.25E-39	ILC2
Itgb3	0.731	0.267	0.028	3.85E-39	ILC2
Klrc2	1.525	0.624	0.02	3.24E-288	NKs
Klra9	1.967	0.419	0.007	8.28E-280	NKs
Klrb1f	1.066	0.513	0.014	6.15E-262	NKs
Klra4	1.729	0.325	0.004	2.18E-243	NKs
Klri2	1.413	0.479	0.019	2.73E-191	NKs
Gzmb	2.472	0.581	0.033	4.47E-181	NKs
Gzma	3.956	0.769	0.073	8.87E-171	NKs
Klrk13	2.216	0.966	0.138	1.50E-160	NKs
Cma1	1.035	0.274	0.006	3.64E-158	NKs
Eomes	1.016	0.436	0.02	1.51E-153	NKs
Klrc11	1.649	0.547	0.039	1.29E-137	NKs
Car2	1.619	0.556	0.044	3.18E-129	NKs
Fasl	0.893	0.41	0.023	1.36E-122	NKs
Samd31	1.096	0.496	0.037	1.97E-117	NKs
Il2rb2	1.461	0.701	0.091	8.39E-109	NKs
Xcl11	2.406	0.598	0.068	3.69E-104	NKs
Serpinb6b1	1.409	0.607	0.071	1.08E-97	NKs
Txk1	1.325	0.701	0.099	8.73E-94	NKs
Ctsw1	1.580	0.803	0.144	1.53E-93	NKs
Klrd13	1.855	0.923	0.243	1.45E-87	NKs
H2-Ob	1.517	0.704	0.184	5.54E-289	B2-like
Mzb11	1.272	0.599	0.123	6.92E-255	B2-like
Cd19	1.176	0.451	0.054	3.62E-254	B2-like
Fcer2a	1.223	0.4	0.036	1.24E-252	B2-like
Fcrla1	1.251	0.492	0.076	3.20E-242	B2-like
Ralgps2	1.234	0.517	0.089	1.36E-241	B2-like
Siglecg	1.275	0.516	0.095	6.67E-231	B2-like
Cd37	1.312	0.84	0.497	2.10E-218	B2-like
Cd55	1.221	0.468	0.082	1.27E-209	B2-like
Rps272	0.647	1	0.999	1.82E-207	B2-like
Mef2c2	1.348	0.774	0.359	2.14E-206	B2-like
Rps191	0.524	1	0.999	1.91E-190	B2-like
H2-Oa2	1.202	0.642	0.21	5.89E-190	B2-like
Rpl18a2	0.545	1	1	2.07E-182	B2-like
Rpl131	0.519	0.999	0.998	1.17E-174	B2-like
Rpl351	0.472	0.999	0.996	5.01E-168	B2-like
Spib2	1.024	0.344	0.049	9.08E-164	B2-like
Fau1	0.476	1	0.997	1.64E-163	B2-like
mt-Co3	0.462	1	0.999	6.53E-160	B2-like
Rps201	0.582	0.999	0.97	1.13E-153	B2-like
Mzb12	1.867	0.738	0.178	8.21E-56	B1-like
Cd79b1	0.542	0.937	0.331	8.08E-39	B1-like
Pou2af11	0.485	0.429	0.075	8.48E-39	B1-like
Cd79a1	0.580	0.929	0.322	1.73E-38	B1-like
Ly6d2	0.554	0.889	0.317	4.88E-36	B1-like
Prr51	0.358	0.349	0.061	1.07E-31	B1-like
Cd191	0.411	0.452	0.102	9.12E-28	B1-like

Gene	avg_ logFC	pct.1	pct.2	p_val_adj	Cluster Name
Dennd5b	0.316	0.302	0.053	3.98E-26	B1-like
Ms4a11	0.357	0.675	0.209	4.36E-25	B1-like
Ebf11	0.340	0.667	0.206	3.53E-24	B1-like
Gm432911	0.483	0.294	0.054	4.64E-24	B1-like
Trp53i11	0.273	0.381	0.082	6.23E-24	B1-like
Fam46c1	0.380	0.373	0.085	3.29E-23	B1-like
Tnfrsf13c1	0.264	0.444	0.109	8.33E-23	B1-like
Fcmr1	0.354	0.603	0.185	2.84E-22	B1-like
Fcrla2	0.379	0.468	0.127	1.17E-21	B1-like
Pdia4	0.526	0.468	0.134	2.20E-21	B1-like
Phgdh1	0.464	0.413	0.107	7.17E-21	B1-like
Rgcc1	0.399	0.389	0.1	2.65E-19	B1-like
Txndc52	1.480	0.595	0.238	1.03E-17	B1-like
Plvap	1.859	0.562	0.014	2.20E-300	SMC foam cells
Gng11	1.919	0.741	0.03	9.10E-297	SMC foam cells
Bmx	1.159	0.446	0.007	2.07E-294	SMC foam cells
Fhl1	1.311	0.482	0.009	3.36E-292	SMC foam cells
Tmem1581	2.480	0.768	0.035	2.73E-285	SMC foam cells
Gkn3	2.103	0.509	0.011	2.91E-285	SMC foam cells
Palmd	0.790	0.304	0.001	1.20E-283	SMC foam cells
Prex2	0.759	0.304	0.001	2.41E-283	SMC foam cells
Selp	0.851	0.366	0.004	4.54E-282	SMC foam cells
Ushbp1	0.775	0.321	0.002	1.45E-277	SMC foam cells
Ptgis	1.125	0.366	0.004	5.14E-273	SMC foam cells
Ccdc80	1.096	0.464	0.009	5.48E-272	SMC foam cells
Unc45b	0.774	0.286	0.001	1.72E-270	SMC foam cells
Gata6	0.791	0.339	0.003	5.74E-269	SMC foam cells
Slco2a1	0.905	0.357	0.004	1.09E-268	SMC foam cells
Tspan6	1.003	0.402	0.006	1.52E-268	SMC foam cells
Synpo	1.039	0.455	0.009	5.57E-268	SMC foam cells
Ldb2	0.677	0.277	0.001	2.44E-267	SMC foam cells
Cyyr1	0.870	0.268	0.001	4.76E-265	SMC foam cells
Fermt2	0.856	0.339	0.003	5.48E-264	SMC foam cells
Pdgfrb	0.851	0.579	0.003	2.94E-286	Fibroblast
Ccl11	1.391	0.421	0.001	4.19E-282	Fibroblast
Aldh1a1	1.070	0.421	0.001	4.45E-282	Fibroblast
Epha3	0.968	0.526	0.002	2.52E-279	Fibroblast
Hoxc6	0.442	0.316	0	1.07E-277	Fibroblast
Gpc6	0.731	0.474	0.002	1.23E-276	Fibroblast
Meg3	2.145	0.789	0.007	2.43E-266	Fibroblast
Bicc1	0.948	0.579	0.003	9.52E-266	Fibroblast
Scara5	1.308	0.421	0.001	4.99E-263	Fibroblast
Foxp2	0.691	0.421	0.001	7.39E-263	Fibroblast
Tmem100	1.301	0.474	0.002	1.33E-262	Fibroblast
Nsg1	0.908	0.474	0.002	5.93E-262	Fibroblast
Wnt5a	0.385	0.263	0	4.68E-257	Fibroblast
Cygb	2.062	0.789	0.007	4.78E-253	Fibroblast
Nox4	0.485	0.368	0.001	2.51E-251	Fibroblast
Bmper	0.818	0.421	0.001	4.62E-246	Fibroblast
Sult5a1	0.570	0.421	0.001	5.70E-246	Fibroblast
Col1a2	3.689	1	0.014	4.19E-241	Fibroblast
Col5a1	1.007	0.474	0.002	1.32E-237	Fibroblast
Col6a3	0.833	0.474	0.002	4.47E-237	Fibroblast

Avg_logFC refers to the average log fold change in gene expression between groups. pct.1 and pct.2 refer to percentage of cells expressing the gene within the identified cluster in room air or aneurysm groups. p_val_adj refers to p values adjusted using Bonferroni correction for multiple comparisons.

TABLE 2: Top 20 differentially expressed genes in each macrophage and monocyte cluster

Gene	avg_logFC	pct.1	pct.2	p_val_adj	Cluster Name
Lyve1	1.904	0.805	0.095	3.49E-194	Resident
Folr2	2.131	0.968	0.314	5.03E-184	Resident
Ccl24	1.939	0.733	0.088	4.68E-167	Resident
Pf4	2.059	0.997	0.592	2.17E-156	Resident
Cd163	1.695	0.733	0.123	5.37E-146	Resident
Ltc4s	1.677	0.848	0.238	6.03E-140	Resident
Sepp1	1.297	1	0.92	4.27E-136	Resident
Cbr2	1.480	0.865	0.242	4.32E-136	Resident
F13a1	1.549	0.966	0.476	7.90E-136	Resident
Fcna	1.662	0.612	0.073	9.02E-133	Resident
Fxyd2	1.488	0.713	0.149	5.55E-124	Resident
Gas6	1.327	0.894	0.332	5.04E-123	Resident
Mrc1	1.325	0.954	0.472	2.31E-116	Resident
Fcgrt	1.389	0.92	0.546	1.86E-109	Resident
Ednrb	1.295	0.54	0.074	1.98E-106	Resident
Ninj1	1.342	0.931	0.668	7.26E-102	Resident
Maf	1.187	0.902	0.449	7.77E-100	Resident
Apoe	2.461	0.721	0.222	8.21E-97	Resident
Cd209f	2.225	0.511	0.075	2.01E-96	Resident
Cd209g	1.644	0.422	0.039	4.08E-94	Resident
H2-Eb1	0.912	0.987	0.904	1.46E-84	Inflammatory
H2-Aa	0.825	0.991	0.939	4.20E-79	Inflammatory
H2-Ab1	0.806	0.996	0.972	3.15E-77	Inflammatory
Cd74	0.815	0.998	0.993	1.87E-74	Inflammatory
Tmem176b1	0.573	0.97	0.789	4.65E-53	Inflammatory
Tmem176a	0.618	0.933	0.687	2.23E-50	Inflammatory
H2-DMb1	0.557	0.912	0.69	4.45E-43	Inflammatory
Fcrls1	0.603	0.858	0.488	3.46E-42	Inflammatory
Ccl12	0.852	0.7	0.395	3.21E-38	Inflammatory
Serinc31	0.445	0.981	0.871	5.63E-38	Inflammatory
H2-DMa	0.453	0.931	0.776	3.63E-36	Inflammatory
Cd811	0.488	0.968	0.749	3.52E-35	Inflammatory
Clec4b1	0.523	0.606	0.281	8.22E-34	Inflammatory
Trf1	0.459	0.959	0.792	1.33E-33	Inflammatory
Cxcl2	0.954	0.634	0.371	4.58E-29	Inflammatory
Mrc11	0.281	0.841	0.469	1.44E-28	Inflammatory
Sepp11	0.282	0.998	0.914	2.18E-28	Inflammatory
Cx3cr1	0.559	0.692	0.425	1.70E-27	Inflammatory
Itm2b1	0.290	1	0.997	2.95E-27	Inflammatory
C1qa1	0.393	0.996	0.876	9.68E-26	Inflammatory
Lgals3	1.598	0.998	0.854	1.67E-163	Trem2 Foamy
Ctsz	0.830	0.996	0.915	3.81E-140	Trem2 Foamy

Gene	avg_logFC	pct.1	pct.2	p_val_adj	Cluster Name
Cd9	1.609	0.882	0.443	7.07E-126	Trem2 Foamy
Ctsb	1.027	1	0.992	4.40E-110	Trem2 Foamy
Cd68	0.853	0.99	0.855	3.86E-109	Trem2 Foamy
Fth1	0.842	1	1	2.98E-107	Trem2 Foamy
Lilr4b	1.051	0.861	0.424	2.44E-106	Trem2 Foamy
Mmp14	0.812	0.62	0.126	7.92E-105	Trem2 Foamy
Syngr1	0.833	0.512	0.077	1.94E-98	Trem2 Foamy
Anxa5	0.733	0.973	0.9	7.97E-98	Trem2 Foamy
Ctsd	1.233	0.986	0.86	1.57E-96	Trem2 Foamy
Gpr137b	0.919	0.741	0.259	6.94E-96	Trem2 Foamy
Cxcl16	0.958	0.918	0.575	3.16E-91	Trem2 Foamy
Ftl1	0.613	1	1	1.43E-88	Trem2 Foamy
Lilrb4a	0.929	0.912	0.649	2.88E-88	Trem2 Foamy
Cstb	1.041	0.953	0.816	1.16E-85	Trem2 Foamy
Prdx1	0.831	0.996	0.958	1.64E-85	Trem2 Foamy
Eif4a1	0.683	0.978	0.871	1.30E-83	Trem2 Foamy
Capg	0.969	0.878	0.639	4.51E-81	Trem2 Foamy
Ctss	0.667	1	0.993	6.78E-81	Trem2 Foamy
Upb1	0.628	0.309	0.01	2.76E-67	Cavity
Cd226	0.444	0.309	0.017	9.67E-52	Cavity
Ear2	1.809	0.723	0.161	3.06E-46	Cavity
Crip11	1.297	1	0.967	6.76E-40	Cavity
Retnla1	3.092	0.851	0.416	1.35E-35	Cavity
Fn1	1.529	0.809	0.32	5.12E-32	Cavity
Clec4b11	1.177	0.83	0.338	1.82E-30	Cavity
Ccl61	1.076	1	0.907	6.06E-29	Cavity
Dok21	0.905	0.83	0.331	2.58E-28	Cavity
Batf3	0.866	0.745	0.27	4.56E-27	Cavity
S100a101	0.938	0.968	0.749	3.79E-26	Cavity
Ryr1	0.388	0.287	0.035	3.37E-25	Cavity
Lpl1	1.451	0.766	0.382	1.76E-22	Cavity
Ccl91	0.755	0.989	0.84	2.60E-21	Cavity
Lyz1	2.568	0.713	0.325	1.51E-20	Cavity
Gfra2	0.338	0.319	0.056	5.37E-18	Cavity
H2-DMa1	0.780	0.957	0.808	1.07E-17	Cavity
Gda	0.750	0.819	0.404	4.04E-17	Cavity
Olfm1	0.669	0.553	0.184	7.12E-17	Cavity
H2-DMb11	0.737	0.957	0.735	1.56E-16	Cavity
Ifit2	1.541	0.689	0.051	9.19E-81	IFNIC
Ifit3b	1.212	0.541	0.031	1.56E-73	IFNIC
Cmpk2	1.133	0.607	0.047	3.24E-67	IFNIC
Ifit1	1.721	0.705	0.08	4.40E-60	IFNIC
Ifit3	2.103	0.82	0.126	1.34E-57	IFNIC
Mx1	0.755	0.492	0.034	6.90E-56	IFNIC
Rsad2	1.750	0.639	0.072	4.06E-53	IFNIC

Gene	avg_logFC	pct.1	pct.2	p_val_adj	Cluster Name
Oasl1	1.012	0.541	0.051	5.17E-49	IFNIC
Isg15	1.888	0.918	0.295	9.31E-38	IFNIC
Cxcl10	1.740	0.393	0.034	3.80E-37	IFNIC
Phf11d	1.288	0.787	0.198	1.69E-33	IFNIC
Mnda	1.427	0.918	0.29	6.46E-33	IFNIC
Iigp1	1.234	0.443	0.051	9.86E-33	IFNIC
Gm4955	1.056	0.738	0.172	6.25E-30	IFNIC
Ifi44	0.618	0.311	0.025	1.30E-29	IFNIC
Ifi47	1.194	0.82	0.233	1.94E-29	IFNIC
A530040E14Rik	0.622	0.426	0.053	2.09E-28	IFNIC
Pydc3	0.549	0.377	0.041	7.57E-28	IFNIC
Usp18	1.174	0.656	0.146	3.93E-27	IFNIC
Phf11b	1.340	0.869	0.343	4.46E-26	IFNIC
Hp	1.604	0.802	0.197	1.25E-103	Classical Monocytes
Ms4a4c1	1.336	0.918	0.349	2.81E-95	Classical Monocytes
Plac8	1.802	0.948	0.5	4.62E-90	Classical Monocytes
Sirpb1c	1.282	0.884	0.325	8.50E-86	Classical Monocytes
Ly6c2	1.722	0.776	0.242	1.54E-84	Classical Monocytes
Gm9733	1.083	0.556	0.085	1.52E-81	Classical Monocytes
Tmsb101	1.330	1	0.856	3.86E-80	Classical Monocytes
Emb	1.081	0.871	0.394	3.16E-73	Classical Monocytes
Mcemp1	0.962	0.642	0.156	1.13E-69	Classical Monocytes
Gsr	1.125	0.81	0.306	4.89E-66	Classical Monocytes
Napsa	0.950	0.892	0.437	6.50E-65	Classical Monocytes
Chil3	2.237	0.741	0.284	1.99E-64	Classical Monocytes
Ifitm31	0.840	1	0.969	2.00E-61	Classical Monocytes
Ccr22	1.069	0.957	0.516	4.17E-61	Classical Monocytes
Ifitm61	1.164	0.716	0.246	6.61E-59	Classical Monocytes
Sirpb1b	0.910	0.703	0.238	1.63E-57	Classical Monocytes
Ms4a6c1	0.794	0.978	0.856	1.34E-54	Classical Monocytes
Rplp0	0.508	1	0.981	2.90E-54	Classical Monocytes
H3f3a	0.561	1	0.969	5.44E-54	Classical Monocytes
Vcan	0.492	0.254	0.017	9.39E-54	Classical Monocytes
Ace	1.439	0.707	0.067	1.87E-112	Non-classical Monocytes
Eno3	1.666	0.675	0.078	2.25E-95	Non-classical Monocytes
Adgre4	1.424	0.699	0.085	4.99E-94	Non-classical Monocytes
Treml4	1.349	0.634	0.068	2.21E-89	Non-classical Monocytes
Ear21	1.678	0.797	0.146	7.84E-77	Non-classical Monocytes
Itgal	1.388	0.691	0.13	4.77E-68	Non-classical Monocytes
Pglyrp1	2.110	0.764	0.191	6.52E-64	Non-classical Monocytes
Gngt21	1.603	0.992	0.671	6.36E-61	Non-classical Monocytes
Trem3	1.056	0.472	0.064	1.26E-51	Non-classical Monocytes
Plac81	1.618	0.935	0.53	1.26E-42	Non-classical Monocytes
Nr4a1	1.110	0.593	0.14	2.33E-42	Non-classical Monocytes
Napsa1	1.291	0.894	0.466	1.61E-40	Non-classical Monocytes

Gene	avg_logFC	pct.1	pct.2	p_val_adj	Cluster Name
Cd300e	0.790	0.301	0.032	2.61E-37	Non-classical Monocytes
Cebpb1	1.122	0.984	0.861	3.01E-36	Non-classical Monocytes
Ly6i	1.170	0.52	0.12	1.32E-34	Non-classical Monocytes
Lst11	0.995	0.951	0.829	2.87E-34	Non-classical Monocytes
Ldlrad3	0.869	0.463	0.097	4.93E-34	Non-classical Monocytes
Samsn1	1.182	0.724	0.294	6.23E-34	Non-classical Monocytes
Rps27	0.513	1	0.998	7.43E-34	Non-classical Monocytes
Gsr1	1.078	0.789	0.34	5.22E-33	Non-classical Monocytes

Avg_logFC refers to the average log fold change in gene expression between groups. pct.1 and pct.2 refer to percentage of cells expressing the gene within the identified cluster in room air or aneurysm groups. p_val_adj refers to p values adjusted using Bonferroni correction for multiple comparisons.

TABLE 3: Differences in proportion of macrophage and monocyte clusters

Cluster Name	Cell Count Room Air	Cell Count Aneurysm	% Room Air	% Aneurysm	P-val	FDR (Benjamini–Hochberg)
Resident Mac	52	72	0.0841	0.0875	0.9008	1.0000
Inflammatory Mac	216	209	0.3495	0.2539	0.0002	0.0061
Trem2 Foamy Mac	200	302	0.3236	0.3670	0.0955	1.0000
Cavity Mac	5	30	0.0081	0.0365	0.0006	0.0137
IFNIC_MAC	42	16	0.0680	0.0194	0.0001	0.0046
Classical Monocytes	55	140	0.0890	0.1701	0.0001	0.0046
Non-classical Monocytes	48	54	0.0777	0.0656	0.3203	1.0000

FDR refers to false discovery rate and % column refers to cell proportions expressed as decimal numbers.

TABLE 4: Gene ontology pathway analysis of differentially expressed genes

Cluster Name	GO Pathway Name	GO_id	adj_p_val	log_adj_p_val
Resident				
	response to stress	GO:0006950	1.59E-08	7.799025
	endocytosis	GO:0006897	1.63E-06	5.787818
	vasculature development	GO:0001944	3.28E-06	5.483987
	regulation of cell population proliferation	GO:0042127	9.17E-06	5.037421
	leukocyte activation	GO:0045321	4.71E-04	3.326847
Inflammatory				
	inflammatory response	GO:0006954	1.47E-06	5.831308
	chemokine-mediated signaling pathway	GO:0070098	2.18E-05	4.662333
	myeloid leukocyte migration	GO:0097529	6.57E-04	3.182151
	T cell activation	GO:0042110	7.54E-04	3.122735
	macrophage apoptotic process	GO:0071888	6.90E-03	2.161105
	interleukin-1 beta production	GO:0032611	2.57E-02	1.590690
Trem2 Foamy				
	response to oxygen-containing compound	GO:1901700	2.23E-11	10.651347
	vesicle-mediated transport	GO:0016192	3.90E-09	8.408476
	organic substance catabolic process	GO:1901575	5.50E-09	8.259435
	response to lipid	GO:0033993	8.90E-08	7.050606
	regulation of catalytic activity	GO:0050790	4.36E-05	4.360215
	cellular response to lipoprotein particle stimulus	GO:0071402	2.18E-03	2.662512
	inorganic cation transmembrane transport	GO:0098662	3.96E-03	2.402489
Cavity				
	peptide biosynthetic process	GO:0043043	2.16E-08	7.665971
	cytoplasmic translation	GO:0002181	7.22E-06	5.141599
	antigen processing and presentation of peptide antigen via MHC class II	GO:0002495	4.90E-05	4.310187
	ribosomal small subunit biogenesis	GO:0042274	2.56E-03	2.591881
IFNIC				
	defense response to virus	GO:0051607	2.46E-35	34.608923
	response to interferon-beta	GO:0035456	8.79E-22	21.055937
	type I interferon signaling pathway	GO:0060337	4.72E-06	5.326441
	ISG15-protein conjugation	GO:0032020	2.50E-03	2.601631
	antigen processing and presentation of peptide antigen via MHC class I	GO:0002474	7.29E-03	2.137559
Classical Mono				
	defense response	GO:0006952	6.54E-18	17.184159
	leukocyte cell-cell adhesion	GO:0007159	2.56E-11	10.592488
	regulation of cytokine production	GO:0001817	1.26E-11	10.899498
	reactive oxygen species metabolic process	GO:0072593	2.50E-05	4.602698
	formation of cytoplasmic translation initiation complex	GO:0001732	1.15E-03	2.939335
Non-classical Mono				
	leukocyte cell-cell adhesion	GO:0007159	1.15E-15	14.940179
	T cell activation	GO:0042110	3.31E-12	11.479972
	cell motility	GO:0048870	4.62E-06	5.335804
	leukocyte adhesion to vascular endothelial cell	GO:0061756	1.95E-02	1.709640

TABLE 5: Differentially expressed genes in aneurysm vs room air clusters

Gene	avg_logFC	pct.1	pct.2	p_val_adj	Cluster Name
Slpi	-1.476	0.208	0.923	3.56E-18	Resident
Jchain	-2.107	0.333	0.865	2.11E-10	Resident
Ccl5	-1.045	0.458	0.865	1.13E-08	Resident
Spp1	-1.708	0.708	0.962	1.65E-07	Resident
Hspa8	-0.406	0.986	0.981	0.01175849	Resident
Slpi	-0.558	0.239	0.88	1.02E-45	Inflammatory
Ccl5	-0.775	0.488	0.912	6.13E-31	Inflammatory
Jchain	0.450	0.354	0.87	6.66E-29	Inflammatory
Hspa8	-0.488	1	0.995	7.44E-22	Inflammatory
Dnaja1	-0.599	0.737	0.87	1.58E-18	Inflammatory
S100a8	-0.497	0.325	0.722	3.51E-12	Inflammatory
Uba52	-0.427	0.885	0.921	4.72E-11	Inflammatory
Nkg7	-0.489	0.23	0.569	2.44E-09	Inflammatory
Rps27rt	-0.387	0.9	0.954	7.15E-06	Inflammatory
Mgp	-0.727	0.196	0.458	1.34E-05	Inflammatory
Hsp90ab1	-0.341	0.947	0.954	2.84E-05	Inflammatory
Cacybp	-0.351	0.545	0.662	7.61E-05	Inflammatory
Gm10076	-0.325	0.914	0.949	0.00011444	Inflammatory
Gm9843	-0.280	0.914	0.921	0.00017202	Inflammatory
Wdr89	-0.318	0.77	0.819	0.00019972	Inflammatory
Saa3	-0.266	0.077	0.282	0.00134353	Inflammatory
Gm10073	-0.277	0.804	0.801	0.0019433	Inflammatory
S100a9	-0.330	0.215	0.458	0.00629766	Inflammatory
Asah	-0.324	0.89	0.917	0.00716636	Inflammatory
Pon2	-0.297	0.545	0.634	0.00974419	Inflammatory
Ifitm3	0.331	0.981	0.991	0.01378571	Inflammatory
Jchain	-1.083	0.371	0.89	5.22E-61	Trem2 Foamy
Ccl5	-0.733	0.497	0.915	5.16E-44	Trem2 Foamy
Slpi	-0.568	0.341	0.925	3.26E-41	Trem2 Foamy
Uba52	-0.567	0.927	0.985	7.37E-28	Trem2 Foamy
Ccl8	-0.651	0.732	0.92	2.79E-25	Trem2 Foamy
Dnaja1	-0.585	0.805	0.915	1.07E-18	Trem2 Foamy
Nkg7	-0.489	0.175	0.58	4.11E-17	Trem2 Foamy
Mgp	-0.405	0.096	0.455	3.77E-15	Trem2 Foamy
Hspa8	-0.399	1	1	2.72E-14	Trem2 Foamy
Rps27rt	-0.473	0.884	0.945	1.07E-13	Trem2 Foamy
Mmp3	-0.255	0.02	0.255	1.26E-11	Trem2 Foamy
Gm100761	-0.410	0.937	0.97	4.23E-11	Trem2 Foamy
Gm101161	-0.365	0.917	0.965	1.34E-06	Trem2 Foamy
Hsp90ab1	-0.318	0.934	0.97	2.63E-05	Trem2 Foamy

Gene	avg_ logFC	pct.1	pct.2	p_val_adj	Cluster Name
Hspa51	-0.391	0.907	0.99	2.84E-05	Trem2 Foamy
Hspa1a	-0.474	0.255	0.51	0.00041674	Trem2 Foamy
Rpl23a-ps31	-0.271	0.934	0.95	0.00145085	Trem2 Foamy
Klf2	-0.333	0.255	0.485	0.0057108	Trem2 Foamy
Pf4	-0.463	0.404	0.61	0.00606328	Trem2 Foamy
Gm100731	-0.298	0.758	0.825	0.00842483	Trem2 Foamy
Wdr891	-0.292	0.738	0.83	0.00994126	Trem2 Foamy
Mmp121	-0.719	0.308	0.53	0.02637331	Trem2 Foamy
Dnajb1	-0.276	0.248	0.43	0.04914961	Trem2 Foamy
Slpi	-1.258	0.25	0.976	0.00011562	IFNIC
Jchain	-1.295	0.312	0.929	0.00050801	IFNIC
Uba52	-0.697	0.971	0.964	2.79E-16	Classical Monocytes
Ccl5	-1.156	0.371	0.927	4.08E-12	Classical Monocytes
Rps27rt	-0.488	0.914	0.964	0.0014707	Classical Monocytes
C1qa	-0.335	0.65	0.964	0.00424598	Classical Monocytes
Ly6e3	0.327	0.986	1	0.00640179	Classical Monocytes
Mgp	-0.498	0.05	0.364	0.00640652	Classical Monocytes
C1qb2	-0.536	0.786	0.982	0.00686134	Classical Monocytes
Rps28	-0.255	1	1	0.01338051	Classical Monocytes
Gm100763	-0.433	0.964	0.982	0.02781251	Classical Monocytes
Jchain	-1.180	0.148	0.667	8.74E-05	Non-classical Monocytes
Ccl84	-0.974	0.389	0.875	0.00013429	Non-classical Monocytes
Uba52	-0.747	0.833	0.979	0.00112264	Non-classical Monocytes
Slpi	-1.015	0.37	0.771	0.00680686	Non-classical Monocytes
C1qb3	-0.607	0.611	0.958	0.0108371	Non-classical Monocytes
Spp13	-1.627	0.537	0.917	0.02348405	Non-classical Monocytes

Avg_logFC refers to the average log fold change in gene expression between groups. pct.1 and pct.2 refer to percentage of cells expressing the gene within the identified cluster in room air or aneurysm groups. p_val_adj refers to p values adjusted using Bonferroni correction for multiple comparisons.

SUPPLEMENTARY TABLE 1: Immunohistochemistry antibodies

Target	Fluorophore/ Conjugate	Company	Clone	Catalog Number
CD68 (1:100)	Alexa Fluor 647	BioLegend	FA-11	137004
CD68 (1:100)	Alexa Fluor 594	BioLegend	FA-11	137020
CD68 (1:100)	Biotin	BioRad	FA-11	MCA1957B
CD45.1 (1:100)	Alexa Fluor 647	BioLegend	A20	110720
CD45.2 (1:100)	Alexa Fluor 647	BioLegend	104	109818
BrdU (1:50)	Biotin	BioLegend	MoBu-1	317904
Biotin (1:200)	Streptavidin-HRP	Perkin Elmer		NEL750001EA
Ki67	Primary	Abcam	SP6	Ab16667
Ki67	eFlour 660	Invitrogen	20Raj1	50-5699-82
Biotin (1:200)	Streptavidin – Cy3	Invitrogen		434315
Rat IgG2a	Alexa Fluor 647	BioLegend	RTK2758	400526
Mouse IgG2a	Alexa Fluor 647	BioLegend	MOPC-173	400234
Mouse IgG2a	Alexa Fluor 594	BioLegend	MRG2a-83	407509
Goat anti rabbit IgG	Alexa Flour 568	Invitrogen		A11011

SUPPLEMENTARY TABLE 2: Flow cytometry antibodies

Target	Fluorophore/ Conjugate	Company	Clone	Catalog Number
B220	APC-Cy7	BD Biosciences	RA3-6B2	552094
B220	BV421	BD Biosciences	RA3-6B2	562922
Biotin	Streptavidin – Qdot 605	Life Technologies		Q10101MP
Biotin	Streptavidin – BV 421	Bd Biosciences		563259
BrdU	FITC	BD Biosciences		559619
CCR2	BV786	BD Biosciences	475301	747966
CCR2	APC	R and D	475301	FAB5538A-100
CD115	PE/Cy7	BioLegend	AF598	135523
CD115	BV421	BioLegend	AF598	135513
CD115	APC	BioLegend	AF598	135508
CD117	APC	Thermo Fisher	2B8	17-1152-82
CD11b	PE/Dazzle594	BioLegend	M1/70	101255
CD11b	PE	BD Biosciences	M1/70	553311
CD11b	APC-Cy7	BD Biosciences	M1/70	557657
CD11c	APC-Cy7	BioLegend	N418	117323
CD127	APC-Cy7	BioLegend	A7R34	135039
CD135	BV421	BioLegend	A2F10	135313
CD150	PerCP-Cy5.5	BioLegend	TC15-12F12.2	115921
CD150	PerCP-eFluor 710	Thermo Fisher	mShad150	46-1502-82
CD16/32	BV711	BioLegend	93	101327
CD16/32	APC-Cy7	BD Biosciences	2.4G2	560541
CD3	APC-Cy7	BD Biosciences	17A2	555275
CD3	PE	BD Biosciences	17A2	555275
CD31	FITC	BD Biosciences	MEC 13.3	561813
CD34	FITC	BD Biosciences	RAM34	553733
CD34	PE	BD Biosciences	RAM34	551387
CD4	Alexa Fluor 700	BD Biosciences	RM4-5	557956
CD45	Alexa Fluor 700	BioLegend	30-F11	103127
CD45	FITC	BD Biosciences	30-F11	561088
CD45	BV421	BD Biosciences	30-F11	563890
CD45.1	FITC	BD Biosciences	104	553775
CD45.2	eFluor 450	eBioscience	104	48-0454-82
CD45.2	BV421	BD Biosciences	104	562895
CD48	PE/Dazzle594	BioLegend	HM48-1	103437
CD48	Biotin	Thermo Fisher	HM48-1	13-0481-85
CD8A	FITC	BD Biosciences	53-6.7	554856
CD90.2	APC-Cy7	BioLegend	30-H12	105327
CxCR4	BV650	BD Biosciences	2B11	740526
F4/80	PerCP-Cy5.5	BioLegend	BM8	123127
F4/80	PE-Cy7	BioLegend	BM8	123114
Ly6C	BV711	BioLegend		128037
Ly6C	Pe-Cy7	BioLegend	HK1.4	128018
Ly6G	APC	BD Biosciences	1A8	405712

Target	Fluorophore/ Conjugate	Company	Clone	Catalog Number
Lyve-1	Biotin	Thermo Fisher	ALY7	14-0443-80
MHC II	Alexa Fluor 700	Thermo Fisher	M5/114.15.2	1120-09
NK1.1	PE	BD Biosciences	PK136	406517
Rat IgG2a	Biotin	BD Biosciences	R35-95	553928
Rat IgG2b	APC	R and D	141945	IC-031A
SCA-1	BV650	BioLegend	D7	108143
TER-119	APC-Cy7	BioLegend	TER-119	116223
TER-119	PE	BD Biosciences	TER-119	553673